

Old Dominion University

ODU Digital Commons

Electrical & Computer Engineering Theses & Dissertations

Electrical & Computer Engineering

Spring 2020

Virtual SATCOM, Long Range Broadband Digital Communications

Dennis George Watson

Old Dominion University, dwats017@odu.edu

Follow this and additional works at: https://digitalcommons.odu.edu/ece_etds



Part of the [Digital Communications and Networking Commons](#), [Signal Processing Commons](#), and the [Systems and Communications Commons](#)

Recommended Citation

Watson, Dennis G.. "Virtual SATCOM, Long Range Broadband Digital Communications" (2020). Doctor of Philosophy (PhD), Dissertation, Electrical & Computer Engineering, Old Dominion University, DOI: 10.25777/4vcn-my13
https://digitalcommons.odu.edu/ece_etds/211

This Dissertation is brought to you for free and open access by the Electrical & Computer Engineering at ODU Digital Commons. It has been accepted for inclusion in Electrical & Computer Engineering Theses & Dissertations by an authorized administrator of ODU Digital Commons. For more information, please contact digitalcommons@odu.edu.

VIRTUAL SATCOM
LONG RANGE BROADBAND DIGITAL COMMUNICATIONS

by

Dennis George Watson
B.S. May 1980, United States Naval Academy
M.S. September 1985, Naval Postgraduate School
M.S. June 2000, National Defense University

A Dissertation Submitted to the Faculty of
Old Dominion University in Partial Fulfillment of the
Requirements for the Degree of

DOCTOR OF PHILOSOPHY

ELECTRICAL AND COMPUTER ENGINEERING

OLD DOMINION UNIVERSITY
May 2020

Approved by:

Linda Vahala (Director)

Dimitrie Popescu (Member)

Otilia Popescu (Member)

Jose Fernandez (Member)

ABSTRACT

VIRTUAL SATCOM: LONG RANGE BROADBAND DIGITAL COMMUNICATIONS

Dennis George Watson
Old Dominion University, 2020
Director: Dr. Linda Vahala

The current naval strategy is based on a distributed force, networked together with high-speed communications that enable operations as an intelligent, fast maneuvering force. Satellites, the existing network connector, are weak and vulnerable to attack. HF is an alternative, but it does not have the information throughput to meet the distributed warfighting need. The US Navy does not have a solution to reduce dependency on space-based communication systems while providing the warfighter with the required information speed.

Virtual SATCOM is a solution that can match satellite communications (SATCOM) data speed without the vulnerable satellite. It is wireless communication on a High Frequency (HF) channel at SATCOM speed. We have developed an innovative design using high power and gain, ground-based relay systems. We transmit extremely wide-wideband HF channels from ground stations using large directional antennas. Our system starts with a highly directional antenna with a narrow beam that enables increased bandwidth without interfering with other spectrum users. The beam focus and power provide a high SNR across a wideband channel with data rates of 10 Mbps; 1000 times increase in HF data speed.

Our modeling of the ionosphere shows that the ionosphere has more than adequate bandwidth to communicate at 3000 km and high speeds while avoiding detection. We designed a flexible structure adjustable to the dynamic ionosphere. Our design provides a high-speed communications path without the geo-location vulnerability of legacy HF methods.

Our invention will benefit mobile users using steerable beamforming apertures with wide bandwidth signals. This dissertation will focus on three areas: examination of the ionosphere's ability to support the channel, design of a phased array antenna that can produce the narrow beam, and design of signal processing that can accommodate the wideband HF frequency range.

Virtual SATCOM is exciting research that can reduce cost and increase access to long range, high data rate wireless communications.

Copyright, 2020, by Dennis George Watson, All Rights Reserved.

This dissertation is dedicated to hard work and perseverance.

ACKNOWLEDGMENTS

Many people have contributed to the successful completion of this dissertation. I want to thank my committee members for their patience and hours of guidance on my research and editing of this manuscript. The untiring efforts of my advisor, Dr. Linda Vahala, deserve special recognition. Also, Dr. Fernandez, who guided me through an understanding of the complex mathematics of ray propagation in the ionosphere. Dr. Dimitri Popescu and Dr. Otilia Popescu were very helpful in the development of this dissertation.

The results published in this paper were obtained using the HF propagation toolbox, PHaRLAP, created by Dr. Manuel Cervera, Defence Science and Technology Group, Australia. This toolbox is available by request from its author.

I also need to acknowledge the Elmer's in the Chesapeake Amateur Radio Service (CARS). This group of amateur radio enthusiasts are real "doers" in the electromagnetic spectrum. Jeff Kayser, Bill Runyon, Bill Mellema, and John Copper have assisted with my understanding of the RF spectrum through hands-on radio operations.

Finally, and most importantly, I want to acknowledge Amy, my wife, for her unwavering support. Her assistance in writing the paper and keeping me moving was critical to the successful completion. Her support was incredible, and I could not have done it without her.

NOMENCLATURE

AC	Alternating Current
ACR	Array Control Room
ADC	Analog-to-Digital Converters
ADNS	Automatic Digital Network System
AESA	Active Electrically Scanned Array
AM	Amplitude Modulation
ALE	Automatic Link Establishment
ARQ	Automatic Repeat Request
ATO	Air Tasking Orders
BER	Bit Error Rate
BLOS	Beyond Line of Sight
CANES	Consolidated Afloat Networks and Enterprise Services
COSPAR	Committee on Space Research
CW	Continuous Wave
DAC	Digital to Analog Converter
dB	Decibel
dB _i	Decibel referenced to isotropic antenna
dB _m	Decibel referenced to milliwatt
dBW	Decibel referenced to a watt
DC	Direct Current
DoD	Department of Defense
DSP	Digital Signal Processor
DSTO	Defence Science and Technology Organization (Australia)
ECU	Element Control Units
EM	Electromagnetic
EMS	Environmental Monitoring Station
EW	Electronic Warfare
FCC	Federal Communications Commission
FDM	Frequency Division Multiplex
FFT	Fast Fourier Transform
FM	Frequency Modulation
FCMW	Frequency-Modulated Continuous Wave

FPGA	Field-Programmable Gate Arrays
HF	High Frequency (3-30 MHz)
HFDF	High Frequency Direction Finding
Hz	Hertz
IFFT	Inverse Fast Fourier Transform
IRI	International Reference Ionosphere
ISI	Inter Symbol Interference
ISR	Intelligence, Surveillance, and Reconnaissance
ITU	International Telecommunication Union
JWICS	Joint Worldwide Intelligence Communications System
kHz	Kilo Hertz
km	Kilo meters
LAN	Local Area Network
LIS	Lightning Imaging Sensor
LPD	Low Probability of Detection
LPDA	Log Periodic Dipole Antenna
LPMA	Log Periodic Monopole Antenna
LPI	Low Probability of Intercept
LTE	Long Term Evolution
Mbps	Megabits per Second
MHz	Mega Hertz
MILSTD	Military Standard
MIMO	Multiple Input multiple Output
MUOS	Mobile User Objective System
NATO	North Atlantic Treaty Organization
nm	Nautical Mile
NIPRNET	Non-classified Internet Protocol Router Network
OFDM	Orthogonal Frequency Division Multiplexing
OTD	Optical Transient Detector
OTHR	Over the Horizon Radar
PA	Power Amplifier
PHaRLAP	Provision of High Frequency Raytracing Laboratory for Propagation Model
PLA	People's Liberation Army
PWR	Power

QAM	Quadrature Amplitude Modulation
QPSK	Quadrature Phase Shift Keying
RF	Radio Frequency
RMS	Route Mean Square
ROTHR	Relocatable Over the Horizon Radar
RX	Receiver
SATCOM	Satellite Communications
SCR	System Control Room
SDR	Software Defined Radio
SIGINT	Signals Intelligence
SIPRNET	Secret Internet Protocol Router Network
SNR	Signal to Noise Ratio
SSB	Single Sided Band
STANAG	Standardization Agreement (NATO)
TADC	Time-Based Analog-to-Digital Converter
TRMM	Tropical Rainfall Measuring Mission
TX	Transmitter
URSI	International Union of Radio Science
US	United States
USS	United States Ship
UWB	Ultra-Wide Band
VSWR	Voltage Standing Wave Ratio
WAN	Wide Area Network
WBHF	Wideband Frequency Modulation
WCDMA	Wideband Code Division Multiple Access
W-OFDM	Wideband Orthogonal Frequency-Division Multiplexing
WSPR	Weak Signal Propagation Reporting

TABLE OF CONTENTS

	Page
LIST OF TABLES	XII
LIST OF FIGURES	XIII
Chapter	
1. INNOVATIVE CONCEPT.....	1
1.1 Our Original Concepts and Contributions of this Work:.....	3
1.2 Areas of Study	4
1.3 Virtual SATCOM Design Flow	5
1.4 Virtual SATCOM Concept of Operations	7
1.5 Key Technology Factors:.....	8
1.6 Another Advantage of Virtual SATCOM, Low Probability of Detection	10
1.7 Another Advantage of Virtual SATCOM, Electronic Scanning to Service Multiple Platforms	10
1.8 The Vulnerability of the SATCOM System Architecture.....	11
1.9 Threats to Satellite Communications	11
1.10 High Cost as a Vulnerability	12
1.11 Technological Capability to Modernize as a Vulnerability	12
1.12 Capacity Limit.....	12
1.13 Information Theory and Link Budget	13
1.14 Virtual SATCOM Forward Link Analysis	14
1.15 Virtual SATCOM Back Link Analysis.....	16
1.16 Comparison of SATCOM to Virtual SATCOM.....	17
1.17 Bandwidth Policy Limitations.....	18
1.18 Prior Research and Current Standards for Wideband HF Systems.....	19
1.19 Review of Current HF Communication Capabilities.....	20
1.20 Virtual SATCOM Ground Station Design	21
1.21 Environment Monitoring Station.....	22
1.22 Signal Control Room.....	23
1.23 Array Control Room.....	24

1.24	Element Control Unit	24
1.25	Vertical Log Periodic Dipole Antenna Array	24
1.26	Virtual SATCOM Mobile Station Design	25
1.27	Virtual SATCOM Mobile Receiver	25
1.28	Omnidirectional Command and Control Network and Sounders	27
1.29	Sounder Operations	28
1.30	Omnidirectional Command and Control Communication	29
1.31	Example Omnidirectional Command and Control Communication	30
2.	BANDWIDTH OF THE IONOSPHERE	32
2.1	Ionosphere Layers	33
2.2	The Volatility of the Plasma	34
2.3	How Free Electrons Affect Ray Path in the Ionosphere	35
2.4	Refractive Index	35
2.5	PHaRLAP Model:	40
2.6	Results of Our Testing.	42
2.7	Validation of PHaRLAP Model	46
3.	HF NOISE ANALYSIS	47
3.1	SiMIAN Noise Model Improvement	48
3.2	Lightning Strike Noise	48
3.3	Galactic Noise	49
3.4	Propagation	49
3.5	Absorption Model	49
3.6	Summarizing the Noise Floor in HF Band	50
4.	ANTENNA DESIGN AND SIGNAL PROCESSING	52
4.1	Introduction	52
4.2	Radiation Mechanisms of Antennas	52
4.3	Dipole Antenna	53
4.4	Directional Antenna Designs	53
4.5	Log Periodic Array Antenna	54
4.6	Virtual SATCOM Design of Log Periodic Antenna for Antenna array.	56
4.7	Log Periodic Antenna Design Procedure for Virtual SATCOM	56
4.8	Results of Virtual SATCOM Design using Matlab LPDA Design Program	59

4.9	Virtual SATCOM Antenna Array	60
4.10	Virtual SATCOM Linear Array Design	61
4.11	Two Element Arrays.....	61
4.12	N-Element Linear Array	64
4.13	Virtual SATCOM Radiation Pattern Analysis Using MATLAB.....	68
4.14	Phase Steering	71
4.15	Directivity and Gain	71
4.16	Radiation Intensity and Radiation Power Density	72
4.17	Radiation Intensity of Antenna Arrays	73
4.18	Non-Uniform Amplitude of Array Elements.....	76
4.19	Smart Antennas	80
4.20	Analysis Performance Degradation Due to Non-Linearity and Phase Noise.....	81
4.21	Signal Processing for Virtual SATCOM	83
4.22	Delay Spread.....	84
4.23	Flat Fading	85
4.24	Inter Symbol Interference	86
4.25	The Magnitude of Signal Processing	87
4.26	OFDM.....	89
4.27	Virtual SATCOM Data Block Design	89
4.28	Weakness of MILSTD 188-110D Appendix D, Wide Bandwidth Channels.....	91
4.29	Our Solutions to MILSTD188-110D Wideband Modulation High Symbol Rate.....	92
4.30	Software Defined Radios (SDR) Meet digital Signal Procession Requirements.....	94
5.	CONCLUSIONS.....	95
	REFERENCES	96
	APPENDIX A.....	101
	APPENDIX B	110
	APPENDEX C	115
	VITA.....	135

LIST OF TABLES

Table	Page
1. Data Rate Analysis for Various Scenarios.....	14
2. Comparison of Data Rate between Satellite and HF Link.....	17
3. The output of Model from Guam Looking North on Sept 2, 2016.....	46
4. MATLAB Results of LPDA Design.....	59
5. Half Power Beam Width (HPBW) for Arrays at select frequencies.....	68
6. Directivity across the Virtual SATCOM Spectrum.....	76
7. Comparison of MILSTD Symbol rate and Delay Spread.....	92
8. Virtual SATCOM Modulation using MILSTD188-110D modified with OFDM.....	93

LIST OF FIGURES

Figure	Page
1. Virtual SATCOM moves the relay point from space to the surface.....	1
2. Shows the Virtual SATCOM design flow.....	6
3. Virtual SATCOM Spider Architecture.....	8
4. With ground stations in Guam, Hawaii, and California, the Pacific is connected from the USA to China.....	9
5. Virtual SATCOM Diagram.....	22
6. Virtual SATCOM Functional Diagram.	23
7. Mobile Unit Antenna Configuration and Functional Diagram.....	26
8. Omnidirectional Environmental Sounding and Command and Control Network.....	27
9. Chirp sounders were receivers that were used by mobile units to determine the best propagation path in the HF band of interest.....	28
10. Once mobile unit checks in on omnidirectional C2 Net, the directional AESA system will begin to transmit to the mobile unit to establish a link.....	29
11. Picture of an FT user interface. K4DGW is responding to a CQ request from AC9HP.....	31
12. The graph shows the concentration of gases in the atmosphere. For example, at an altitude of 300 km, there are approximately 10^{14} O ₁ atoms [20].....	32
13. Diagram of ionosphere layers during day and night.....	34
14. A simple diagram is showing ray traveling from lower to higher plasma frequency.....	35
15. Chart of effective collision frequency vs altitude at a midlatitude on an average day [13].....	37
16. Shows electron density for a low and high sunspot number (R) during day and night.....	38
17. Shows Earth magnetic contour lines in nano Teslas (nT) for the western Pacific Ocean.....	38
18. PHaRLAP Model flow chart.....	43
19. Local Midnight PHaRLAP graph of ray propagation looking north.....	44
20. Local Noon PHaRLAP graph of ray propagation looking north.....	44
21. The graph shows the highest and lowest frequency that meets the test of traveling 3000 km and landing on a precise location.....	45

	Page
22. Graph shows effective bandwidth during 24-hour period for Guam on September 2, 2016	45
23. Common dipole antenna.....	53
24. Dipole Log periodic dipole array.....	55
25. Computed contours of constant directivity versus τ and σ . [41]	56
26. Relative characteristics impedance of a feeder line as a function of relative characteristics impedance of a dipole element [41].....	58
27. Virtual SATCOM antenna element design. It is a vertical wire LPDA suspended from towers.....	60
28. Diagram of two-element antenna array with uniform amplitude.....	62
29. Diagram of a two-element array with separation distance (d) and direction angle (θ)...	62
30. On the left is a diagram of an N element array that is evenly spaced with uniform amplitude.....	64
31. Graph of $ (\sin/x) $	65
32. Shows the 3D pattern of 200 dipole element array at 7MHz with 10m spacing.....	69
33. Shows 3D pattern of 200 dipole element array at 14 MHz with 10m spacing.....	69
34. Shows 3D pattern of 200 dipole element array at 21 MHz with 10m spacing.....	70
35. Shows 3D pattern of 200 dipole element array at 28 MHz with 10m spacing.....	70
36. Diagram of Non-uniform amplitude array. Each of the N elements has its output modified by a phase shift (b) and amplitude weighting (W).....	77
37. Aperture gain of a 200-element isotropic array with uniform spacing of 10m at 7, 14 and 28 MHz.....	79
38. Diagram of a smart antenna array with a digital signal processor.....	80
39. The diagram shows how a notional smart antenna would adjust the weighting to a 10-element array.....	81
40. The diagram shows the power fall from an amplifier at high power.....	82
41. Adaptive Pre-Distorter will adjust the input to the amplifier and maintain linear output.....	83
42. Diagram of two ray paths. One at refraction altitude of 300 km and the other at a refraction altitude of 400 km.....	85
43. The diagram shows how delay spread causes inter-symbol interference.....	87
44. Functional diagram of digital processing in the Virtual SATCOM system.....	88

	Page
45. The diagram shows how high-speed applications are sorted into data blocks for transmission.....	90
46. Diagram of 26 OFDM subchannels, each 1800 Hz wide.....	93

CHAPTER ONE

INNOVATIVE CONCEPT

Virtual SATCOM is wireless communication at satellite communication (SATCOM) data speeds on a high frequency (HF) skywave channel (3-30MHz) without a physical satellite. The relay function of the satellite is moved from space to a terrestrial (ground) station. Virtual SATCOM employs bent signal paths versus line of sight (LOS) paths to connect over the horizon users on high speed digital channels. The high data rate is a result of ultra-wide bandwidth of 3 MHz and directional high gain antenna with 1° of beam width which results in >20 dBi of gain. In this paper, a long range and high data rate are defined as 2000-3000 Km (~ 1000 -2000 miles) and data rates greater than 10 Mbps.

The Achilles heel of the United States Department of Defense's (DoD) modern networked warfare is the communication satellite. Adversaries including nation-states, terrorists, and criminals, understand this vulnerability. They are poised to attack with electromagnetic jamming, cyber-attack, directed enemy, and kinetic weapons, as discussed in an unclassified DoD report to Congress in 2016 [1]. The United States needs a SATCOM alternative to mitigate the space vehicle vulnerability. Virtual SATCOM will deliver communications at SATCOM speed (>10 Mbps), thus reducing the risk. It is an affordable and low-risk solution. It could be deployed regionally and scaled up for worldwide capability.

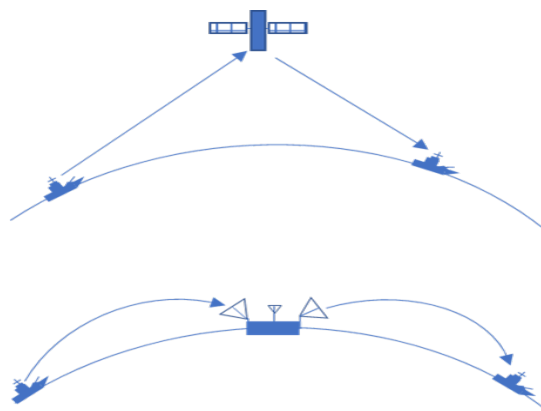


Figure 1. Virtual SATCOM moves the relay point from space to the surface. The top diagram shows a satellite relaying a signal. The bottom picture shows a relay station on the surface and bent rays relaying a signal.

This new concept is possible due to improvements in digital signal processing, software defined radio equipment, and automatic link capabilities. Unlike a spaced based system, a ground system that can be repaired and upgraded with commercially available equipment will improve performance at reduced

costs throughout the life cycle. To appreciate the cost of SATCOM systems, the MOUS satellite system cost over \$6B for five satellites.

The key to this project is understanding the ionosphere. The ionosphere's HF skywave propagation channel can provide the bandwidth needed to support long range high data rate communications. The ionosphere has been used for over the horizon communication for many years. Signals in the HF band (3-30MHz), sometimes called shortwave, are diffracted (bent) in the ionosphere and redirected back to Earth thousands of km downrange. However, these narrowband signals have weaknesses that limit capability. The typical data rate capacity of HF links is less than 10 kbps with a few systems that can reach 100 kbps under favorable conditions. HF links are an order of magnitude below SATCOM systems. This work will show that current flaws can be mitigated, and an HF skywave path can transport information at Mbps speeds and compete with or compliment geosynchronous satellite systems. The satellite's altitude allows the use of line of sight frequencies and enables the satellite to see both the uplink and downlink transceivers. Figure 1 shows a view of a SATCOM and Virtual SATCOM system.

The virtual SATCOM architecture starts with a base station that has an AESA (active electrically scanned array) of vertical log periodic dipole antennas (LPDA) that can steer narrow beams with wideband signals onto mobile platforms. This concept is a complete reversal of current HF communication architectures. Current practice is wide (omnidirectional) beams with narrow bandwidths to avoid interference. In our design, this wide frequency bandwidth and narrow beamwidth feature increase the signal to noise ratio (SNR) and bandwidth thus increasing data speed inside the beam without interfering with the spectrum outside the beam.

Signals that travel via the ionosphere are prone to multipath interference due to delay spread resulting in frequency selective fading and inter-symbol interference. Refractions cause the multipath off multiple layers in the ionosphere. In the past, delay spread has limited the data speed. Our system takes advantage of modern wideband signal modulation techniques to avoid this limitation. Software defined radios (SDR) with digital signal processing using orthogonal frequency division multiplexing (OFDM) modulations divides a high-speed digital channel into many slower sub-channels. Slower data rate sub-channels are resistant to multi-path effects. The sub-channels are combined by an inverse fast Fourier transform (IFFT) process just before transmission. At the other end, the receiver applies a fast Fourier (FFT) process to decompose the signals back into the sub-channels. The parallel streams of many slower sub-channels are then combined back into a single high-speed data channel.

Another limitation of current HF radio operation is the policy of fixed frequency allocations. This is an inefficient policy for a medium that varies with time. If the assigned frequency allocated to a user encounters a loss of service due to signal fading, it is not permitted to adjust to a new workable frequency without assignment of additional frequencies. In the Virtual SATCOM concept, the system must

automatically adjust channel frequency to maintain long-range propagation without loss of service due to fading. The signal is bound inside a narrow beam, so the frequency agility and bandwidth are not major negative issues. The narrow beam reduces the impact on other users. For example, when sailing a ship, the mariner must continuously adjust sails and heading to reap the benefit of the natural wind to propel the ship. The sailor can navigate the ship to the destination but must adapt the course as the natural wind changes. In Virtual SATCOM, the system must also adjust frequencies within the HF band adjusting to the frequencies that will diffract to a specific location on a given day/time. The US electromagnetic policy agency is the Federal Communication Commission (FCC). The FCC has developed policies for spectrum sharing for mobile cellular applications [2]. The policy allows the leasing of the spectrum as secondary users. The secondary user must ensure there is no interference with the primary user. That stated, there is precedence to show that the US has made progress in allocating spectrum to meet the needs of emerging capabilities.

Signal bandwidth is a parameter that determines maximum signal throughput. Unfortunately, current frequency allocation in the HF spectrum is normally narrow bandwidth with the assumption of omnidirectional (360°) propagation. A key to high-speed throughput is greater bandwidth. The passband of the ionosphere was studied, and this dissertation shows that 3 MHz of bandwidth is characteristically available. 3MHz is 1000 times greater than the standard 3 kHz allocation for one signal. However, to allocate this much bandwidth to an omnidirectional signal that propagates for thousands of km is not practical. Our proposed system requires the use of directional antennas at a base station for both transmitting and receiving. A focused beam will increase the signal to noise at the mobile receiver. More importantly, it will also reduce the interference to other spectrum users. Within the narrow beam, the entire bandpass of the ionosphere can be used. Note, a directional antenna at the mobile location is not required. Instead, low power will be used to avoid interference with other users of the spectrum.

1.1 Our Original Concepts and Contributions of this Work:

The list below shows our contribution to changing the pyridine on how to communicate in the high frequency (HF) spectrum to generate significantly better data rates.

1. Developed a viable novel concept and design that can change military communications.
2. Completed a tradeoff analysis of data rate vs. frequency, bandwidth, noise level, antenna gain, transmitter power, and efficiency.
3. Modified a radio frequency (RF) propagation program to analyze the ionosphere across four seasons and time of day in various locations. Results confirm bandwidth is available almost 24/7.

4. Designed a wideband LPDA antenna for a 7-28 MHz frequency range for the enormous antenna array.
5. Designed and modeled a 200-element array to show the beamforming capabilities.
6. Designed a command and control network to monitor and adjust parameters in real-time.
7. Developed a modulation scheme using MILSTD188-110D with OFDM modulation to enable high data rates in a harsh multipath environment.
8. Used Active Electronic Scanned Array (AESA) for communication channel that capitalizes on a directional beamforming antenna array coupled with a high-power transmitter and high gain antenna that results in high signal to noise ratio (SNR) on the receiver.
9. Used wideband channels (WB). We used a 3 MHz vs. 3kHz bandwidth which yields a high data rate (>10 Mbps).
10. Employed Virtual SATCOM frequency reuse for low probability of detection (LPD), and Anti-Jam (AJ) capabilities.
11. Identified Virtual SATCOM as increasing the usefulness of HF in the 21st Century by changing the paradigm on how to communicate on HF.

1.2 Areas of Study

This dissertation will focus on three areas. First and most important, we consider whether the ionosphere can support the channel conditions needed for high data rate communications. Understanding that the environment is dynamic, we determine the parameters needed to operate in this dynamic environment. This range of maneuver and rate of change will define the parameters that the ground station and remote terminal must meet.

The second area of focus will be the ground station. The premise is that the ground station antenna will use directional beams versus omnidirectional propagation. The directional beam will increase gain, and the result is higher SNR between the mobile terminal and the ground station. The focused beam will also limit unintended signal energy into other user equipment. To prevent interference, the beam confines the energy into a narrow space and allows the terminal and ground station to open the bandwidth of the channel without interfering with other spectrum users. To put it into a size perspective, an HF ground station with a beamforming array capable of 1° of focus is 2 km in total length. This is too large for even the largest ships. This size is the driver for a ground station to relay to mobile units with smaller antenna apertures.

Additionally, the ground station will have to change the direction of the beam to service multiple users. These two constraints preclude the use of mechanical steering to move the beam. The obvious

choice is an electronically steered array of antennas. Over the horizon, radar (OTHR) systems that exist today use directional steering to move their radar beam. As discussed in [3], the AN/TPS-71 (ROTHR) system has a separate array for the transmit and receive portions of the radar system. One advantage of this bistatic configuration is a reduction of transmitter energy reflecting from near objects and picked up by the receiver. The Virtual SATCOM system operates in a hub and spokes architecture. The ground station receives all communication from mobile terminals. The connections can then be forwarded via a gateway to another IP network or rebroadcast to another mobile platform. The use of a hub for mobile to mobile may seem like a redundant path, but it provides needed advantages to the platforms. The high gain and high-power base station ensure proper signal strength at the receiver of the mobile terminal. This way the terminals can use minimal power received by high gain ground station yet ensure a high-power signal is relayed to the other mobile platform.

The third area of study will be the design limitations of the mobile system. The objective is to keep this equipment to the minimum necessary to meet the range and data rate requirements. The starting point for mobile platforms is a single dipole antenna with wide bandwidth (>3 MHz) tunable reception. Other designs include mechanical steerable Log Periodic or Duo-conical antennas. These antennas are larger but offer better bandwidth profiles. Other required equipment is a software defined radio that can digitize and demodulate multiple signal formats.

1.3 Virtual SATCOM Design Flow

This paper follows a design flow that begins with defining the need in a broad sense. While looking at the weaknesses of both current SATCOM and HF skywave communications paths. This results in crucial design parameters that the system should meet. These parameters start with data speed but also include parameters like bandwidth, transmit power, antenna gain, path losses, etc. The next function is an analysis of the propagation medium. HF skywave is possible due to the free electrons in the ionosphere. The ionosphere is a dynamic environment that requires a design that can adjust to the situation as it changes. This work uses a ray tracing ionosphere model to examine the environment to design an antenna that can maneuver in the dynamic environment. Next, we created an antenna array to operate in this environment to include the antenna elements. Finally, we developed a system of systems architecture to include the process of command and control, environment monitoring, frequency control and allocation, antenna control, traffic management processes including signal modulation and data rate. Figure 2 shows this design flow.

Virtual SATCOM Design Flowchart

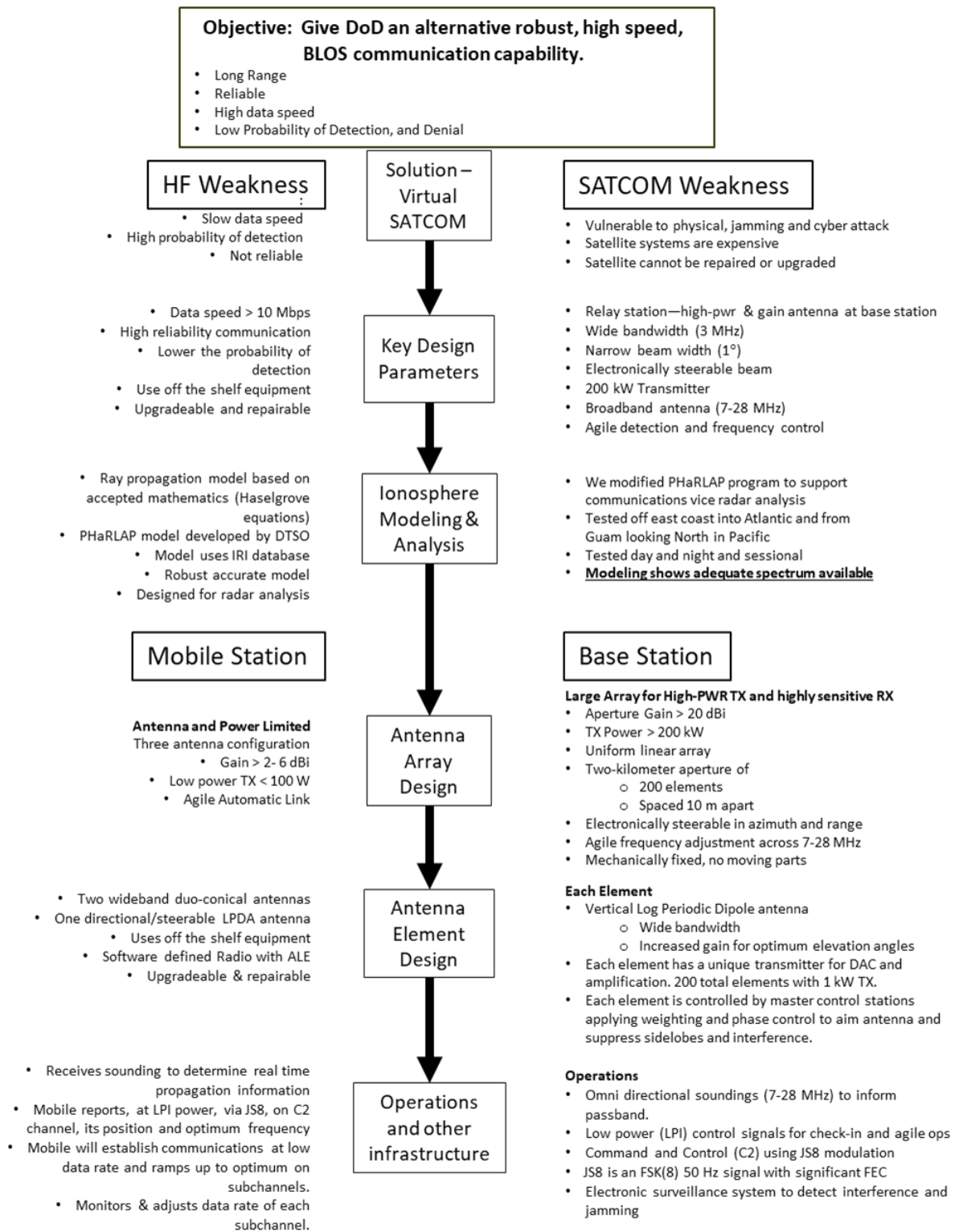


Figure 2. Flowchart Shows the Virtual SATCOM design flow.

1.4 Virtual SATCOM Concept of Operations

The concept of operations for virtual SATCOM is shown in Figure 3 and Figure 4. It is a high gain ground-based antenna to generate an electronically steerable high-power beam to relay mobile to mobile users or connect mobile users to other network systems, e.g., intelligence, surveillance, and reconnaissance (ISR) resources. Ground basing of the steerable antenna is necessary because the size of an HF system is too large for mobile units (2 km). Using beam steering to aim the beam at the correct azimuth and frequency electronically will result in a beam bending back to an intended mobile recipient downrange. A feedback loop will keep the beam on target. Beam steering is common to radar systems but not widely used in communication systems. For this virtual SATCOM communication application, beam steering is needed to avoid interference with other users of the same spectrum. With segregation, the bandwidth can be increased without interfering with others. An added benefit is an increased SNR at the mobile platform.

The ionosphere is dynamic, and the refraction angle changes as the free electron concentration of the upper atmosphere changes. The system must continually update the steering to maintain the signal on the intended mobile user. Beam aiming must be continuously updated to keep the signal energy on the mobile unit while the ionosphere changes. This requires feedback from the mobile unit regarding signal quality. This is similar to the mobile cellular systems where the mobile equipment reports a signal strength of other channels [4].

By steering the beam, the base station can timeshare by moving the focused signal to multiple users. Mobile units can communicate beyond the line of sight (BLOS) using the base station to relay digital networks and communications between mobile users and connect to other off-site ISR networks. To over-simplify, the system operates as a hub and spoke mobile cellular architecture but at a much greater range. The range from the base station to the mobile user is up to 3000 km (1620 NM). The high-gain base station's antenna increases the SNR at the receiver on both the forward link and backlink while preventing unintended interference with other users outside the narrow beam. Preventing unintentional interference is a crucial consideration for approval by the International Telecommunication Union and Federal Communication Commission (ITU/FCC).

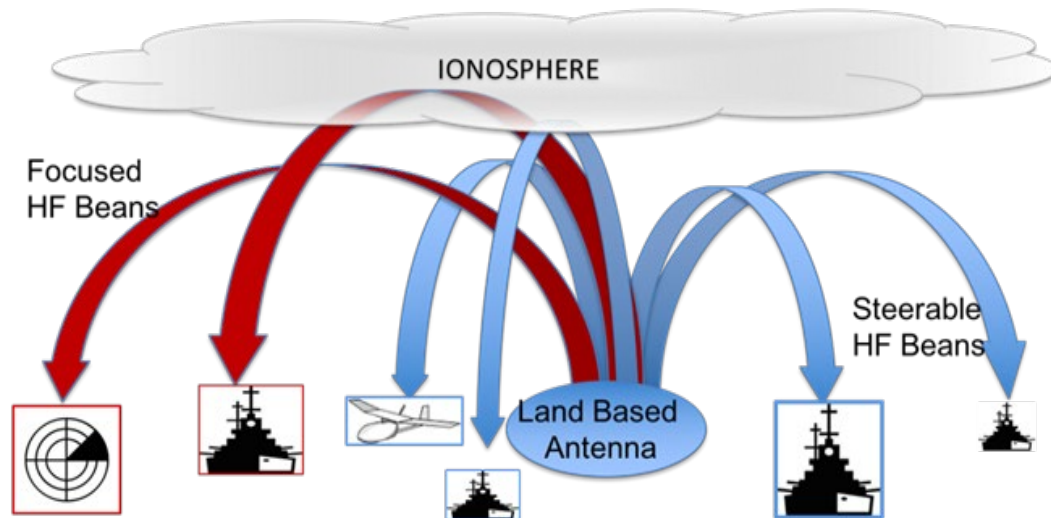


Figure 3. Virtual SATCOM Spider Architecture. Focused beams from base station are bent by ionosphere to land on designated locations. Both friendly and adversary units can be serviced with network communications or electronic warfare (EW) techniques, e.g. jamming.

High SNR plus ultra-wide bandwidth results in high-speed links (>10 Mbps). This speed significantly exceeds the current HF data link capabilities, which are typically 9.6 kbps. Ground stations in Hawaii, Guam, and California could service most of the Pacific Ocean. Frequency reuse is possible due to the separate beams. This defeats adversary jamming and electronic surveillance and enables the electronic counter-surveillance of adversaries.

1.5 Key Technology Factors:

1. Can the ionosphere support the bandwidth required? On a given day, what is the amount of frequency and bandwidth that will follow a path from the ground station to the mobile user and from the mobile user back to the ground station? This dissertation will show how frequency changes affect the degree of refraction and, therefore, where the ray returns to the surface. Rays of frequencies that do not “land” at the receiver’s location will not be detected. By rejecting rays that land short or long, the bandwidth of rays that will work is the bandwidth for that daytime and ionospheric conditions. Bandwidth drives the information rate. The bandwidth of the ionosphere must be wide enough to carry high data rate signals. We have picked 3 MHz as a base to determine parameters for modulation schemes, etc. However, the data shows that most of the time the bandwidth is more than 3MHz.

2. To take advantage of the bandwidth available, can an aperture (antenna) be designed that generates the radiation pattern needed to project the electromagnetic field at the required power, azimuth, and elevation to allow high-speed data flow? Can the radiation pattern (beam) be adjusted quickly enough to adapt to a changing ionosphere to target a specific mobile user? Additionally, can the beam move quickly enough to time share service between multiple users?

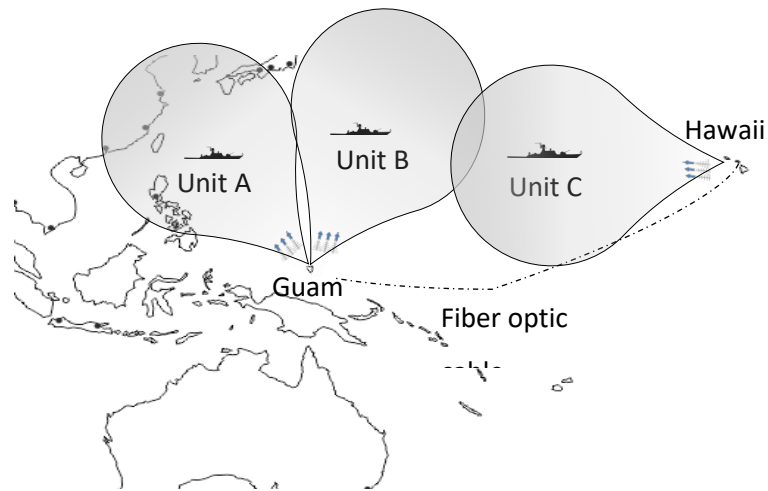


Figure 4. With ground stations in Guam, Hawaii and California, the Pacific is connected from the USA to China. Unit A, B and C can communicate with each other via the base stations in Guam and Hawaii.

3. This system requires the receiver to provide feedback to the transmitter on the quality of the signal. The feedback will enable the system to adjust in real-time and maintain a high-speed link. The system will divide the available spectrum bandwidth into subchannels. Orthogonal Frequency Division Multiplex (OFDM) is state of the art for high-speed communication in multipath channels. It efficiently divides a wide bandwidth frequency allocation into numerous subchannels. The subchannels are spaced orthogonally so that the sidebands cancel out. This enables the subchannels to be placed closer together. This frequency compression allows more parallel channels within a given bandwidth. Each subchannel will carry a different data stream. With feedback from the receiver, the transmitter can change modulation on the subchannels and use the best channels for data transmission.

1.6 Another Advantage of Virtual SATCOM, Low Probability of Detection

One tactical disadvantage of current HF skywave communications is adversary detection and localization of HF emissions. It is common for adversaries to establish Signals Intelligence (SIGINT) sites that attempt to exploit HF communications. If the adversary can determine a line of bearing of a target signal from a few locations, the intersection of the lines of bearing can be used to localize the target's positions. The advantage of the systems proposed in this dissertation is the ability to reduce the mobile unit's transmission signal power to reduce the probability of detection.

The 20-dBi gain of the base station has an 18-dB advantage over an omnidirectional antenna. Therefore, the mobile transmitter can reduce transmitted power by 20 dB from the typical communication link between omnidirectional antennas. For example, if a 1000-watt (30 dBW) transmitter is needed for omni to omni antenna configurations the 20 dB reduction results in a 10 dBW transmission or 10 watts. A 20-dB reduction in transmitted power even from an omnidirectional antenna, would significantly reduce the probability of detection. If the mobile platform employed a directional antenna, for example, a log-periodic dipole with 6 dB of gain, the mobile transmission would be even more challenging to detect by an adversary. When two or more mobile platforms want to link together, they can all transmit at minimal power to allow detection by the high gain ground station. The ground station will rebroadcast the signal back to all units in the network using high power and a high gain antenna. Though the adversary may detect the ground station transmission, the probability of detection of the mobile platform is significantly reduced.

1.7 Another Advantage of Virtual SATCOM, Electronic Scanning to Service Multiple Platforms

An antenna with 20 dBi of gain in the HF frequency range is massive. Using the AN/TPS-71 ROTHAR radar as a test platform, we see that the system is a bistatic system with separate receive and transmit antenna arrays. In the literature, this is commonly called quasi-monostatic since the distance between transmitter and receiver (about 100 km) is small relative to the range to the target (>2000 km). The TPS-71 receiver is a linear array of 372 vertical twin monopoles. It has a total length of 2.6 km (1.6 miles). The transmitter, at another location, is a two-band linear array of 16 vertical log periodic antennas for each band, a total of 32 antennas. This transmit/receive system is too large for mobile systems but is reasonable as the antenna system at ground stations that can service multiple mobile platforms. To maintain connectivity with numerous mobile platforms with directional beams requires the ability to move the beam steering from platform to platform. TPS-71 is a radar system that scans or moves the transmit and receive beam to put the transmitted sign energy where it is needed. Due to the size, mechanical scanning is not practical, so phased steering is required to steer the beam.

The Virtual SATCOM system can perform numerous missions. The primary objective of this system is command and control (C2), i.e., connecting units in an information-sharing network. The system can support other missions — for example, Electronic Warfare against an adversary system. Electronic Warfare i.e., jamming is denying the use of the electromagnetic spectrum to the adversary while assuring friendly use. Due to the spatial segregation of the beams, the base stations' high-power transmitter and high gain antenna can direct jamming energy onto adversaries while communicating.

1.8 The Vulnerability of the SATCOM System Architecture

A typical SATCOM system has three pieces: 1) the ground station that acts as a gateway to internets and controls the satellite, 2) the mobile terminal that is usually a mobile platform like a ship or aircraft, and 3) the satellite vehicle that acts as a high-altitude relay or transponder that receives uplink signals on one frequency and retransmits as a downlink signal on another frequency. Satellites use frequencies above the HF band that do not bend appreciably as they pass through the ionosphere. The high altitude of the space vehicle enables the satellite to see both the uplink and downlink transceivers.

1.9 Threats to Satellite Communications

Potential adversaries see satellite systems as crucial vulnerabilities. For example, China is focusing on counter-space, offensive cyber operations, and electronic warfare (EW) capabilities meant to deny their adversaries the advantages of modern information-driven systems.

China's People's Liberation Army (PLA) is acquiring a range of technologies to improve China's counter-space capabilities. In addition to the development of directed energy weapons and satellite jammers, China is also developing anti-satellite skills and has undoubtedly made progress on the anti-satellite missile system it tested in July 2014. In the summer of 2014, China conducted a space launch that had a similar profile to the January 2007 test [5]. China's state-run news agency, Xinhua, reported on July 24, 2014 that the military had announced a successful missile intercept test. According to Xinhua, China's Ministry of National Defense stated on its website that the test "achieved the preset goal." In 2013, China launched an object into space on a ballistic trajectory with a peak altitude above 30,000 km, which could have been a test of technologies with a counter-space mission against geosynchronous orbit. According to a 2013 press release from the Chinese Academy of the Sciences' National Space Science Center, the sounding rocket was launched from Xichang Satellite Launch Center and carried payloads for studying the high-energy particles in the upper atmosphere and near-Earth space.

"The launch appeared to be on a ballistic trajectory nearly to geosynchronous Earth orbit," Pentagon spokeswoman Lt. Col. Monica Matoush wrote in an email to SpaceNews on May 16, 2013 [6].

The launch profile was not consistent with traditional space-launch vehicles, ballistic missiles, or sounding rocket launches used for scientific research, the report stated.

PLA strategists regard the ability to use space-based systems—and to deny them to adversaries—as central to enabling modern informationized warfare. Although PLA doctrine does not appear to address space operations as a unique operational “campaign,” space operations will likely form an integral component of other PLA campaigns as well as serve a key role in enabling actions that counter third-party intervention.

1.10 High Cost as a Vulnerability

In addition to vulnerability, space systems are expensive. For example, the cost of the US Navy’s MUOS is \$7 billion for five satellites [7]. Space systems require costly components to operate in the harsh space environment. Since repairs cannot be accomplished once a system is launched, the manufacturing costs are high to build in reliability. The launch costs are also expensive and carry several risks.

1.11 Technological Capability to Modernize as a Vulnerability

The long development timeline and the inability to upgrade space vehicles after launch is a technological vulnerability. For example, the MUOS satellite system, the newest SATCOM system launched in 2012, incorporates a 3rd generation communication technique called wideband code division multiple access (WCDMA) [8]. Though this is an upgrade to the existing (ancient) systems, it is already behind the times. In 2020, state of the art in cellular communications is 4th generation with 5th generation being deployed. A terrestrial-based system with 3G technology can migrate to 4th generation OFDM systems, but MUOS will likely still be using a 3rd generation technology when 6th or 7th generation systems are standard.

1.12 Capacity Limit

Capacity is another weakness of a satellite system. The concept of Data Fusion is the process of integrating multiple data sources to produce more consistent, accurate, and useful information than any single data source. If the communications path is limited, the ability of the sensors is reduced resulting in lower confidence in the fusion analysis. The proliferation of autonomous systems that operate beyond the horizon has demanding communication requirements. To rely only on satellite systems to relay sensor data is likely a single point vulnerability. The Navy’s vision of robust networks where every sensor is connected to every “shooter” requires numerous information channels. Satellite channels may not meet this requirement in a wartime setting.

1.13 Information Theory and Link Budget

Within Information Theory [9], the Shannon–Hartley theorem (equation 1) shows the maximum rate at which information can be transported over a communications channel with a given bandwidth in the presence of noise. Bandwidth and SNR are the limiting parameters. Theoretical channel capacity (C) [bps] is a function of the bandwidth (B) in Hz, noise power (N_o) in W/Hz, and power at the receiver (P_r) in W.

$$C = B \log_2(1 + SNR) \quad (1)$$

where

$$SNR = \frac{P_r}{BN_o}$$

The Friis transmission equation (equation 2) sometimes called the link budget, models the power at the receiver. The equation is presented in numerous publications including: [10], [11], [12], and [13]. The power at the receiver is a function of the power transmitted (P_t) in watts; gain of the antenna at the transmitter and receiver (G_t and G_r) in dBi; wavelength (λ) of the signal in meters; and range (R) between the transmitter and receiver in meters.

$$\frac{P_r}{P_t} = G_t G_r \left(\frac{\lambda}{4\pi R} \right)^2 \quad (2)$$

Converting to decibels (dB), where P_L is the free space path loss:

$$P_{r,dB} = P_{t,dB} + G_{t,dB} + G_{r,dB} - P_L$$

$$P_{L,dB} = 20 \log \left(\frac{4\pi R}{\lambda} \right)$$

For example, if B is 3 MHz and signal to noise (SNR) is 15 times (or ~12 dB) the noise power, then the channel capacity is $C = 12$ Mbps. However, if bandwidth, B , is 3 kHz, the capacity is only 12 kbps. As bandwidth increases, SNR decreases, so P_r must be increased to maintain the same SNR. Virtual SATCOM needs +42 dB of P_r increase to account for the increased bandwidth (30 dB of bandwidth and 12 dB of SNR). Virtual SATCOM must increase P_t and G_t to meet the desired SNR. The Virtual SATCON base station design produces a base station gain (G_t) of +20 dBi and a base station power of (P_t) of 200 kW which is 23 dB over a 1 kW transmitter.

An ultra-wide bandwidth (3 MHz) signal transmitted from a typical omnidirectional communication antenna would interfere with many other users of the spectrum. In practice, the two ways to share the spectrum are to lower the transmitted power significantly or to separate the wideband channel from other users spatially. Lowering the power will reduce the SNR, so our design proposes a high gain antenna to focus the energy into a spatially narrow 1° beam and thus reduce the energy on other users of the same spectrum. From the ground station to the mobile, we use a high power very narrow beam to avoid interference with other users.

Table 1. Data Rate Analysis for Various Scenarios

Scenario	Freq [MHz]	C [Mbps]	E_b/N_0 [dB]	SNR [dB]	B [Hz]	N_0 [W/Hz]	P_r [dBW]	P_t [W]	P_t [dBW]	G_t [dBi]	G_r [dBi]	P_L [dBW]	λ [m]	Range [m]	L [dB]
Operator input	x				x	x		x		x	x			x	x
Forward link	7	28.267	18.62	28.36	3E+06	1.0E-14	-46.87	200000	53	20	2	118.88	42.86	3E+06	3
	14	22.286	13.63	22.34	3E+06	1.0E-14	-52.89	200000	53	20	2	124.90	21.43	3E+06	3
	21	18.807	13.63	18.81	3E+06	1.0E-14	-56.41	200000	53	20	2	128.42	14.29	3E+06	3
	28	16.360	8.95	16.32	3E+06	1.0E-14	-58.91	200000	53	20	2	130.92	10.71	3E+06	3
Forward link	7	11.006	22.71	33.13	1E+06	1.0E-14	-46.87	200000	53	20	2	118.88	42.86	3E+06	3
Low bandwidth	14	9.008	17.56	27.11	1E+06	1.0E-14	-52.89	200000	53	20	2	124.90	21.43	3E+06	3
BW=1 MHz	21	7.841	17.56	23.59	1E+06	1.0E-14	-56.41	200000	53	20	2	128.42	14.29	3E+06	3
	28	7.016	12.63	21.09	1E+06	1.0E-14	-58.91	200000	53	20	2	130.92	10.71	3E+06	3
Forward link	7	22.306	13.64	22.36	3E+06	1.0E-14	-52.87	200000	53	14	2	118.88	42.86	3E+06	3
Low Gain	14	16.281	8.99	16.34	3E+06	1.0E-14	-58.89	200000	53	14	2	124.90	21.43	3E+06	3
Gt=14 dBi	21	12.771	8.99	12.81	3E+06	1.0E-14	-62.41	200000	53	14	2	128.42	14.29	3E+06	3
	28	10.666	4.81	10.32	3E+06	1.0E-14	-64.91	200000	53	14	2	130.92	10.71	3E+06	3
Forward link	7	25.283	16.10	25.36	3E+06	1.0E-14	-49.87	200000	53	20	2	118.88	42.86	3E+06	6
	14	19.321	11.25	19.34	3E+06	1.0E-14	-55.89	200000	53	20	2	124.90	21.43	3E+06	6
	21	15.873	11.25	15.81	3E+06	1.0E-14	-59.41	200000	53	20	2	128.42	14.29	3E+06	6
High RX/TX losses	28	13.468	6.79	13.32	3E+06	1.0E-14	-61.91	200000	53	20	2	130.92	10.71	3E+06	6
Forward Link Average	17.500	16.035	12.944	20.40	3E+06	1.0E-14	-56.02	200000	53	18.50	2	125.78	22.32	3E+06	3.75
Scenario	Freq [MHz]	C [Mbps]	E_b/N_0 [dB]	SNR [dB]	B [Hz]	N_0 [W/Hz]	P_r [dBW]	P_t [W]	P_t [dBW]	G_t [dBi]	G_r [dBi]	P_L [dBW]	λ [m]	Range [m]	L [dB]
Back link	7	4.745	7.36	14.12	1E+06	1.0E-15	-75.88	100	20	6	20	118.88	42.86	3E+06	3
Reduced Noise	14	2.898	3.48	8.10	1E+06	1.0E-15	-81.90	100	20	6	20	124.90	21.43	3E+06	3
BW=1 MHz	21	1.952	1.67	4.58	1E+06	1.0E-15	-85.42	100	20	6	20	128.42	14.29	3E+06	3
Tx=100W, 6 dBi	28	1.386	0.66	2.08	1E+06	1.0E-15	-87.92	100	20	6	20	130.92	10.71	3E+06	3
Back Link Average	17.500	2.745	3.291	7.22	1E+06	1.0E-15	-82.783	100	20	6	20	125.78	22.32	3E+06	3
Ship to ship	7	2.227	1.47	5.66	1E+06	1.0E-15	-84.34	100	20	6	2	109.34	42.86	1E+06	3
	14	0.941	1.47	-0.36	1E+06	1.0E-15	-90.36	100	20	6	2	115.36	21.43	1E+06	3
Range=1000km	21	0.495	1.47	-3.88	1E+06	1.0E-15	-93.88	100	20	6	2	118.88	14.29	1E+06	3
Tx=100W, 6 dBi	28	0.299	1.47	-6.38	1E+06	1.0E-15	-96.38	100	20	6	2	121.38	10.71	1E+06	3
Ship to Ship Average	17.500	0.991	1.47	-1.24	1E+06	1.0E-15	-91.24	100	20	6	2	116.24	22.32	1E+06	3

1.14 Virtual SATCOM Forward Link Analysis

Table 1 lists the channel capacity for six different scenarios varying one of the input parameters. The range is 3,000 km for all situations except ship to ship which is set to 1000 km. The reason for the

reduced range for the ship to ship is that the data rate was very low at 3000 km and judged not to be a viable scenario. The power of the Tx and gain of Tx antenna are based on similar over the horizon radar systems, e.g., AN/TPS-71. Noise power was derived from studies of various ionosphere conditions [14] [15] [16] [17] [18] and [19]. The 3 MHz bandwidth was a tradeoff between the bandwidth required to enable high data rate, but it was not so wide that signal to noise ratio reduction significantly affects data throughput. The frequency range (7-28 MHz) was based on the availability of the ionosphere discovered through our modeling of the ionosphere and the physical size of the antenna. Frequencies below 7 MHz will significantly increase the size of each antenna element and require additional elements to meet the narrow beamwidth requirements. The table shows that lower frequencies (7 MHz) experience less propagation loss. Our analysis starts with a two dBi dipole mobile antenna for reception and six dBi gain for the mobile unit transmitter. All scenarios experience better throughput at the lower end of the frequency range due to reduced free space path loss.

The forward link data rate is the most important. The system is designed to connect mobile to mobile customers and connect mobile users to the sizeable amounts of shore to ship information products. This includes significant amounts of ISR (intelligence, surveillance and reconnaissance) data. Other high data documents are air tasking orders (ATO), which is a large file that needs to be relayed to all ships to ensure mobile units do not inadvertently attack friendly aircraft with anti-air weapon systems.

The forward link from the ground station to the mobile unit is presented in the first four scenarios. The first scenario is the expected normal mode and results in a minimum of 16 Mbps data rate. The inputs to this run include a 200 kW transmitter at a bandwidth of 3 MHz and a range of 3000 km. Noise spectral density was input at -140 dBW/Hz. This noise density level is a conservative estimate, 25 dB above most of the literature [20]. Also added was a -3dB attenuation loss to account for absorption in the D and E layers. For antenna gain, two dBi was used for the mobile receiver and six dBi for the mobile transmitter. The ground station antenna gain is 20 dBi.

In scenario two, the bandwidth is reduced to 1 MHz, and the average data rate is 9 Mbps, just under the design goal of 10 Mbps. However, if the lower frequencies around 7 MHz are available, the data rate is above the 10 Mbps level.

In the third scenario, the gain of the ground station antenna array is reduced to 14 dBi, and the data rate is above 10 Mbps at all frequencies. In the fourth scenario, the absorption loss was increased to 6 dB, and this still resulted in data rates above 10 Mbps at all frequencies. The average data rate for all four scenarios across the 7-28 MHz frequency range is 16.77 Mbps which exceeds the 10 Mbps design goal.

1.15 Virtual SATCOM Back Link Analysis

The backlink from the mobile unit to the base station does not have the same high data throughput. The driving factor for this is a reduction in transmitter power. To provide a low probability of detection, the mobile unit's power has been reduced to 100 W. This is a 33 dB reduction compared to the forward link. In the transmit mode, the mobile will employ a steerable, horizontal log periodic dipole antenna. This antenna will have a minimum of 6 dB of gain with low sidelobes off-boresight. For example, the Alaris RPL-10-30 [21] has a gain of 9 dBi and operates in the 10-30 MHz range. It has an 8-meter beam length and could be installed on top of a ship's mast with some thorough engineering. It meets MILSTD-810 environmental standards. In the backlink scenario, the noise power was reduced to -150dBW/Hz and bandwidth was reduced to 1 MHz. The average data rate is 3 Mbps and would be adequate data offload from a mobile maritime platform. When lower detection probability is required, the mobile unit can reduce power to 10 W.

The final scenario is provided as a reference point to show the advantage of using the ground station as a relay. Here the transmitting unit employs a directional antenna with six dBi of gain to another unit's omnidirectional antenna. The range has been reduced to 1000 km to minimize the free space path loss. Even at this much closer range, the data rate is half the rate when using the ground-based relay station. In other words, if two ships are 1000 km apart, they will see twice the data rate if they relay the information through the relay station that is 3000 km away from both units.

The Virtual SATCOM ultra-wide bandwidth signal uses a 1000 time larger bandwidth compared to current (3 kHz) narrow-band modulations and results in a much higher information rate. An advantage of the low power mobile Tx is that an adversary's HF Direction Finding (HFDF) and Signals Intelligence (SIGINT) capability is reduced because the power of the signal is reduced in the direction of the HFDF and SIGINT systems. Another tactic is to use the high power directional base station as a jammer against adversary HFDF, SIGINT and over the horizon radar equipment to cover friendly communications; note, the jamming will not affect the connections, so simultaneous jamming and communications on the same frequency are possible because of the directional beam.

1.16 Comparison of SATCOM to Virtual SATCOM

Table 2. Comparison of Data Rate between Satellite and HF Link

<p>Example 1 SATCOM Geostationary orbit at 36000km; Range =36e6 m; Power of transmitter (P_t)=20W =13 dBW; Gain of satellite antenna= 33dBi Frequency (F_c) = 4 GHz Wavelength (λ) = .075 m; Free Space Pass loss =P_L</p> $P_L = 20\text{Log}_{10}\left(\frac{4\pi R}{\lambda}\right)$ $P_L = 20\text{Log}_{10}\left(\frac{4\pi 36e6}{.075}\right) = 195.6\text{dB}$ $P_{r\text{ dB}} = P_t + G_t - P_L = 13 + 33 - 195.6 = -149.6\text{ dBW}$ <p>Calculating the energy per bit:</p> $\frac{E_b}{N_o} = \frac{P_r T_b}{N_o} = \frac{P_r}{N_o R_b} \rightarrow \text{SNR} = \frac{P_r}{N_o} = R_b \left(\frac{E_b}{N_o} \right)$ $R_b = \frac{\left(\frac{P_r}{N_o} \right)}{\left(\frac{E_b}{N_o} \right)} \rightarrow 10\text{Log}(R_b) = \left(\frac{P_r}{N_o} \right)_{\text{dB}} - \left(\frac{E_b}{N_o} \right)_{\text{dB}}$ <p>Assume noise lvl (N_o) at 4 GHz =-204 dBW/Hz</p> $\left(\frac{P_r}{N_o} \right)_{\text{dB}} = -149.6 - (-204) = 54.4\text{ dB/Hz}$ <p>Assuming systems need 10 dB of E_b/N_o then:</p> $\left(\frac{E_b}{N_o} \right)_{\text{dB}} = 10\text{ dB}$ $10\text{Log}(R_b) = 54.4 - 10 = 44.4_{\text{dB}}$ <p><u>Bit rate = $10^{4.44}$ = 27.5 kbps</u></p>	<p>Example 2 Virtual SATCOM HF Link; R=3000km =3e6 m, Power of TX (P_t) =200 kW=53dBW, Gain of TX=20 dBi F_c=15 MHz; Wavelength (λ) = 20 m; Free Space Pass loss = P_L</p> $P_L = 20\text{Log}_{10}\left(\frac{4\pi R}{\lambda}\right)$ $P_L = 20\text{Log}_{10}\left(\frac{4\pi 3e6}{20}\right) = 125.5\text{dB}$ $P_{r\text{ dB}} = P_t + G_t - P_L = 53 + 20 - 125.5 = -52.5\text{ dBW}$ <div style="border: 1px solid black; padding: 5px; margin: 10px 0;"> <p>Because of the shorter path and longer wavelength, the Virtual SATCOM is 97 dBW more powerful at the receiver.</p> </div> <p>Where: E_b= Energy per bit= $P_r * T_b$ [Ws] N_o= noise power; [W/Hz] T_b=time per bit; [s] P_r= power at receiver =$R_b * E_b$ [W] R_b= bit rate = $1/T_b$ [s^{-1}] SNR = signal to noise ratio</p> <p>Assume noise lvl (N_o) at 15 MHz = -140 dBW/Hz</p> $\left(\frac{P_r}{N_o} \right)_{\text{dB}} = -52.5 - (-140.0) = 87.5\text{ dB/Hz}$ $\left(\frac{E_b}{N_o} \right)_{\text{dB}} = 10\text{ dB}$ $10\text{Log}(R_b) = 87.5 - 10 = 77.5_{\text{dB}}$ <p><u>Bit rate = $10^{7.75}$ = 56.23 Mbps</u></p>
<p>HF Virtual SATCOM link has two thousand times the data rate of the SATCOM link.</p>	

Table 2 is a comparison of SATCOM and Virtual SATCOM links assuming typical power, antenna gain, and frequency of the systems. Satellites must produce their power with solar energy so 20 watts is a reasonable transmitter output. Modern satellites use high gain antennas to compensate for the lower transmitter output [22]. The 33 dBi estimate used here is a generous gain estimate.

The Virtual SATCOM system has a significant bit rate due to a couple of factors. The Virtual system's signal distance is 12 times less, and the wavelength is 267 times greater than the satellite system. These two inputs drive down the free space path loss. Even though the Virtual system's noise level is much higher, the power and range advantage can move data faster. Some SATCOM systems operate at higher frequencies in the Ku and Ka bands with high gain antennas, but the higher frequency increases the free space path loss. Generally, all geosynchronous satellite systems face the same limitations in range and power. The long-distance to the geosynchronous orbiting vehicle and the limited power of the solar-powered transmitter limit the data rate. The advantage the satellite does have is the bandwidth available in the higher frequency bands. To compete with SATCOM, Virtual SATCOM needs additional bandwidth. Frequency reuse is the solution.

1.7 Bandwidth Policy Limitations

The propagation advantage of the HF spectrum for BLOS communications has been exploited since the 1920s. Early users of the spectrum employed a wireless telegraph type service using Morse code on narrowband CW transmitters. First broadcast services operated AM, FM and single sideband (SSB) signal modulations. Today, typical SSB analog voice communication is allocated a 3-kHz of bandwidth. Though each country manages the spectrum within its borders, the International Telecommunication Union (ITU) [23], an agency of the United Nations, assists in the management for signals that will cross borders. The ITU allocates global radio spectrum and develops the technical standards that ensure networks and technologies seamlessly interconnect without interference. The HF propagation channel travels thousands of kilometers, and many customers use a narrow band architecture within the HF band. This frequency allocation process is rigid and slow to change. It is out of date considering the capabilities of emerging HF techniques. The current stringent allocation process is not efficient in managing the use of the dynamics of the ionosphere. For example, if the frequency allocated is not optimum for the current ionosphere the signal may not reach the receiver. A more dynamic frequency allocation system will allow systems to find the optimum channel conditions.

Additionally, the narrow bandwidth limits the data speed of the system. The current ITU and FCC policies for HF frequency allocations have not changed to accommodate the requirement to operate at high data rates. The ITU/FCC perspective is that frequency allocation and bandwidth restrictions do prevent interference between users. The Virtual SATCOM solution to interference is directional channels

that connect customers through directional beams that deliver reliable signal power and bandwidth for high data rate transmissions. Our solution allows frequency reuse of the optimum frequencies on any given day.

1.18 Prior Research and Current Standards for Wideband HF Systems

There is abundant research on the various pieces required for this concept. Reference [24] is a model for OTH radar performance, much like a program called Provision of High-frequency Raytracing Laboratory for Propagation (PHaRLAP) model that was used in this work. The PHaRLAP model was designed for radar operations, but we have modified the program for our communications system. HF communications have been well researched since Marconi's experiments in 1901. In 1955 and 1963, Dr. J. Haselgrove [25] and [26] developed a ray tracing mathematics based on Hamiltonian equations that predicts the HF ray path through the anisotropic ionosphere. Her work was incorporated into the PHaRLAP program developed by Dr. Cervera [14] and others to predict radar performance for the Australian Department of Defence.

The Virtual SATCOM system requires wide bandwidths up to 3 MHz. The US Air Force has studied 3 MHz bandwidths as presented in [27]. They developed a technique to measure the transfer function of the ray path and correcting for it in real-time. Their testing up to a bandwidth of 3 MHz shows that the correlation technique is feasible, and the correction is valid for several seconds. In [28] Fabrizio discusses an experiment using four different adaptive beamforming techniques for OTHR. The paper reports success was operating in a bistatic mode. Though this is a radar system, logically, HF communications systems can apply similar adaptive beamforming signal processing to improve the reliability of data transmission.

Many countries operate OTHR systems, including Australia, China, France, Iran, Russia, and the United States [29]. These systems employ large land-based antennas to focus the beam in the area to be searched. The beam is electronically steered in azimuth to search within the designated area. Typically, the receiver and transmitter are separated by approximately 100 km to prevent short-range clutter affecting the system. The operators use knowledge of the channel conditions gained from ionosonde to know the optimum frequencies to reach the desired search range. The systems typically transmit at a bandwidth of 100 kHz. The systems are frequency agile to adjust frequency to move the beam and adapt to the changing ionospheric conditions. The frequency allocation is contingent on the radar system using real-time knowledge of the spectrum and agility to avoid interfering with other users of the spectrum. In the case of the US AN/TPS-71, OTHR systems in Texas, Virginia, and Puerto Rico, the systems beams are used to search areas that are mainly over water and are less likely to interfere with other users.

There are many articles on the use of electronically steerable directional antenna systems for radars [3] [29] [28], but very few address the system's application to communication systems. Somewhat unique are radar designs that operate at HF frequencies. At these frequencies, the beamforming task requires many elements that are spaced 10-20 meters apart. This results in a considerable array, on the order of a few kilometers. The United States, Australia, China, Russia and France are a few of the countries that operate OTHR systems in the HF frequency range.

There is published research on wideband HF communications [13] [30] [31], and the US military has adopted a wideband frequency modulation (MILSTD-188-110D) called WBHF, but the maximum bandwidth is 48 kHz. Our system uses a 3 MHz channel, which is 62 times larger than WBHF and 1,000 times the bandwidth of a standard 3 kHz HF communications channel.

Our research is unique in that we are combining the requirement for a large electronic steerable array across an ultra-wideband frequency bandwidth. In Information Theory, bandwidth and SNR are the variables that limit information speed. Our approach includes a directive aperture to increase SNR across an ultra-wideband signal.

1.19 Review of Current HF Communication Capabilities

The HF spectrum (2-30 MHz) is allocated to many users and is divided into many narrow bandwidth slices. Today, data is sent to support a wide variety of applications, including chat, email, situation awareness, file transfer, and network information exchange. Many applications require error-free data and utilize a reliable acknowledged (ARQ) based data link to ensure proper transfer of the data. STANAGs are standards developed by NATO that define processes, procedures, terms, and conditions for common military or technical procedures or equipment between the member countries of the alliance. The most popular standards are STANAG 5066 and STANAG 4538 which send error-free data and adapt to channel conditions. In [32] Johnson provides an overview of military HF communication standards.

STANAG 5066 has become the choice of many military organizations for data communications. The building blocks of the STANAG 5066 system is a computer connected to a wired network (Ethernet). Data intended for transmission is passed through a crypto device and then to a modem that converts the data to analog signals (ones and zeros) that are sent to the radio for transmission. The STANAG 5066 systems is a computer linked to a wired network, a modem, crypto gear, and a radio with automatic link capability.

A modern HF system should have an HF management system that can include Automatic Link Establishment (ALE) features. ALE features adjust the frequencies to maintain connectivity as the propagation path changes. Mil-STD-188-141 is a series of military standards that define how this data link layer will operate.

Typically, ALE systems have a list or table of frequencies. The transmitter and receiver cycle through those frequencies to find a frequency with the best propagation channel. If the channel is lost, the system will search, acquire, and reconnect on a new frequency. MIL-STD-188-110D [33] is a set of standards that define the modem's output. For example:

- Appendix A describes the requirements for an optional local area network (LAN) interface for radio data modems.
- Appendix B describes a 39-tone parallel mode
- Appendix C describes the HF waveform for data rates above 2400 bps in 3 kHz channels. These may be termed narrowband, medium data rate (MDR) waveforms.
- Appendix D describes the HF data modem waveforms for use with single contiguous bandwidths from 3 kHz to 48 kHz.

Only MILSTD 188-110D, Appendix D standards present HF modulations that appreciably increase the data speed on an HF network. However, the higher data rate modulations employ very high symbol speed and noise-sensitive modulation. These parameters will likely fail in long-range BLOS HF scenarios due to multipath interference and HF environmental noise. In Chapter 4, this dissertation presents a better way to modulate the wideband signal that results in a higher data rate and improved BER.

1.20 Virtual SATCOM Ground Station Design

Figure 5 and Figure 6 present the Virtual SATCOM Systems Diagram and Functional Diagrams. The system is composed of six parts. The Environment Monitoring Station (EMS) will assist the Systems Control Room in evaluating the ionosphere and help mobile units join the Virtual SATCOM system. The System Control Room (SCR) is the central control station for the entire system controlling what information systems (application) are connected to which mobile units. The Array Control Room (ACR) will control the beam steering input to the Element Control Units (ECU). The ECU will convert the digital signal from SCR into an RF signal for the LPDA antenna array. There is one ECU for every antenna element, 200 in total.

Virtual SATCOM Systems Diagram

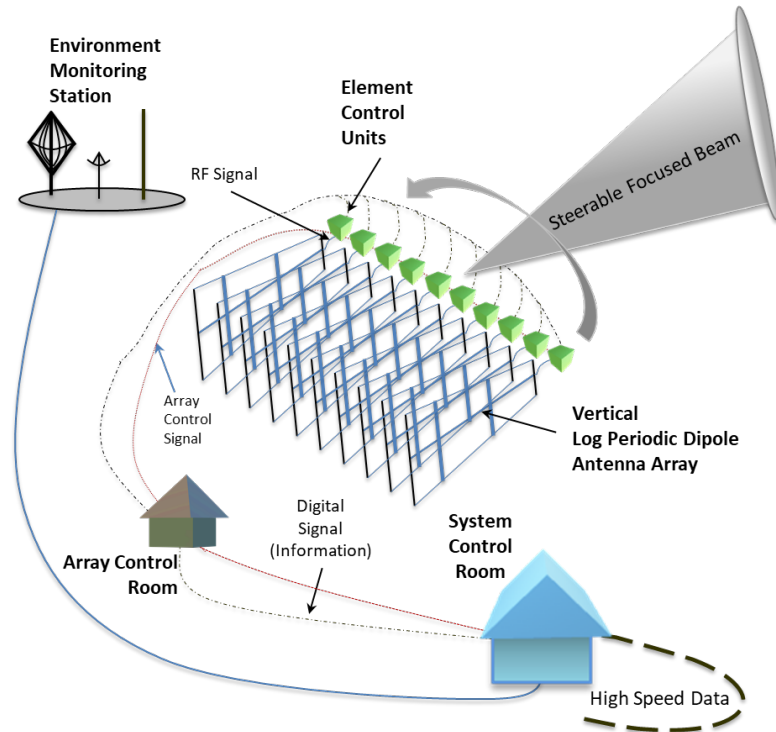


Figure 5. Virtual SATCOM Diagram.

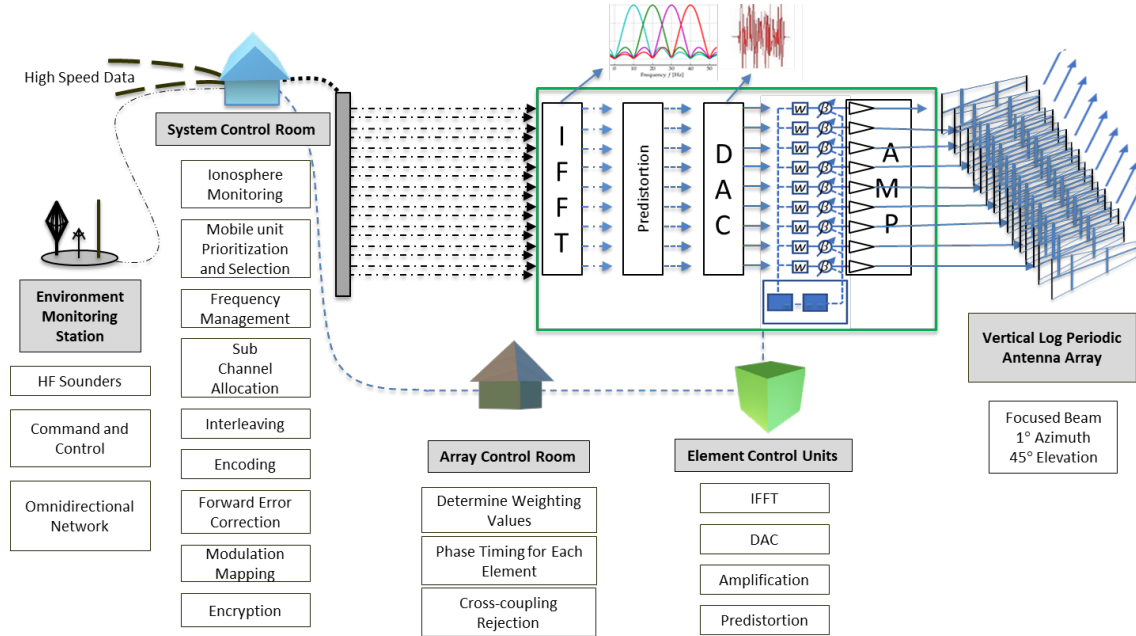
1.21 Environment Monitoring Station

The first purpose of the EMS is to provide a real-time picture of the ionosphere for the entire operational theater. The second purpose is an omnidirectional narrow band low data rate command and control link with mobile units to coordinate inclusion in the Virtual SATCOM network. This EMS will have a series of vertical and oblique sounders to see the environment. In the 1950s and 1960s, Naval ships had an onboard system called a chirp sounder. A chirp sounder [34] is a system of transmitters at ground sites and receivers on mobile units. Only the frequencies that can propagate will be received. The transmitted signal is scanned across the entire band (7-28 MHz). The frequencies received by the ship will inform them what frequencies will operate. There are modulation and techniques outside of military systems that can work at very low power range of millivolts. One method is called the Weak Signal Propagation Reporting (WSPR) system. Though the amateur radio community uses the WSPR system, the software is open source and the DoD could use the system on DoD authorized frequencies.

The ship will need to communicate with the Virtual SATCOM their position and the best-operating frequencies before joining the network. In Chapter 4, we present a narrow band, the low power

system with a low probability of detection by adversaries. The EMS will coordinate the initial command and control required to initiate the connection via an omnidirectional antenna system.

Figure 6. Virtual SATCOM Functional Diagram.



1.22 Signal Control Room

The Signal Control Room (SCR) is the central control location for the system. The SCR will take input from EMC to determine which units want to join the network and what are the best frequencies to communicate. The SCR will prioritize mobile units and allocate frequencies to be used for each unit. The frequency allocation will include what information systems i.e. email, chat, etc. and the amount of data that needs to be transmitted. In Chapter 4, this dissertation shows how the system will allocate applications to data blocks for transmission. Data blocks are 161 kHz frequency blocks that include two 24 kHz and two 48 kHz MILSTD 188-110D modulations. The advantage of the MILSTD modulation is that the interleaving, forward error correction and modulation type i.e. QPSK, 16 QAM has been determined. Within each data block are monitoring, and command and control signals to monitor the bit error rate and then adjust and control the modulation path as required. An innovation that this dissertation presents is the use of an OFDM technique in the MILSTD188-110D standard. We are using MILSTD188-110 3 kHz modulations compressed into 48 and 24 kHz bandwidths. Virtual SATCOM's design advantage is the flexibility to adjust the beam, the frequency, the bandwidth, and the power, in real-time. Therefore, during periods when the available spectrum is limited, the SCR can adjust to ensure efficient use of the bandwidth available.

1.23 Array Control Room

The Array Control Room (ACR) performs the function of controlling the antenna array steering. It is an automated control room that calculates the weighting and phase shift for each antenna. Virtual SATCOM utilizes smart antenna processing, which means it uses adaptive digital processing to adjust the weighting and phase to properly steer the antenna in the desired direction keeping the beamwidth as narrow as required to avoid interference with other users of the spectrum. When the ground station is operating as a receiver, the ACR will adjust the weighting to reject interference and jamming from different directions.

1.24 Element Control Unit

The Element Control Units (ECU) primary function is the conversion of the symbol stream from a digital to analog RF signal. In this design, there are 200 ECUs, one for each antenna. The ECU uses an Inverse Fast Fourier Transform to convert digital symbols in the time domain into sub frequencies in the frequency domain. The sub frequencies are converted back into the time domain, depending on the bandwidth set by the SCR. The ECU will apply the weighting and phase shift determined by the ACR. The ECU will amplify the signal and feed it to the antenna element. There is a feedback loop that will ensure that the output of the amplifier matches the intended value output from the IFFT. This function will add a predistortion signal onto the subchannels amplitude to ensure the output signal is correct. This is a vital function to ensure 200 individual antenna elements are in sync to properly steer the beam.

1.25 Vertical Log Periodic Dipole Antenna Array

Each ECU will control one vertically polarized LPDA antenna. The design includes 200 elements with a 10-meter separation between elements. The LPDA antenna is inherently a broadband resonator and the Virtual SATCOM antenna is designed to operate between 7 and 28 MHz at 3 MHz of bandwidth. Narrowband antennas do have the ability to resonate from 7-28 MHz but not across 3 MHz at low VSWR. The 10-meter separation is driven by the half wavelengths of the highest frequency, 28 MHz. The total length needed to enable the generation of a narrow 1° beam is just under 2 km. The antenna array design is a crucial contribution to this work and is further discussed in Chapter 4. Though the LPDA design was chosen due to the broadband feature, it will also contribute to the total directivity of the array. The LPDA vertical orientation will narrow the beam in the elevation direction while the 200-element design will narrow the beam in the azimuth direction. The physical antenna will be a wire antenna meaning the wires will be held up by towers. This is the same configuration as the transmitter antennas of

the TPS-71 ROTH system, but in the Virtual SATCOM design, there is six times the number of antennas (200 vs. 32). Note, the ROTH receiver has over 300 antennas.

The design has flexibility and redundancy. The choice of a 200-element array with an ECU for each antenna will allow numerous configurations. For example, one beam using every fourth antenna operating at 7 MHz could be paired with two beams at 14 MHz using 150 antennas leaving 50 antennas remaining. The beamwidth will be larger, but the operational tempo may require more beams and broader beamwidths.

As stated, the strategic advantage of a Virtual SATCOM system is relaying via a ground station allowing the mobile user to operate at much less power and gain while receiving high data rate signals. In the next section, the shipboard architecture is presented.

1.26 Virtual SATCOM Mobile Station Design

On top of Figure 7 is the silhouette of a mobile unit. It shows the addition of three new antennas. Two conical monopoles receive antennas, one on the bow and one amidships, and a directional horizontal log periodic antenna on the mast. The directional LPDA antenna is mechanically steerable in azimuth and is horizontally orientated to focus the energy in azimuth. Note: the figure shows the antenna in a vertical orientation to visualize on a 2-D graphic.

1.27 Virtual SATCOM Mobile Receiver

In the normal receive mode, the incoming signal energy will resonate on the conical antennas. Two antennas provide redundancy and may be able to be combined in a MIMO mode. The advantage of the conical antenna is like the log-periodic in the broadband capability. This is important for an antenna that will be receiving over a 3 MHz bandwidth. The conical antenna is not new; 20 years ago, the US Navy had many ships with this type of antenna before SATCOM replaced HF as the principal BLOS signal path. The Dis-cage antenna is one example of a shipboard HF conical antenna.

Virtual SATCOM Mobile System

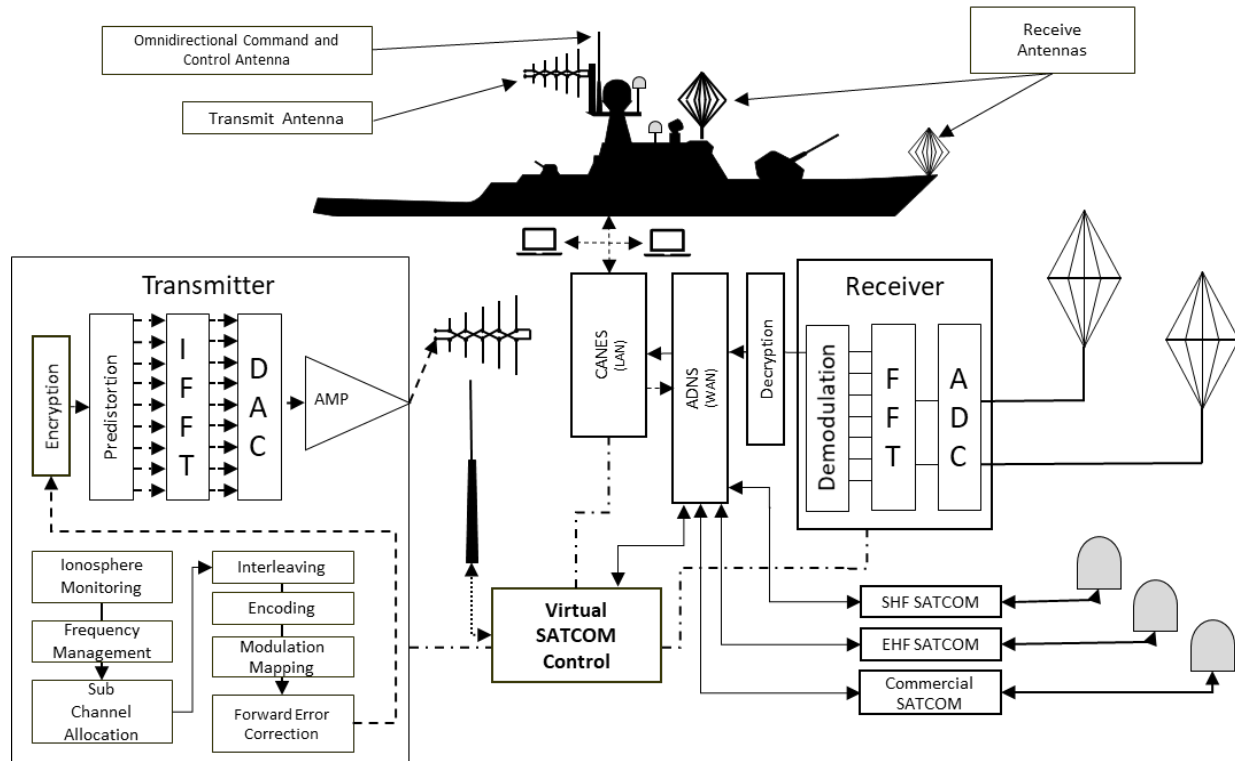


Figure 7. Mobile Unit Antenna Configuration and Functional Diagram.

The ADC will convert the RF signal from the antenna to digital and then apply a Fast Fourier Transform to convert the time domain signal to a multi-frequency OFDM signal for demodulation in a software defined radio. The digital message will be decrypted to remove the encryption applied before transmission. The data flows into the ship's Automatic Digital Network System (ADNS). ADNS uses off the shelf protocols, processors and routers to efficiently connect the ship's digital communication systems to the ship's internal network system called Consolidated Afloat Networks and Enterprise Services (CANES). It is helpful to think of the ADNS as the ship's WAN connecting to other ships and shore sites and CANES as the ship's LAN connecting the workstations to off-ship customers.

When the ship is transmitting, workstations or radios traffic will be routed by the ADNS to the Virtual SATCOM control system. The system will initiate a connection to the Virtual SATCOM system via a low probability of detection, narrow band, weak power signal. The Virtual SATCOM ground station will allocate bandwidth to the unit to begin connection at low bandwidth and then will increase the bandwidth as required once connectivity is established. More detail is provided in Chapter 4. Once connected the appropriate signal processing tasks generate an encrypted digital signal that is converted to

a multichannel frequency domain in the Inverse Fast Fourier Transform (IFFT) and then converted to a time-domain analog signal (DAC) and amplified as required before transmission on the LPDA antenna that has been mechanically steered to that designated ground station.

The advantage of a directional LPDA antenna for transmitting is the ability to increase gain in one direction while decreasing gain in another. For example, a ship in the western Pacific Ocean can point the LPDA antenna at the ground station to the southeast with 6-9 dBi of gain while reducing signal energy propagation in the direction of a potential adversary to the west. However, the choice of the antenna to transmit or receive function can be interchanged to provide the best way to meet operational requirements.

1.28 Omnidirectional Command and Control Network and Sounders

Connection to the Virtual SATCOM network starts with an understanding of the environment and communication via an omnidirectional command and control (C2) system to establish wideband high data rate information flow. The Environmental Monitoring station is a network of ground and shipboard stations with various tools to measure the ionosphere in real-time and share that information with other locations. The data is used to build and monitor a real-time state of the ionosphere to select the best frequencies for Virtual SATCOM operations. As illustrated in Figure 8, the west Pacific Ocean with sounders and beacons in various locations can provide both vertical and oblique soundings. In the 1950 and 1960s, the US Navy operated an oblique propagation system called a chirp sounder. Ground sites would transmit a linear changing FM signal starting at the low end of the band and ending at the highest

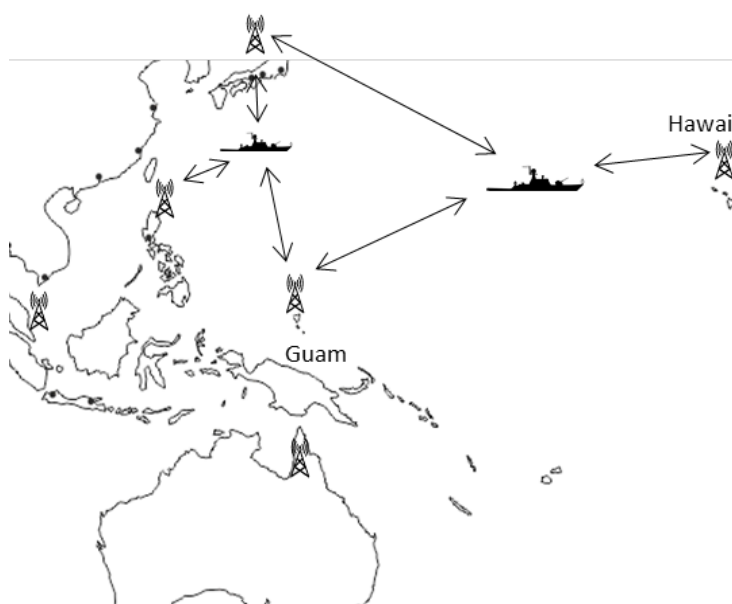


Figure 8. Omnidirectional Environmental Sounding and Command and Control Network. Using LPD low power low data rate communications, the mobile unit can establish communication from a ground control station.

frequency in the band. The receiver was on ships and they would monitor for signal energy. When energy was received from a ground site, it indicated that energy transmitted from that site would propagate to the ship (Figure 9). This would inform the ship on which frequencies were best to communicate with that site. By encoding the transmitted signal, the mobile receiver would know the best frequencies for initial contact with desired locations.

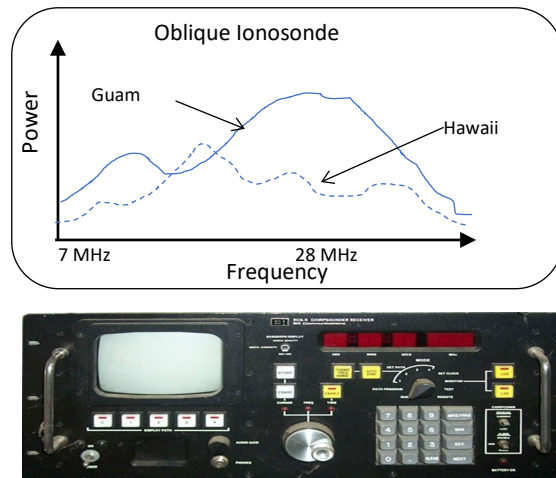


Figure 9. Chirp sounders were receivers that were used by mobile units to determine the best propagation path in the HF band of interest. The receiver would show the best frequencies for propagation. A similar system will be used for Virtual SATCOM services.

1.29 Sounder Operations

- Provides real-time Omnidirectional oblique ionosphere soundings, transmitted by base stations (Guam and Hawaii) to mobile platforms to establish the best frequencies for communication.
- Transmitter sweeps FMCW beacon from 7 to 28 MHz.
- Mobile units only receive signals with suitable propagation parameters.
- Mobile units relay location and best frequency for communications on C2 frequencies of 10, 15, 20 & 25 MHz using narrowband modulation using FT8 like modulation.
- The base station will respond on check-in frequency with specific communication frequency, modulation, etc. for the unit check-in.
- A directional AESA signal is transmitted by the base station to mobile platforms to establish communication, as shown in Figure 10.

- Once locked on, the base station will initiate communications at narrow bandwidth and slow data rate then increase bandwidth as the propagation environment is determined.
- Once connected, the mobile unit and base station use Agile ALE techniques to maintain the best link.
- A mobile unit will transmit the quality of service via set aside frequencies to help maintain high throughput data flow.

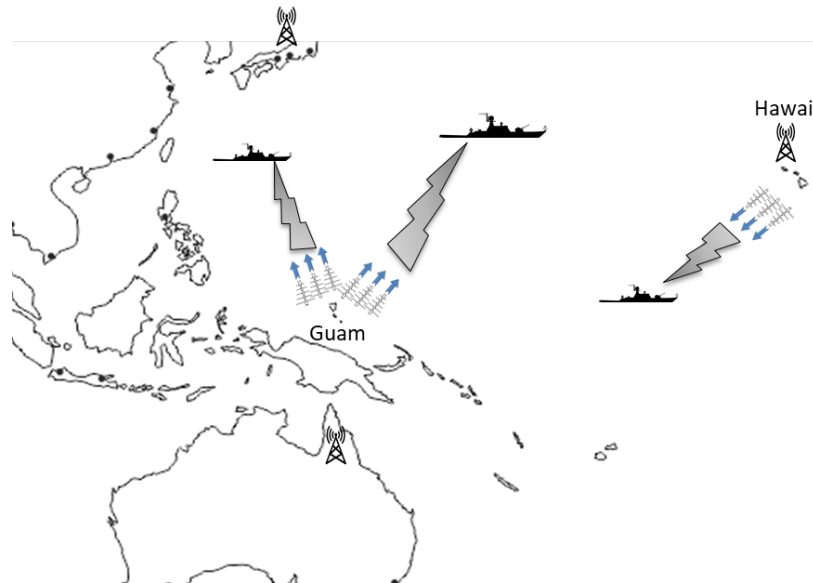


Figure 10. Once the mobile unit checks in on omnidirectional C2 Net, the directional AESA system will begin to transmit to the mobile unit to establish a link.

1.30 Omnidirectional Command and Control Communication Modulation

Mobile units will transmit their location and requests via coded narrowband low power communication. This system is similar to the FT8 and JS8 modulation schemes used in amateur radio. FT8 is an open-source code that operates on the amateur HF frequencies. The FT8 system transmits call sign, position and power level to the requesting caller. The user interface of an FT communications exchange is shown in Figure 11. This amateur radio modulation has had great success with thousands of contacts each day. The system is very reliable due to the extra bits used for FEC and synchronization. It is a reliable way to enable naval units to establish contact without compromising location. This DoD system will not use amateur band frequencies but could use the same modulation techniques with different information on DoD allocated frequencies. A Navy application of this modulation would include coded location and best frequencies for connection and size data to be transferred. Below are the technical parameters of the system:

- Transmit and receive sequence period length: 15 sec

- Bandwidth: 50 Hz within a 3 kHz window
- Modulation is 8-FSK, tone at a frequency spacing of 6.25 Hz
- Message length: 75 bits + 12-bit CRC
- Forward error correction (FEC) code: Low-density parity-check (LDPC) at (174,87)
- The time slot is divided into 79-time intervals
- 58 intervals allotted for the message + FEC + CRC
- 21 intervals allotted for SYNCH TONES
- Synchronization is a 7x7 Costas arrays transmitting 7 Synch tones at the start, middle, and end of a message.
- 79-time intervals, of 0.16-second duration. Thus, each symbol transmitted for 0.16 s.
- Total message duration: 12.64 seconds
- Decoding threshold: -20 dB
- Multi-decoder finds and decodes all signals in the passband of 3 kHz.
- Optional auto-sequencing and autoreply

Figure 11 is a graphic of the interface. The top of the graphic is a waterfall display showing signals versus time. The top is the newest signals and the bottom is the oldest. The lower area shows how the signals are decoded. Here call sign K4DGW has made contact with AC9HP. The two stations exchange call sign, position and received power. Once the operator initiates the connection the two radios automatically exchange the information. The total time for all exchanges is 75 seconds.

1.31 Example Omnidirectional Command and Control Communication

Omnidirectional oblique ionosphere sounders transmit from base stations in Guam and Hawaii. Mobile units monitor for signal strength and frequency to determine the best frequencies for communication. USS XYZ's sounding in Figure 9, shows the best frequency is 20 MHz from Guam. USS XYZ would transmit in code their call sign and location on predetermined check-in frequencies. Even if detected, the coding prevents an adversary from locating the unit. The power is low, so it is difficult for adversary HFDF equipment to determine the ship's location. The ground stations will transmit instructions via omnidirectional C2 system to the USS XYZ, the check-in frequency, modulation and bandwidth of the narrow beam signal. Once a narrow bandwidth signal is stable between the ground station at Guam and the USS XYZ, the bandwidth will increase to meet the information flow rate required. The ground station and the ship will continue to monitor the data flow and adjust. As the ionosphere changes, the ground station will adjust what bandwidth and modulations are working. More discussion on how frequencies are managed is presented in Chapter Four.

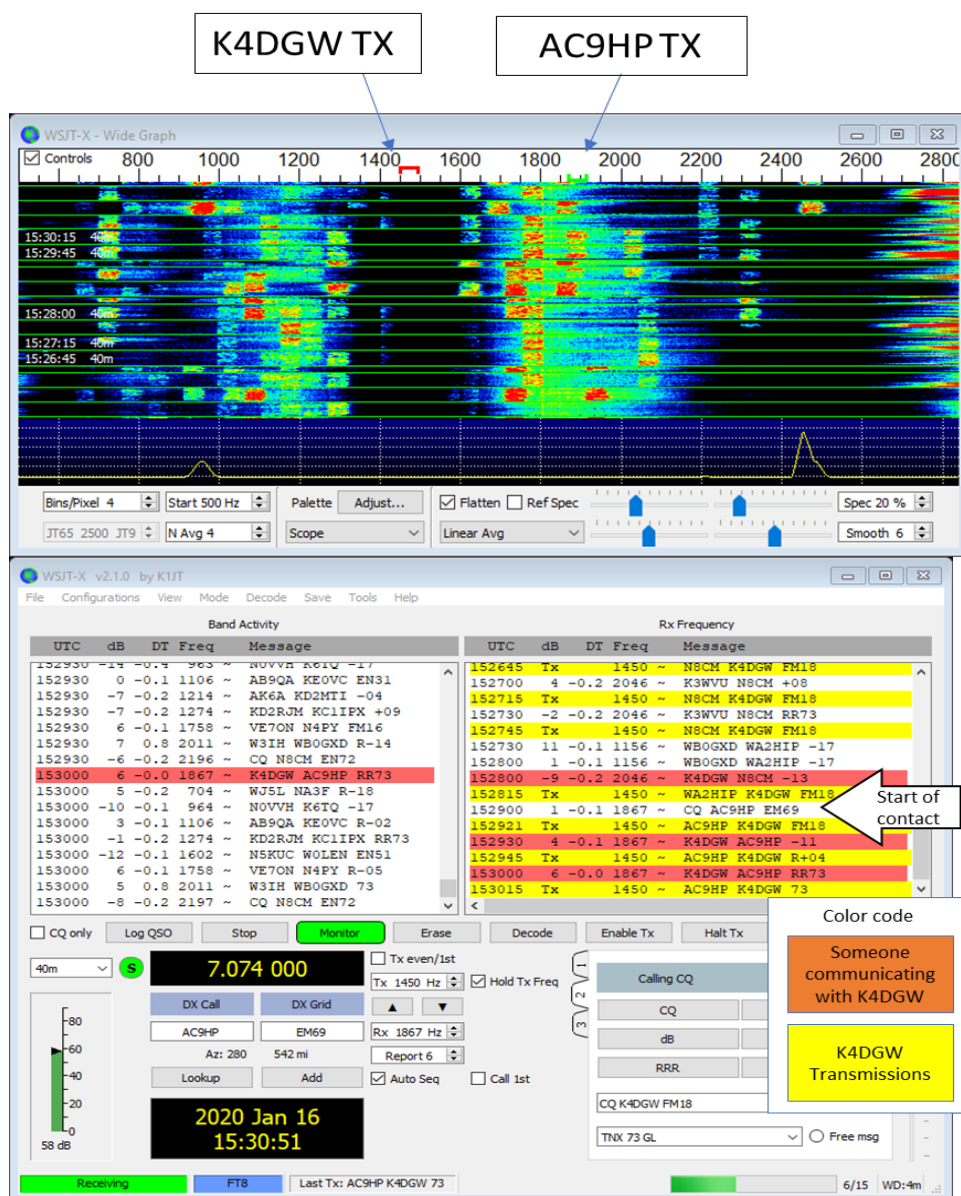


Figure 11. Picture of an FT user interface. K4DGW is responding to a CQ request from AC9HP. K4DGW is transmitting on frequency 1450 to 1500 Hz above 7.074 MHz. AC9HP is transmitting from 1867 to 1917 Hz above 7.048 MHz. The two stations are 542 miles apart and K4DGW is transmitting at 25 Watts.

CHAPTER TWO

BANDWIDTH OF THE IONOSPHERE

Ionization is when a neutrally charged atom loses an electron and becomes positively charged. The Earth's ionosphere, exposed to the radiation from the sun, is composed of layers of particles that have ionized when high energy ultra-violet and x-rays (photons) break electrons away from the atoms. For example, equation 3 shows monotonic oxygen when exposed to ultraviolet photons gives up an electron and becomes positively charged.



Monotonic oxygen is concentrated in a layer at a given altitude due to gravity. This process produces many free electrons at this altitude. These layers of free electrons react to signals, i.e. communication electromagnetic (EM) waves and oscillate at the signal's frequency thus refracting the signal back to Earth and is detected by a receiver thousands of kilometers away. The ionosphere acts like a metal reflector above the Earth. This is the process that enables the signal to travel over the horizon (OTH).

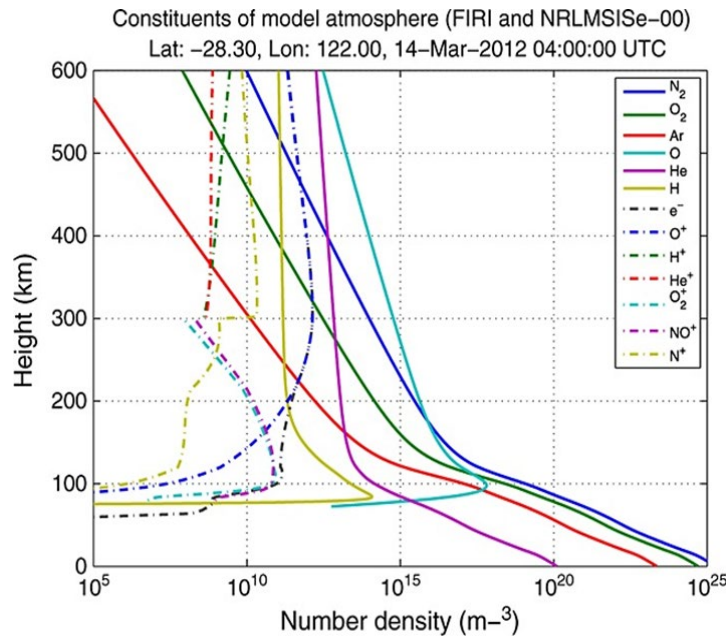


Figure 12. Graph shows the concentration of gases in the atmosphere. For example, at an altitude of 300 km there are approximately 10^{14} O_1 atoms [20].

Besides refracting EM energy, the ionosphere protects the surface of the Earth from this hazardous radiation exposure. It is a complex inhomogeneous, anisotropic, non-linear, time-varying environment. Providing evidence that this natural phenomenon is harnessed for long range wide bandwidth communications required precision modeling of the ionosphere's plasma with an interactive ray tracing simulation that shows the bandwidth limits of the channel paths from the transmitter to receiver. At ODU, we modified an EM propagation program designed for OTHR radar system development called PHaRLAP. It was developed by the Australian Defence Science and Technology Group to assist in the development of next-generation OTHR systems. Our simulations show that the ionosphere can support the wide bandwidth necessary to communicate at speeds comparable with SATCOM systems.

The ionosphere, roughly 85-1,000 km above the Earth, is sometimes referred to as “nature’s satellite” because of the physical phenomenon of bending individual radio waves back to the Earth’s surface. As shown in Figure 12, below the ionosphere (<85 km), down to the Earth’s surface, the gases in the atmosphere (air) are mixed continuously by the sun’s heating the surface. Therefore, ionization concentration is deficient. In contrast, above 85km, there is little mixing, so the atoms and molecules become stratified due to gravity. Lighter gases rise to the top and more dense particles stack below. The atmosphere’s gases stratify (stack-up) into layers, based on density. In the presence of radiation, some gases experience ionization. Consequently, a significant number of ions are prevalent at the altitude of these layers. The ion itself is too massive and does not contribute to the refraction. It is the free electrons generated by the ionization that contribute. Since the free electrons are less massive, they exhibit significant oscillations in the presence of an oscillating EM signal.

2.1 Ionosphere Layers

As seen in Figure 13, during the day, the ionosphere divides into four layers: D, E, F1, and F2. The lowest is the D layer at 85km, and the highest layer is the F2 layer at approximately 350 km. In the D layer, the predominant ion-molecule is nitric oxide. At night, the D layer quickly depletes the free electrons. It dies within a few minutes of the sunset because the recombination rate at 85 km is high due to the higher atmospheric density. The D layer collapse is a desirable outcome because in the D layer collision between free electrons and ions is high, thus absorbing the signal energy and attenuating the signal energy. The key during the day is to operate far enough above the D layer plasma frequency, so electrons do not react in this layer. The electron density of the D layer is lower than the F layers, so the plasma frequency is less. At night the F1 and F2 layers combine and stay ionized through the darkness due to the low ion density resulting in a lower probability of recombination. At approximately 300 km, the F layer is less dense, so the ions are more spaced out.

Consequently, the probability of collision is less, and the time to recombine is longer. Therefore, even after the sun has set below the horizon, the F layer still has enough free electrons to refract communication signals throughout the night. The F layer's ion concentration drops during the night but not to a level that prevents communications. Because of the altitude of the F layer, the refracted signals travel much further before coming back to the surface. This makes the F layer the primary layer for over the horizon skywave communications.

The degree of ray bending is a function of the free electron concentration in the ionosphere and the frequency of the communication signal. The free-electron concentration changes as a function of time of day, along with the season, location and other factors like sunspot number. Therefore, the transmitter signal needs to change frequency to propagate to a precise location. The mathematics algorithm that models this propagation path was developed initially by Dr. Jenifer Haselgrove in 1963 [26] and based on Hamiltonian principles. The algorithms developed by Haselgrove are incorporated into the PHaRLAP program.

2.2 The Volatility of the Plasma

Our studies have shown that there are consistency and reliability in the ionosphere. However, some dynamics that play a significant role in when, and at what frequencies the ionosphere can support communications. The concentration of free electrons determines the degree of refraction and the number

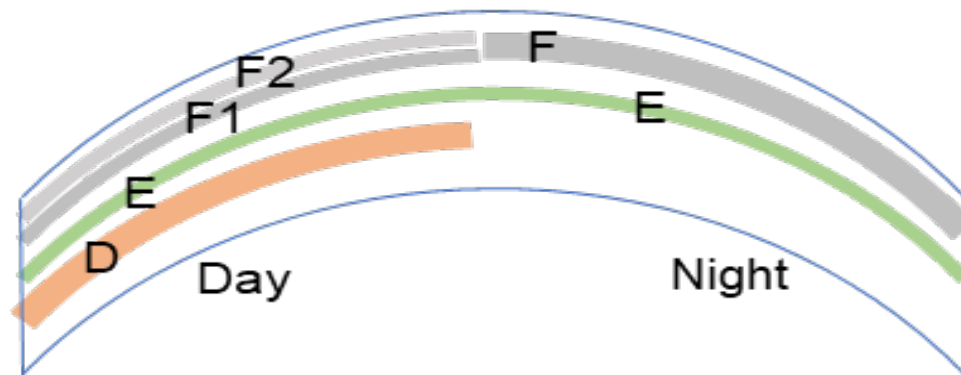


Figure 13. Diagram of ionosphere layers during day and night.

of free electrons is dominated by the intensity of photon radiation from the sun. Photon concentration is affected by the time of day, season, sunspot number, and other factors. Photons affect ion concentration and ion concentration affects the amount of refraction. The use of a directional antenna that can adjust frequency, azimuth, and elevation can direct a beam of EM energy (a signal) to a specific location. Additionally, it can maintain connections with that location by changing frequency and elevation as the plasma of the ionosphere changes.

2.3 How Free Electrons Affect Ray Path in the Ionosphere.

This simplified version of Snell's law (equation 4) shows the relationship between the angles of incidence and refraction for waves passing through a boundary of different media, such as layers in the ionosphere. In Figure 14, we apply Snell's law to the boundary layer in the ionosphere.

$$n_1 \sin \phi_1 = n_2 \sin \phi_2 \quad (4)$$

If ϕ_1 is the angle of incidence in a medium with an index of refraction n_1 , then ϕ_2 is the angle of refraction in medium n_2 (angle between the outgoing ray and the normal). If $n_1 > n_2$, then $\sin \phi_2 > \sin \phi_1$ and $\phi_2 > \phi_1$. If the plasma frequency increases from n_1 to n_2 , then $n_1 > n_2$. As a result, ϕ_2 must be greater than ϕ_1 .

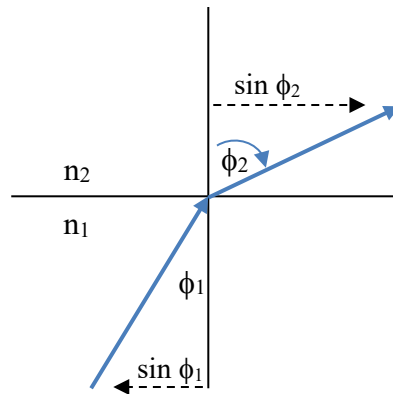


Figure 14. Simple diagram showing ray traveling from lower to higher plasma frequency. As plasma frequency increases, index of refraction decreases, so, $n_1 > n_2$. Therefore, $\sin \phi_2$ is greater than $\sin \phi_1$ causing the ray to bend back toward the horizon. As this process continues, the ray's direction bends completely back to the surface.

2.4 Refractive Index

An understanding of how refractive index changes is central to understanding how the ray will bend. On the surface of the Earth, up to 60 km, the reactive index is approximately 1, and there is little refraction. The density of the atmosphere at lower altitudes is dense and ions have a short life cycle before collision and absorption. At higher altitudes in the ionosphere, this cannot be assumed and must be analyzed to understand signal propagation. The variable parameters that define the refractive index are signal frequency, free electron concentration, Earth magnetic flux in relation to signal path and collision frequency between free electrons and other particles (ions and neutral atoms). In Budden [13] equation 5 provides a formula for a cold electron magnetoplasma with electron collisions that is very similar to the Appleton-Hartree formula.

$$n^2 = 1 - \frac{X(U - X)}{U(U - X) - (1/2)Y^2 \sin^2 \Theta \pm \left\{ (1/4)Y^4 \sin^4 \Theta + Y^2 \cos^2 \Theta (U - X)^2 \right\}^{\frac{1}{2}}} \quad (5)$$

where:

$$X = \left(\frac{Ne^2}{\epsilon_0 m} \right) \frac{1}{\omega^2} \quad \bar{Y} = \left(\frac{e\bar{B}}{m} \right) \frac{1}{\omega} \quad U = 1 - i \left(\frac{\nu}{\omega} \right)$$

Here N is the number of free electrons (m^{-3}), e is the charge on an electron in coulombs (C), ϵ_0 is the permittivity of free space 8.85×10^{-12} (F/m), and ω is the angular frequency of the signal ($2\pi f$) (s^{-1}). \mathbf{B} is the magnetic flux vector of the Earth's magnetic field (ϕ_B). ν is the collision frequency of free electrons in s^{-1} and Θ is the angle between the Earth's magnetic flux and wave direction.

For the X term, Budden factors out the signal frequency and calls this term angular plasma frequency, then:

$$\omega_p^2 = \left(\frac{Ne^2}{\epsilon_0 m} \right) \text{ and } X = \frac{\omega_p^2}{\omega^2}$$

For the Y term, factor out the signal frequency and call this term angular gyro frequency for electrons.

$$|\omega_H| = \left(\frac{e\bar{B}}{m} \right) \text{ and } |\bar{Y}| = \frac{\omega_H}{\omega}$$

The U term has the least effect on propagation at high altitudes (F layer) and little effect at low altitude, as indicated in the example below. Example: calculate the U term at the height of 70 and 300 km at a frequency of 15 MHz: ($\omega = 2\pi f = 2\pi 15 \times 10^6$). From chart below; $\nu = 10^2$ at 300 km and $\nu = 10^7$ at 70 km.

$$U(300\text{km}) = 1 - i \left(\frac{\nu}{\omega} \right) = 1 - i \left(\frac{10^2}{9.4 \times 10^7} \right) = 1 - i 1.06 \times 10^{-6} = 1 \angle 0^\circ$$

$$U(70\text{km}) = 1 - i \left(\frac{\nu}{\omega} \right) = 1 - i \left(\frac{10^7}{9.4 \times 10^7} \right) = 1 - i 0.1064 = 1.006 \angle 6^\circ$$

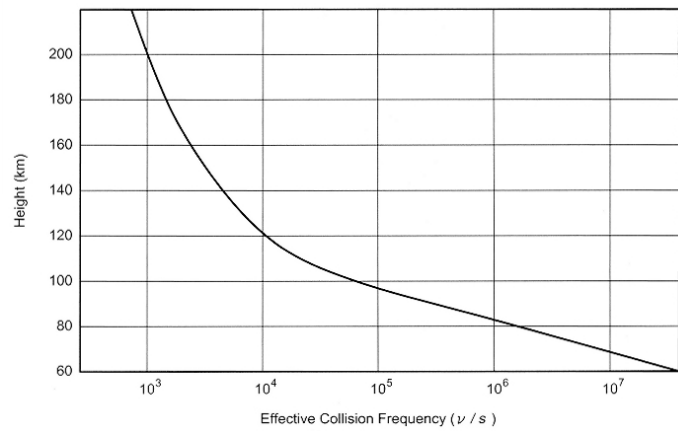


Figure 15. Chart of effective collision frequency vs. altitude at a midlatitude on an average day [13] page 12.

Substituting $U = 1$ into equation 6 results in:

$$n^2 = 1 - \frac{X(1-X)}{1-X - (1/2)Y^2 \sin^2 \theta \pm \left\{ (1/4)Y^4 \sin^4 \theta + Y^2 \cos^2 \theta (1-X)^2 \right\}^{\frac{1}{2}}} \quad (6)$$

To calculate n^2 from X and Y on a typical day, we need to estimate the following: signal frequency is 15 MHz, so angular frequency (ω) is $2\pi f = 9.43 \times 10^7$. Using the charts below, we calculated 10^{11} free electrons per m^3 and Earth's magnetic flux at 50,000nT.

This results in:

$$X = \left(\frac{Ne^2}{\epsilon_0 m} \right) \frac{1}{\omega^2} = \left(\frac{10^{11} (1.6 \times 10^{-19})^2}{8.85 \times 10^{-12} (9.1 \times 10^{-31})} \right) \left(\frac{1}{(9.4 \times 10^7)^2} \right) = \left(\frac{3.18 \times 10^{14}}{8.84 \times 10^{15}} \right) = 3.6 \times 10^{-2}$$

$$Y_{\max} = \left(\frac{|B|e \cos \Theta}{m} \right) \frac{1}{\omega} = \left(\frac{(50000 \times 10^{-9})(1.6 \times 10^{-19}) \cos \Theta (1)}{(9.1 \times 10^{-31})} \right) \left(\frac{1}{(9.4 \times 10^7)} \right) = \frac{8.8 \times 10^6}{9.4 \times 10^7} = 9.4 \times 10^{-2},$$

where Θ is the angle between the signal direction and the Earth's magnetic flux. Y is at a maximum when Earth's magnetic flux and ray normal are in the same direction (0°) and at zero when ray normal and flux are 90° out of phase.

In the F layer, the collision frequency is low, so U tends to 1 as can be seen in the Appleton-Hartree formula for the refractive index in a cold electron magnetoplasma:

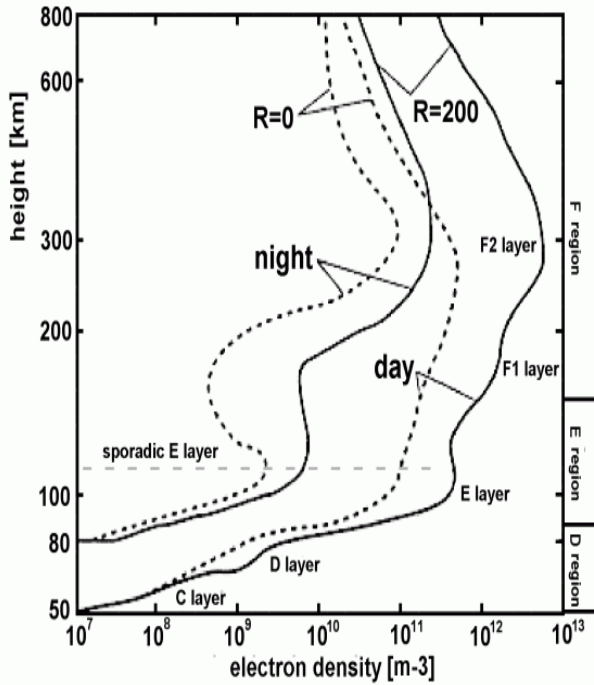


Figure 16. Shows electron density for a low and high sunspot number (R) during day and night.

Taken from:

http://roma2.rm.ingv.it/en/research_areas/4/ionosphere

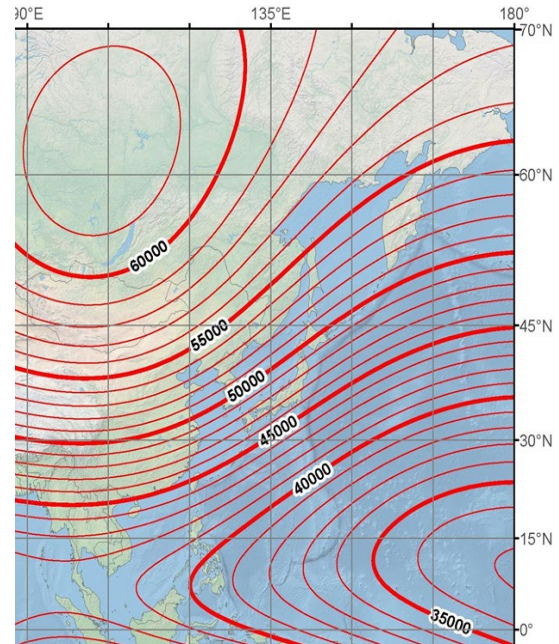


Figure 17. Shows earth magnetic contour lines in nano Teslas (nT) for western Pacific Ocean.

Taken from:

<https://www.ngdc.noaa.gov/geomag/WMM/image.shtml>

$$n^2(X = .036, Y = .096, \Theta = 0^\circ) = 1 - \frac{.036(1 - 0.036)}{1 - 0.036 - \cancel{(.5)(.096^2)(0)} \pm \left\{ \cancel{(.25)(.096^4)(0)} + (.096)^2(1)(1 - .036)^2 \right\}^{\frac{1}{2}}}$$

$$n^2(X = .036, Y = .096, \Theta = 0^\circ) = 1 - \frac{.0347}{.964 \pm .09254} = 0.9672, 0.9602$$

$$n = 0.9835, \text{ and } 0.9799$$

$$n^2(X = .036, Y = .096, \Theta = 90^\circ) = 1 - \frac{.036(1 - 0.036)}{1 - 0.036 - (.5)(.096^2)(1) \pm \left\{ (.25)(.096^4)(1) + (.59)^2(0)(1 - .036)^2 \right\}^{\frac{1}{2}}}$$

$$n^2(X = .036, Y = .096, \Theta = 90^\circ) = 1 - \frac{.0347}{.9594 \pm .004608} = 0.9640, 0.9637$$

$$n = 0.9818, \text{ and } 0.9817$$

The average n is 0.981725, with a standard deviation of 0.0025. Applying the average to equation 6 and assuming n_1 is 1.0 and ϕ_1 is 75 degrees and n_2 is .0.981725, then ϕ_2 is 80 degrees or a 5-degree bend towards the horizon. As the ray travels through additional layers, it continues to bend back towards the surface of the Earth.

Index of refraction is a measure of the bending of a ray when passing from one medium into another. In this case, from one layer of the ionosphere to the next. In the plasma, the index of refraction is a complex term. For a collision-less plasma, this is simplified to the complex index of refraction in equation 7 and 8 [13]:

$$n = \sqrt{1 - \frac{f_p^2}{f^2}} \quad (7)$$

$$n = \sqrt{1 - \frac{\left(\frac{1}{2\pi} \sqrt{\frac{N_e e^2}{m \epsilon_0}} \right)^2}{f^2}}$$

$$n = \sqrt{1 - \frac{\left(\frac{1}{2\pi} \sqrt{\frac{10^{11} (1.6 \times 10^{-19})^2}{(9.1 \times 10^{-31})(8.85 \times 10^{-12})}} \right)^2}{(1.5 \times 10^7)^2}}$$

$$n = 0.9819$$

The index of refraction using equation 7 is very close to what was obtained in the Appleton equation (equation 6).

On the Earth surface (below the ionosphere), N_e is negligible, so plasma frequency, $f_p=0$ and index of refraction (n) is 1.0. However, in the ionosphere, the critical frequency (f_p) is not zero so n is less than 1. Using the example above, if $n=0.982$ and equation 4 (Snell's Law) with $\phi_1 = 75^\circ$ then $\phi_2 = 80^\circ$. Successfully refracting the ray back toward Earth. Successive refractions, as the ray travels through many layers, will bring it back to the surface.

A more simplified formula for plasma frequency, where f_p in MHz is the plasma frequency defined as:

$$f_p = \frac{1}{2\pi} \sqrt{\frac{N_e e^2}{m \epsilon_0}} \cong 9 \times 10^{-3} \sqrt{N_e} \quad (8)$$

where N_e is the number of free electrons per cm^3 .

As mentioned earlier, this dissertation uses the PHaRLAP ray tracing model to quantify the availability of bandwidth to support a Virtual SATCOM system. The model was modified to show how much of the spectrum would refract onto a precise location. The next section will describe how this model calculated the successive refractions along the ray's path.

2.5 PHaRLAP Model:

In 2014 the Australian Defence Science and Technology Organization (DSTO) developed an HF ray tracing toolbox called PHaRLAP to study the propagation of radio waves through the ionosphere. The 2-D raytracing engine is an implementation of the 2-D equations developed by Coleman, based on the Haselgrove equations [35] [25]. This raytracing tool was developed by Dr. Manuel Cervera, of the DSTO and has been used in many papers to estimate the performance of over the horizon radars (OTHR) and other projects.

The PHaRLAP model uses a MATLAB program to calculate the refraction of RF waves and plot the ray path. The tool takes the International Reference Ionosphere (IRI) data and builds an electron density model. The IRI is an international project sponsored by the Committee on Space Research (COSPAR) and the International Union of Radio Science (URSI), see [36]. The IRI produces an empirical standard model of the ionosphere based on all available data sources. For a given location, time, and date, IRI provides monthly averages of the electron density, electron temperature, ion temperature, and ion composition in the altitude range from 50 km to 2000 km. The data sources are a worldwide network of ionosondes, and incoherent scatter radars and instruments on several satellites.

The PHaRLAP model calculates the plasma frequency for each element in the range-altitude grid for the location specified. It then, through incremental integration, calculates the ray path for a specified frequency given the locations, date, and time, and initial elevation and azimuth of the ray. The program begins with the initial coordinates (x, y, z) as the starting point. Using equations 9, 10, and 11, the program calculates the group velocities at that point ($dx/d\tau$, $dy/d\tau$ and $dz/d\tau$).

$$\frac{dx}{d\tau} = \frac{c}{n} \left(\cos \chi + \sin \chi \frac{1}{n} \frac{\partial n}{\partial \chi} \right) \quad (9)$$

$$\frac{dz}{d\tau} = \frac{c}{n} \left(\sin \chi - \cos \chi \frac{1}{n} \frac{\partial n}{\partial \chi} \right) \quad (10)$$

$$\frac{d\chi}{d\tau} = \frac{c}{n^2} \left(\cos \chi \frac{1}{n} \frac{\partial n}{\partial z} - \sin \chi \frac{1}{n} \frac{\partial n}{\partial x} \right) \quad (11)$$

Since the ionosphere is a nonlinear anisotropic medium, the PHaRLAP model follows an interactive process (Figure 18). First, cutting the volume into a grid and using the electron density from a database solves for the index of refraction for each grid element. With the electron density, ray signal frequency, and incoming elevation angle, it can calculate the refractive index and using an algorithm like Snell's Law, calculate the output angle. By piecing the segments together, the ray path for origin through the ionosphere and then back to the surface can be calculated. Without the refraction ($d\chi/d\tau$) of the ionosphere, the ray would continue out into space. As the ray reaches the ionosphere, the ion concentration increases. For HF band frequencies, the ions change the index of refraction and the new index of refraction leads to a new wave normal angle, i.e. the wave has been bent. The wave velocity and angle lead to a new position. The program continues through this process, calculating incremental changes until the wave reaches the surface or exits the grid.

The PHaRLAP model is based on the Hamilton principle. Dr. Jenifer Haselgrove was the first to derive the Hamiltonian ray tracing equations for HF radio waves through the ionosphere. These equations have been extensively used to study HF radio wave propagation and are the basis of the PHaRLAP program. Where χ is the angle between the wave normal and the respective axis, c is the speed of wave propagation in a vacuum, and n is the refractive index.

The PHaRLAP program divides the area of interest into a grid based on the input range (x) and the altitude range (z). Next, the plasma frequency is calculated based on the IRI date for the date and time to be modeled.

The model traces the signal's ray as it refracts through the ionosphere. The refraction is a function of the free electron density and the signal frequency. The landing point depends on the elevation angle, the degree of refraction (bending), and the altitude of the bending.

The PHaRLAP model calculates the ion density using data downloaded from the International Reference Ionosphere (IRI) database [36].

We modified the model for a single hop point to point analysis. We ran the algorithm at many different frequencies, and elevations recording only rays landing at the locations of a mobile unit 3000 km north of the ground station in Guam. Guam was selected as a test location because of its strategic location in the Western Pacific Ocean.

The idea is: if the ground station transmits at the frequencies and elevations calculated by the model, then those signals will be received at the intended mobile unit's location. The number of rays, 100

kHz apart, equates to more bandwidth. In our testing, the test frequencies are spaced 100 kHz apart with the assumption that the frequencies between the test frequencies will follow the same path.

2.6 Results of Our Testing.

We selected Guam as a transmit location and ran the model every hour for 24 hours on September 2, 2016, to capture the total picture for the day. In Figures 19 and 20, we show propagation paths of rays transmitted north from Guam into the Pacific Ocean (13.4° N, 144.8° E) at midnight and local noon respectively. The color-coding of the background shows the plasma frequency at that range and altitude while rays (in white) are moving from the origin to a landing point on the right. Each graph shows only the rays that would land within 50 km of a point 3000 km north of Guam. In Figure 19 (midnight), there are 36 rays, spaced 100 kHz apart, which equates to 3.6 MHz of bandwidth. Compared to typical HF frequency bandwidth of 3 kHz, this is 1000 times larger than a narrowband signal. In Figure 20, at local noon, there are a total of 176 paths equating to 17.6 MHz of effective bandwidth available.

Figures 21 and 22, and Table 3 shows 24 hours of bandwidth availability. One difference between SATCOM and Virtual SATCOM is for Virtual SATCOM; bandwidth availability is a variable depending on the ionosphere. Most of the time, it is more than adequate, but bandwidth and data speed will be managed to meet communication needs.

In the discussion above, our analysis of the ionosphere shows that typically there is enough bandwidth available to support investment in a Virtual SATCOM system. The next step is to design an antenna array with a transmitter and receiver system that can take advantage of this bandwidth in the High-Frequency RF band.

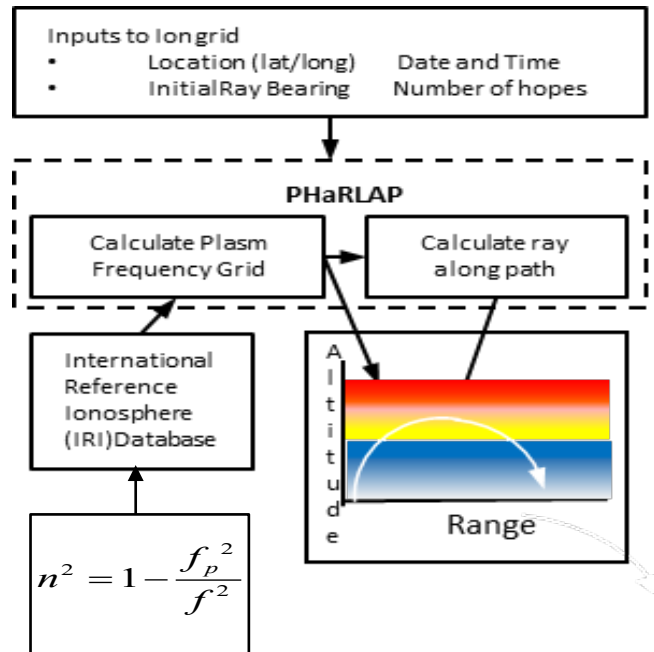


Figure 18. PHaRLAP Model flow chat. Locations, time, date, initial ray elevation, and azimuth angle are input into model. This data is combined with IRI date to computer plasma grid. Ray is plotted incrementally as it reacts to plasma in each grid square.

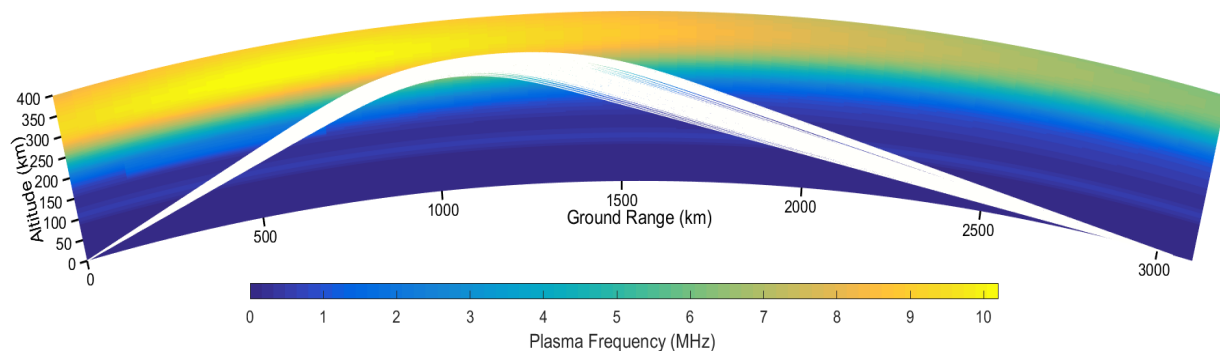


Figure 19. Local Midnight PHaRLAP graph of ray propagation looking north. Each ray is a different frequency and elevation angle. Graph shows only rays landing within 50 km of a point 3000km north of Guam. The plot shows 69 rays with an effective bandwidth of 3.6 MHz.

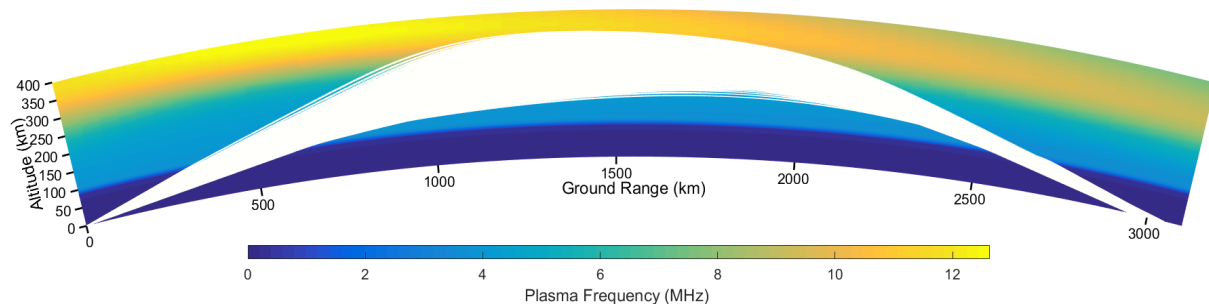


Figure 20. Local Noon PHaRLAP graph of ray propagation looking north. Each ray is a different frequency and elevation angle. Graph shows only rays landing within 50 km of a point 3000km north of Guam. There are 1146 rays between 30-12.5 MHz and elevation angles of 5-15 degrees with and 17.5 MHz of bandwidth.

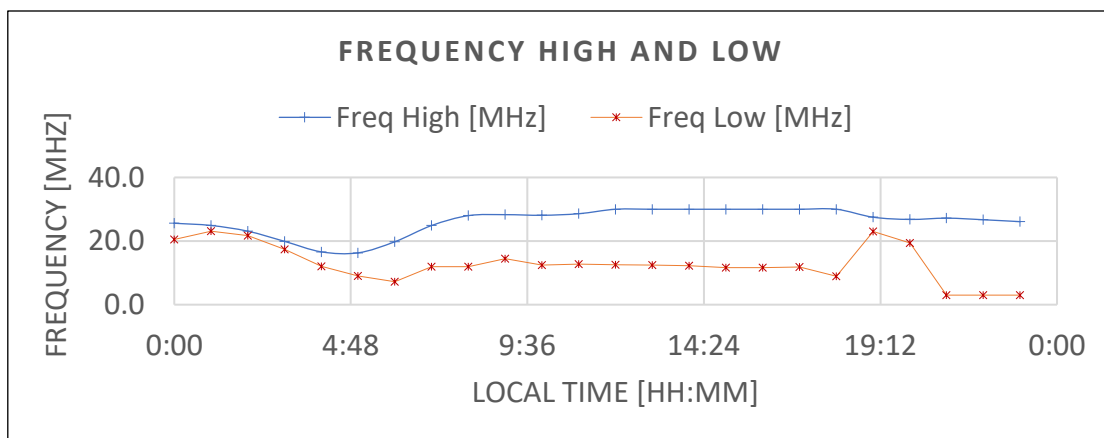


Figure 21. Graph shows the highest and lowest frequency that meet the test of traveling 3000 km and landing on a precise location on September 2nd, 2016.

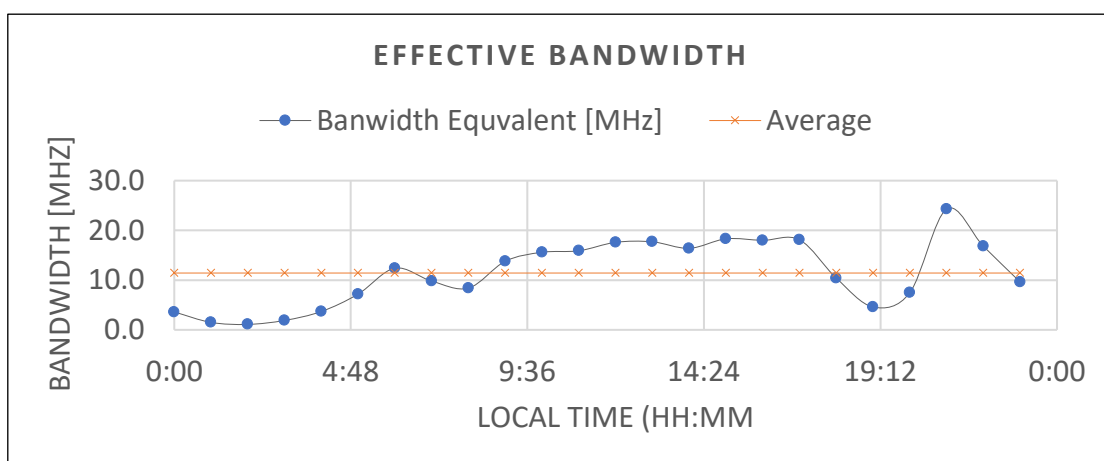


Figure 22. Graph shows effective bandwidth during 24-hour period for Guam on September 2, 2016.

Table 3. The Output of Model from Guam Looking North on Sept 2, 2016

Local Time GUAM	Freq High [MHz]	Freq Low [MHz]	High to Low [MHz]	Count of 100 kHz channels	Bandwidth Equivalent [MHz]
0:00	25.6	20.5	5.1	36	3.6
1:00	24.9	23.1	1.8	15	1.5
2:00	23.1	21.7	1.4	11	1.1
3:00	19.9	17.4	2.5	19	1.9
4:00	16.6	12.0	4.6	37	3.7
5:00	16.3	9.0	7.3	72	7.2
6:00	19.8	7.2	12.6	124	12.4
7:00	24.9	11.9	13.0	98	9.8
8:00	28.0	11.9	16.1	84	8.4
9:00	28.3	14.5	13.8	138	13.8
10:00	28.1	12.4	15.7	156	15.6
11:00	28.6	12.7	15.9	159	15.9
12:00	30.0	12.5	17.5	176	17.6
13:00	30.0	12.4	17.6	177	17.7
14:00	30.0	12.2	17.8	164	16.4
15:00	30.0	11.6	18.4	183	18.3
16:00	30.0	11.6	18.4	180	18.0
17:00	30.0	11.8	18.2	181	18.1
18:00	30.0	8.9	21.1	104	10.4
19:00	27.5	23.0	4.5	46	4.6
20:00	26.8	19.4	7.4	75	7.5
21:00	27.2	3.0	24.2	243	24.3
22:00	26.7	3.0	23.7	168	16.8
23:00	26.1	3.0	23.1	96	9.6
AVERAGE	26.2	12.8	13.4	114.3	11.4

2.7 Validation of PHaRLAP Model

The underlying mathematics of the PHaRLAP program drew on the Fortran program developed by Dr. Coleman [37] and [35]. His work was based on the mathematical work of Dr. Jeanne Haselgrove in 1955 [25]. Her objective was the development of equations that are suitable for numerical integration on a high-speed electric computer. The starting point for her analysis is ray path equations developed by Hamilton in 1837 that are related to geometrical optics for a general anisotropic medium.

CHAPTER THREE

HF NOISE ANALYSIS

Signal to noise ratio (SNR) is an essential parameter in digital communications. It is necessary to understand the ambient noise at the receiver. The HF band propagates for long distances and is sometimes considered a noisy band. The noise that is generated thousands of km away can interfere with HF communications. Even galactic noise from distant stars can affect the HF band. There are many studies on HF band noise and the analyst by Dr. Coleman in 2002 [15] is very comprehensive. Dr. Pederick and Dr. Cervera further improved dr Coleman's model. They developed a model called SiMIAN to calculate the noise level [20]. In this work, the evaluation of noise and absorption is based on the SiMIAN and model. While the theory was built on the Coleman model, the SiMIAN model has made improvements in several areas:

- (1) Added a more accurate absorption model, which is an essential contribution to the noise model particularly at lower frequencies.
- (2) Updated lightning strike models using space-based sensors.
- (3) Added a directional galactic noise model.
- (4) Explored the use of three-dimensional numerical raytracing to model the noise on the O and X polarization modes separately.
- (5) Added a calibration process using noise data from the Jindalee Operational Radar Network (JORN) Frequency Management System (FMS) at Longreach.
- (6) Performed a validation process of the model against noise data from the JORN FMS at Laverton, which is 2160 km away from Longreach

The SiMIAN model provides a suitable estimate of the HF noise floor. The predominant natural noise comes from lightning strikes and galactic noise. A third noise source is the thermal noise within the electrical components. Johnson–Nyquist defined thermal noise in equation 12.

$$N_T = k_B TB \quad (12)$$

where k_B is Boltzmann's constant in joules per kelvin (1.380649×10^{-23} J/K), T is the equipment's absolute temperature in Kelvins, and B is the bandwidth in Hertz. Assuming a temperature of 1250 Kelvin at an altitude of 300 km results in a noise power value of -198 dBW/Hz

Noise is highly anisotropic, with the directional distribution an important factor. The directional narrow beam antenna in the Virtual SATCOM design is a strategic advantage in noise and interference rejection, including jamming. The noise and interference will arrive at the narrow bandwidth receiver from many directions, while the signal of interest will arrive from only one direction. Thus, the ability to reject most of the noise with an antenna with narrow directional control is evident. Long-distance signals have significant path loss reductions and must compete with the noise floor to be accurately decoded. Consequently, the performance of HF radio and radar systems are dependent on the level of the external noise environment. Radar systems are particularly vulnerable to noise since the receiver in these systems must detect the very low energy that is reflected off the targets. The path loss increases at a range to the fourth power rate (R^4). Fortunately, radar systems use directional antennas which would benefit communications systems as well.

3.1 SiMIAN Noise Model Improvement

The line of reasoning is that, at HF, natural external noise originates chiefly from 2 sources, lightning and galactic noise. As seen in equations 13 and 14, the Pederick Cervera summation of natural noise energy, as a function of the solid angle of azimuth (θ) and elevation (ϕ). Where $W(f)$ is the rated energy density of a lightning strike, S_i is the strike rate, G is the galactic noise, and ϕ_i is the elevation at which the noise left the thunderstorm, and L_i is the loss due to both atmospheric absorption and ground reflection. The summation is carried out over each reflection from the ground ($i = 1, 2 \dots n$). Two improvements over the Coleman model are addressing lightning strike energy $W(f)$ as a function of frequency (f) and including a galactic noise contribution. A third improvement is that L_i is calculated differently. These improvements are discussed below.

$$N_i(\theta, \phi) = \left(\frac{\lambda}{4\pi} \right) \frac{W(f)S_i}{L_i \sin(\phi)} \quad \text{for lightning noise} \quad (13)$$

$$N_i(\theta, \phi) = \left(\frac{\lambda}{4\pi} \right) \frac{G(f, \theta, \phi)}{L_i} \quad \text{for galactic noise} \quad (14)$$

3.2 Lightning Strike Noise

In most locations, the primary source of noise is lightning strikes. The SiMIAN separates this into two components: a local component (which propagates to the receiver via line of sight or ground waves, for example, lightning within 100 km) and an ionospheric component (which propagates to the receiver via the ionosphere). The local component is a small area, and accordingly, a small factor. The ionospheric component is the combination of energy from the many lightning strikes across the globe ($\sim 170,000$ per hour), as calculated by Cecil et al. [16]. Cecil's paper documented the publicly available data from the

gridded spaceborne optical sensors: Optical Transient Detector (OTD) on the MicroLab-1 satellite and Lightning Imaging Sensor (LIS) on the Tropical Rainfall Measuring Mission (TRMM) satellite that has been collecting data since 1995. This data is used in the SiMIAN model to define the lightning strike rate (S_i) for a given direction. The Coleman model did not take advantage of the satellite base sensor used by the SiMIAN model.

3.3 Galactic Noise

The other natural source of noise in SiMIAN is galactic noise, which originates from outside the Earth and propagates through the ionosphere. As it requires trans-ionospheric propagation, this noise is only present at higher frequencies or high elevation angles; therefore, radio waves at lower frequencies and low elevation angles cannot penetrate the ionosphere. The SiMIAN model uses the data adapted from Oliveira-Costa et al.'s model of diffuse galactic radio emission [18]. This is a global sky model (GSM) derived from all publicly available total power large-area radio surveys, which can return a predicted all-sky map at any frequency from 10 MHz to 100 GHz. SiMIAN uses the sky map calculated by de Oliveira-Costa et al.'s model at 20 MHz, with the power scaled using ITU-R P.372 [38] to estimate the galactic noise power at other frequencies.

3.4 Propagation

The raytracing to determine the location of relevant noise sources is performed using the Provision of High-frequency Raytracing Laboratory for Propagation model (PHaRLAP) numerical raytracing software. The electron density in the ionosphere was modeled using the IRI data [36], the de facto international standard for the climatological specification of ionospheric parameters. Both the Coleman and SiMIAN models use the IRI data in their calculations. However, the SiMIAN model includes other models to evaluate lower altitude effects.

3.5 Absorption Model

The complex refractive index of the radio wave can be calculated using the well-known Appleton-Hartree formula as described by Budden (equation 15), which accounts for the collision at low altitude. Recall from Chapter 2 that:

$$U = 1 - i \frac{\nu}{\omega} \quad (15)$$

where ν is the collision frequency in collision per sec and ω is the operation angular frequency in radians per second. In the Appleton Hartree formula, U is a frictional term used to account for electron collisions. However, the Appleton Hartree formula assumes that the collision frequency (ν) is constant for all

altitudes and independent of the electron velocity. In the lower ionosphere, this assumption gives erroneous results for the imaginary component χ or v/ω , of the refractive index. Instead, SiMIAN uses the Sen-Wyller formulation [39], which provides more accurate results for the absorption in the lower D and E regions.

In the SiMIAN model, the amount of absorption is calculated using equation 16. It integrates the absorption coefficient χ along a ray path, with the absorption coefficient calculated using the Sen-Wyller formula and the NRLMSISE-00 atmospheric model where k is the wavenumber in m^{-1} . It should be noted that the IRI-2012 model has been upgraded to the NRLMSIS-00 model. The NRLMSISE-00 is a more accurate estimate of the ionosphere layering [40].

$$L = 8.68 \int k \frac{v}{\omega} ds \quad (16)$$

The Sen-Wyller assumes a variable collision frequency based on electron velocity and atmospheric density. Higher electron speeds in a denser atmosphere result in more collisions and higher absorption. In Pederick's paper on the SiMIAN model [20], the author discusses how the Sen Wyller absorption losses are calculated. The sharp increase in electron temperature will contribute to increasing electron velocity. The higher density and higher speed results in higher collision rates. The collision frequency at altitudes below 90 km (D and E region) reads approximately 10^8 collisions per sec. This is a 10^6 increase compared to the F2 layers at approximately 350 km. At HF frequencies, the χ term (v/ω) is much larger at 80 km than at 350 km, accounting for the increased energy absorption passing through the D and E levels. Absorption in the SiMIAN model is typically half the Coleman absorption rate because the Coleman model will attenuate noise too quickly. This is especially true for multi-hop noise rays during the day that must pass through the high absorption D and E regions multiple times. The SiMIAN model shows that absorption in the D and E layer is nominally between -3 and -6 dB. The D and E absorption attenuation is a factor during daylight hours only. At night the D and E layers collapse. The choice of a higher operating frequency (ω) can reduce the absorption effect of the (v/ω) term. In the Virtual SATCOM analysis, a (-3) or (-6) dB absorption loss was included in the analysis to account for the reduction of signal power due to absorption.

3.6 Summarizing the Noise Floor in HF Band

Noise, by its very definition, is random. It extends in various forms across the frequency spectrum, although not always at the same amplitude. Accordingly, there are different categories of noise according to the frequency distribution. As stated, the primary sources of natural HF noise are lightning and galactic noise. The path loss is low so lightning strikes around the world contribute to the global noise level. Galactic noise comes from outside the Earth but is still strong enough to affect the noise floor.

Humanmade noise, classified as interference, can contribute high levels of noise into a system. Humanmade interference generally comes from a given direction and relatively narrow bandwidth compared to natural noise. The interference power level may be higher than natural noise, but the interference can be avoided by using a directional antenna to attenuate the interference. Based on the SiMAIN model, the typical natural noise power density band is -160 dBW/Hz, with directional antennas experiencing less noise than an omnidirectional system. In the Virtual SATCOM analysis, we estimated the noise between -140 dBW/Hz and -150 dBW/Hz. This is a conservative estimate, 20 dB above the SiMAIN model.

CHAPTER FOUR

ANTENNA DESIGN AND SIGNAL PROCESSING

4.1 Introduction

In the previous chapters, the concept of an ultra-wide bandwidth narrow beam architecture was proposed, showing scenarios that could yield high data rate channels. We have demonstrated that the ionosphere has the bandwidth for wideband signals. The signal to noise ratio is an essential input into the Shannon–Hartley theorem that defines the upper-speed limit of data rate in a wireless channel. In this chapter, more detail will be presented on the antenna design that can produce the narrow beam. Additionally, this chapter will provide detail on how the frequency management and signal modulation will be executed.

All wireless systems require an antenna. The antenna is the interface between radio waves propagating through space and electric currents moving in metal conductors. Antenna design is sophisticated, and a capable antenna is designed to resonate well at the desired frequency. The better it resonates, the more effective it will convert alternating currents into propagating electrical signals. During transmission, an oscillating current is applied to the antenna by a transmitter creating a time-varying electric field and magnetic field around the antenna elements. These time-varying fields radiate energy away from the antenna into space as a moving transverse electromagnetic field wave.

4.2 Radiation Mechanisms of Antennas

As discussed in Balanis [41], the antenna is a metallic device that converts currents in the metal to electromagnetic fields that propagate into free space when operating in a transmitter mode. In the receive mode, the antenna converts a propagating electromagnetic field in free space into currents that can be measured by the receiver. In a thin wire, the current I in coulombs/sec can be represented by:

$$I = q_l v \quad (17)$$

where q_l is the charge per length (coulombs/m) and v is the velocity of the charge in (m/s). If the current is time-varying, the derivative with respect to time can be written as:

$$\frac{dI_z}{dt} = q_l \frac{dv}{dt} = q_l a \quad (18)$$

where $a = dv/dt$, is the acceleration of the electrons. If length is 1 unit then:

$$l \frac{dI_z}{dt} = q_l \frac{dv}{dt} = q_l a_z. \quad (19)$$

Equation 17, 18, and 19 show the relationship between charge and current and is the fundamental relation of electromagnetic radiation. If the movement of the charge (current) is not changing, there is no radiation. Direct current (DC) along a straight wire will not radiate but if the wire's path is not straight, or if the current is an alternating current (AC), then radiation will occur. In other words, if the charge is moving with uniform velocity, then there is no radiation unless the wire is curved, bent, discontinuous, terminated or truncated. If the charge is oscillating in a time-motion i.e. alternating current, it will radiate even if the wire is straight.

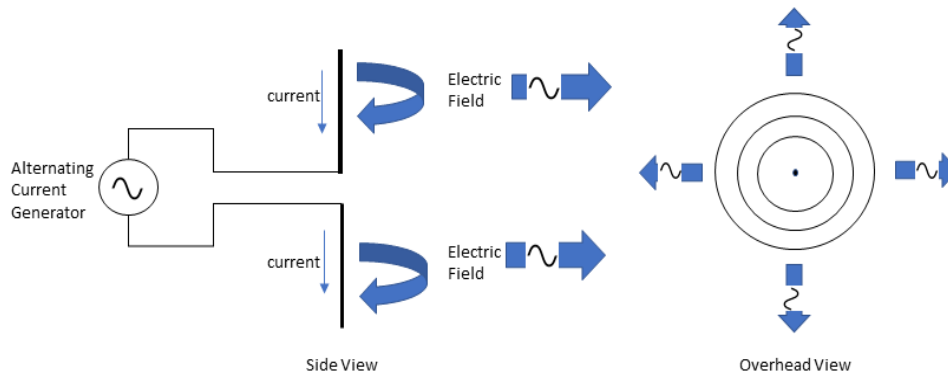


Figure 23. Common dipole antenna. The alternating current moving through the conducting antenna creates an electromagnetic field that propagates away from the antenna in a 360-degree pattern.

4.3 Dipole Antenna

A common communication antenna is the vertical dipole antenna (Figure 23). This antenna propagates signal energy in 360° of azimuth. This omnidirectional pattern is helpful for broadcast transmission to many receivers or when the location of the receiver is unknown.

4.4 Directional Antenna Designs

In point-to-point communication, a dipole antenna is an inefficient geometry to transmit signal energy as most of the energy is wasted as it propagates in all directions. If a more directional antenna was employed, the signal energy in the direction of the receiver is increased. Directive antennas focus the energy, concentrating the signal power in the direction of the receiver to increase the SNR. This focus

term is called directivity or gain and is measured in decibels (dB). If an ideal directional antenna has a 3° beam, then most of the energy is concentrated within 3° . This antenna will have a gain (G) greater than the dipole of:

$$G_{dB_d} = 10 \log_{10} \left(\frac{360}{3} \right) = 21 dB_d \quad (20)$$

Here the gain is measured in dB_d ; the second d in the subscript is a reference to a dipole antenna. There are two primary advantages of directional communications antennas. First is the increased signal power at the receiver resulting in a higher SNR. The second advantage is frequency reuse. By concentrating the signal in a beam, it allows other radios outside the beams to use the same frequencies without interference. This is important in the Virtual SATCOM application because it enables the use of wide bandwidths without interference with others using the same frequencies. Consequently, the bandwidths (frequency range) of the signal can be increased because the beam will not interfere with users outside the beam. As discussed in Chapter 1, the Virtual SATCOM system operates at 3 MHz bandwidth which is 1000 times larger than a typical 3kHz bandwidth channel.

The disadvantage of directional antenna systems, especially with mobile users, is that the systems must steer the antenna in the correct direction. This requires the location (path) knowledge of mobile users. If the directional antenna must service multiple users, it must quickly move the beam amongst the users. HF antennas are relatively large as compared to millimeter systems. For example, a half-dipole vertical polarized antenna designed to operate at 15 MHz is over 30 ft in length. There are directional antenna designs that are mechanically steered, but again, it is a large piece of equipment. One example is a horizontal polarized Yagi antenna. A Yagi–Uda antenna, commonly known as a Yagi antenna, consists of multiple parallel elements in a line, usually half-wave dipoles made of metal rods. Yagi antennas consist of a single driven element connected to the transmitter or receiver with a transmission line and additional parasitic elements, which are not connected to the transmitter or receiver. The parasitic elements act like reflectors, focusing the energy of the beam of the driven element. Usually, the assembly is mounted on a mechanically rotatable mast so that the antenna can swing in 360° .

4.5 Log Periodic Array Antenna

A log-periodic dipole array (LPDA), also known as a log-periodic array, is a multi-element, directional antenna that is designed to operate over a wide band of frequencies (Figure 24). Dwight Isbell and Raymond DuHamel invented it at the University of Illinois in 1958 [41].

The log-periodic is commonly used in communications where it is desired to transmit and receive over wide bandwidth. In the Virtual SATCOM design, the log-periodic zig-zag design with many dipoles is used to cover 7 to 28 MHz. Every element in the LPDA antenna is connected electrically to the feedline along with all the other elements. At any one frequency, most of the elements draw little current except for the resonant dipole element. Each successive element is connected in the opposite phase to the active connection running as a transmission line along with the boom. For that reason, that transmission line can often be seen zigzagging across the support boom holding the elements. Being log-periodic, the antenna's radiation pattern, gain, and driving point impedance is almost constant over its entire frequency range. When matched to the feed line, a standing wave ratio of better than 2:1 is typical. This wide bandwidth performance characteristic makes it an excellent choice for a wideband system.

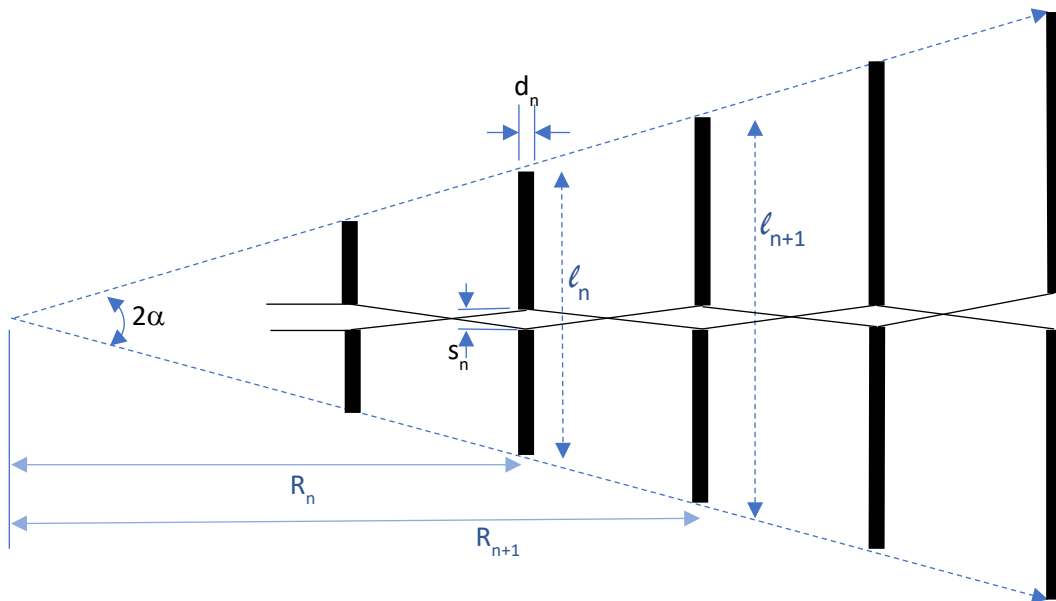


Figure 24. Dipole Log periodic dipole array. Every element in the LPDA design is connected electrically to the feedline along with the other elements. At any one frequency most of the elements draw little current from it. Each successive element is connected in an opposite phase to the active connection running as a transmission line along the boom. For that reason, that transmission line can often be seen zigzagging across the support boom holding the elements.

4.6 Virtual SATCOM Design of Log Periodic Antenna for Antenna array.

As presented in [41], in the design of LPDA antennas, there are three essential parameters to define. First, is the scaling factor (τ), which is the ratio that describes the change in length of each successive element (equation 21). Second, is the spacing factor (σ) (equation 22) that defines the ration of space between dipole elements in relation to their length. And, third, is the angle α , defined as $\frac{1}{2}$ the angle between vectors that pass through the ends of all the elements (equation 23).

$$\tau = \frac{R_n}{R_{n+1}} \quad (21)$$

$$\sigma = \frac{R_{n+1} - R_n}{2\ell_{n+1}} \quad (22)$$

$$\alpha = \tan^{-1} \left[\frac{1-\tau}{4\sigma} \right] \quad (23)$$

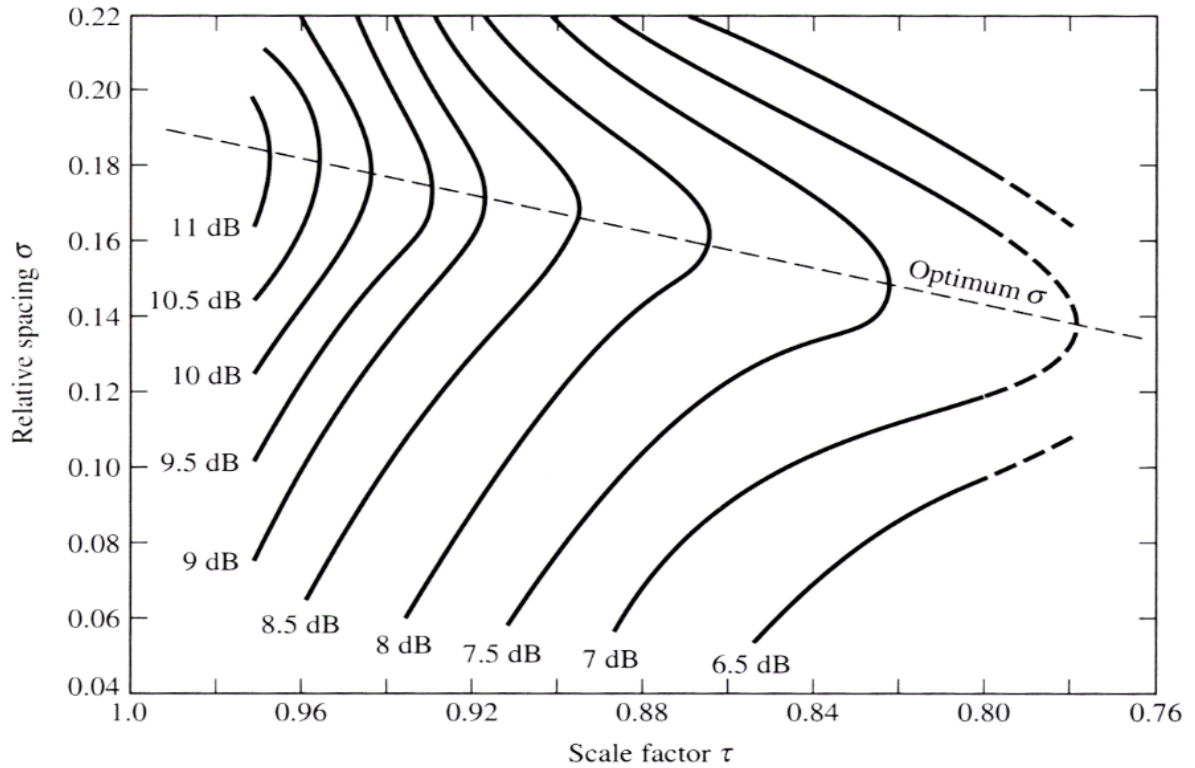


Figure 25. Computed contours of constant directivity versus τ and σ . [41] page, 609.

4.7 Log Periodic Antenna Design Procedure for Virtual SATCOM

The steps below show how the LPDA antenna is designed. This is the procedure used to calculate the dimensions of the Virtual SATCOM elements following the method defined in Balanis [41].

Step one, assume a given directivity and determine τ and σ . For this system, $D_o=7$ dB.

From Figure 25: $\tau=0.78$; $\sigma=0.14$

Step two, determine α using equation (41)

$$\alpha = \tan^{-1} \left[\frac{1-\tau}{4\sigma} \right] = \tan^{-1} \left[\frac{1-0.78}{4(0.14)} \right] = 21.5^\circ$$

Step three, using equation 24 and 25, calculate the bandwidth of the active region B_{ar} and designed bandwidth B_s :

$$B_{ar} = 1.1 + 7.7(1-\tau)^2 \cot \alpha \quad (24)$$

$$B_{ar} = 1.1 + 7.7(1-0.78)^2 \cot(21.5^\circ)$$

$$B_{ar} = 1.1 - 7.7 * 0.048 * 2.539 = 2.038$$

$$B_s = BB_{ar}$$

$$B_s = \left(\frac{28}{7} \right) (2.038) = 8.152 \quad (25)$$

Step four, find the length of the antenna (L) using equation 26:

$$L = \frac{\lambda_{\max}}{4} \left(1 - \frac{1}{B_s} \right) \cot \alpha \quad (26)$$

$$\text{Where } \lambda_{\max} = 2(l_{\max}) = \frac{c}{f_{\min}} = \frac{3e8}{7e6} = 42.9$$

$$L = \frac{42.9}{4} \left(1 - \frac{1}{8.152} \right) 2.539 = 23.9$$

Step five, determine the number of elements (N) using equation 27.

$$N = 1 + \left(\frac{\ln(Bs)}{\ln\left(\frac{1}{\tau}\right)} \right) \quad (27)$$

$$N = 1 + \frac{2.098}{.248} = 9.44, \text{ so: } N = 10 \text{ elements}$$

Step six, determine average characteristic impedance (Z_a) using equation 28:

$$Z_a = 120 \left[\ln \left(\frac{\ell_n}{d_n} \right) - 2.25 \right] \quad (28)$$

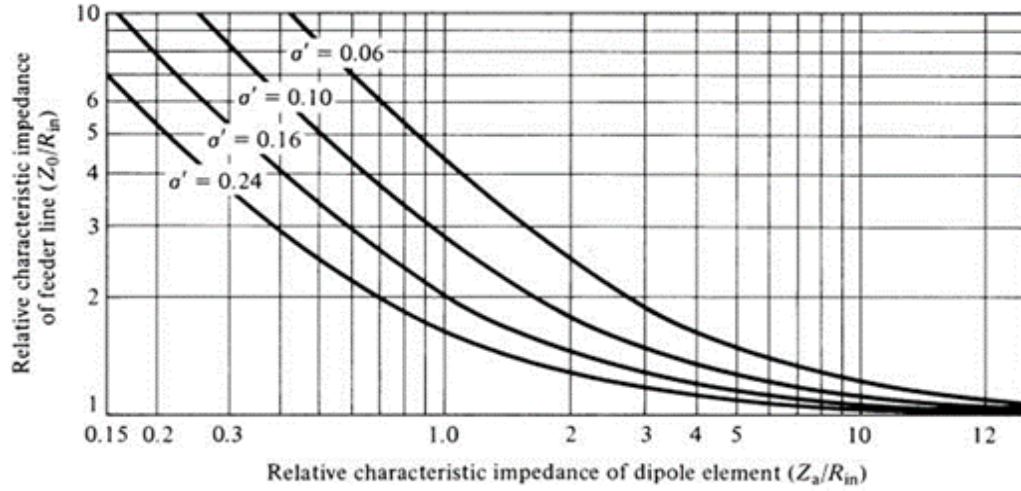


Figure 26. Relative Characteristics impedance of a feeder line as a function of relative characteristics impedance of a dipole element [41], page 611.

where $\frac{\ell_n}{d_n}$ is the length to diameter of the n^{th} element of the array. For this example, assuming $\frac{1}{2}$ inch

copper wire then: $d_{\text{max}} = 0.013$ m at lowest frequency:

$$\ell_{\text{max}} = \frac{\lambda_{\text{max}}}{2} = \frac{42.9}{2} = 21.45$$

$$\frac{\ell_{\text{max}}}{d_{\text{max}}} = \frac{21.45}{0.013} = 1650.0$$

so,

$$Z_a = 120 \left[\ln(1650) - 2.25 \right] = 619 \Omega$$

Using feeder wire of 50 ohms then: $Z_a/R_o = 619/50 = 12.38$

Step seven, determine relative mean spacing (σ') with equation 29 and Z_o/R_{in} using the chart in Figure 26.

$$\sigma' = \frac{\sigma}{\sqrt{\tau}} = \frac{0.14}{\sqrt{0.78}} = 0.159 \quad (29)$$

Using a value of 12.38 for Z_a/R_{in} and $\sigma' = 0.16$ the Z_0/R_{in} is ~ 1.0 , so $Z_0 = R_{in} = 50\Omega$

Step eight, calculate the center to center spacing (s) using equation 30:

$$s = d \cosh\left(\frac{Z_0}{120}\right) \quad (30)$$

$$s = 0.013 \cosh\left(\frac{50}{120}\right) = .015 \text{ m} \approx 0.6 \text{ in}$$

4.8 Results of Virtual SATCOM Design using Matlab LPDA Design Program

Within Matlab R2016a, a subprogram developed by Ramann Mantha [42] was used to provide an analysis of this LPDA antenna. The Design of a Log Periodic Dipole Antenna program designed an antenna that would function between 4.58 MH and 37.7 MHz and is 20 meters longer than the analysis using the Balanis procedure above. The results are listed in Table 4. Both reviews show that an LPDA antenna could be constructed to operate across the bandwidth required.

Table 4. MATLAB Results of LPDA Design

DATA from MATLAB	Value	N = 10.000000	L 9 = 25.214805	R 9 = 29.599988
Enter the Value of Directivity =	7	f1 = 4.580642	L 8 = 19.415400	R 8 = 22.791991
Enter the Lower Cut-Off Frequency (in MHz) =	7	f2 = 37.677431	L 7 = 14.949858	R 7 = 17.549833
Enter the Upper Cut-Off Frequency (in MHz) =	28	$\lambda_{\text{max}} = 65.493000$	L 6 = 11.511391	R 6 = 13.513372
$\sigma =$	0.135	L = 33.768004	L 5 = 8.863771	R 5 = 10.405296
$\tau =$	0.77	L 10 (max) = 32.746500	L 4 = 6.825103	R 4 = 8.012078
$\alpha =$	23.07	R 10 (max) = 38.441543	L 3 = 5.255330	R 3 = 6.169300
$B_{ar} =$	2.05634	L-actual = 34.783765	L 2 = 4.046604	R 2 = 4.750361
$B_s =$	8.225	Spacing factor = 0.0135000	L 1 = 3.115885	R 1 = 3.657778

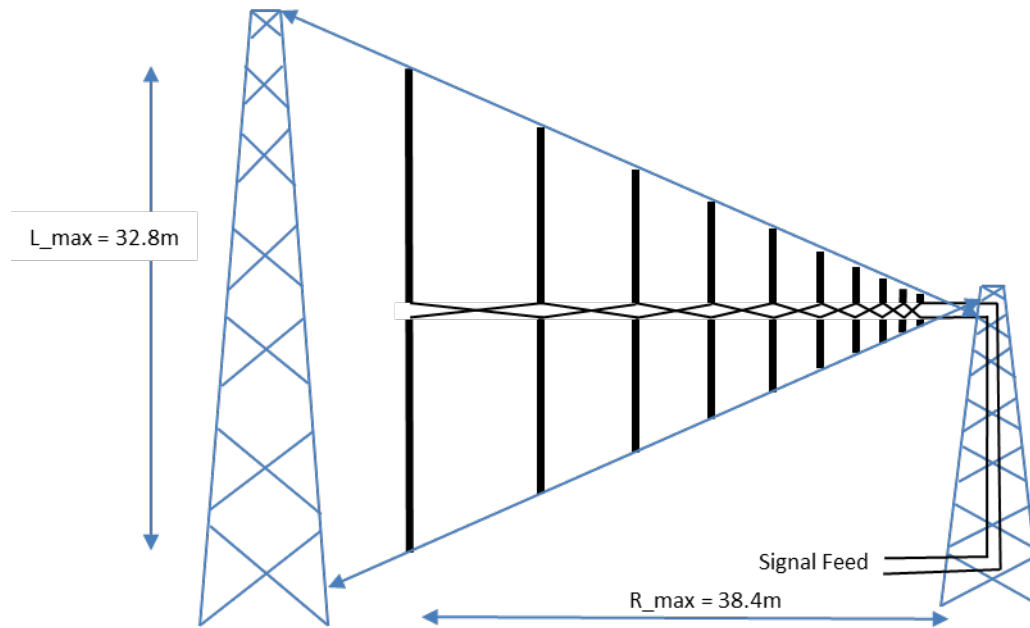


Figure 27. Virtual SATCOM antenna element design. It is a vertical wire LPDA suspended from towers. In the Virtual SATCOM design, 200 elements will be set side by side with 10-meter spacing.

4.9 Virtual SATCOM Antenna Array

The antenna designed above has a gain of 7 dB, and it is a large structure. It is a suitable design for communication from fixed sites, but as a single antenna, it is too large and not an appropriate model for mobile customers. Due to the size of this LPDA antenna in the HF band, a more practical option for a directional system is an electronically scanning array of LPDA elements. The term for this type of antenna is called an active, electronically scanned array (AESA). It is a phased array antenna, which is a computer-controlled where the RF beam can be electronically steered to point in different directions without moving the antenna. The Virtual SATCOM antenna system uses numerous fixed antennas equally spaced and controls the beam steering by varying the phase of the signals to each antenna element. This is accomplished by using the antenna spacing and controlling the phase delay, which will change the direction of the electromagnetic field vector. There are many array geometries including: linear, rectangular and circular. In designing the Virtual SATCOM system, the linear array was selected due to the physical space and cost considerations. The Virtual SATCOM array can be considered a hybrid array with the use of LPDA elements in a linear line. This could be viewed as a rectangular array. In the LPDA, not every component of the antenna array is resonating at the same time, so this design will employ a linear array.

4.10 Virtual SATCOM Linear Array Design

In the Virtual SATCOM concept, the base station is not limited in size and can accommodate an array of many individual elements to focus the radiation in the desired direction. The whole field generated by the array is the vector addition of each element. At this point in the analysis, the mutual coupling is neglected but will be considered later in this dissertation. In an array, the antenna element to element, mutual coupling, describes energy absorbed by one antenna's receiver when another nearby antenna is operating. Mutual coupling is typically undesirable because an adjacent antenna absorbs energy that should be radiated away. To understand the array, a discussion is presented to show the logic of the array architecture. To build an array where the individual element fields interfere constructively depends on:

- The geometric configuration of the array, i.e., linear, circular etc.
- Distance between each element
- Excitation amplitude of each element
- Excitation phase of each element

4.11 Two Element Arrays

I am starting with the assumption that a 2-element array is composed of two infinitesimal small horizontal dipoles positioned along the z-axis, as shown in Figures 28 and 29. Assuming no coupling, the total E field is the addition of the two elements in equation 31 where the phase difference between the elements is β . This implies the same magnitude for both elements. Antenna current is I where l is the antenna length, η is the impedance of free space, and \hat{a}_θ is a unit vector in the θ direction.

$$\bar{E}_t = \bar{E}_1 + \bar{E}_2 = \bar{a}_\theta j\eta \frac{kI_o l}{4\pi} \left\{ \frac{e^{-j\left(kr_1 - \frac{\beta}{2}\right)}}{r_1} |\cos \theta_1| + \frac{e^{-j\left(kr_2 + \frac{\beta}{2}\right)}}{r_2} |\cos \theta_2| \right\}. \quad (31)$$

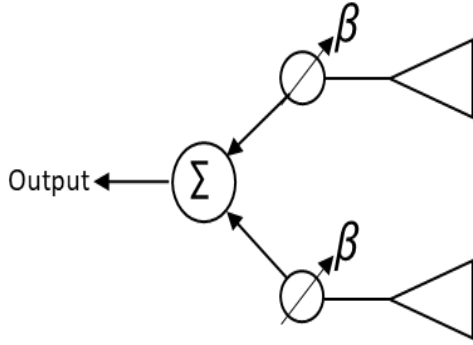


Figure 28. Diagram of two element antenna array with uniform amplitude.

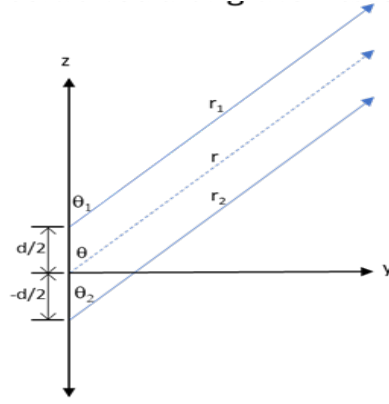


Figure 29. Diagram of two element array with separation of distance (d) and signal direction angle of θ relative to antenna array axis.

In the far-field assume:

$$r_1 = r - \frac{d}{2} \cos \theta \text{ for phase variations}$$

$$r_2 = r + \frac{d}{2} \cos \theta \text{ for phase variations}$$

$$r_1 \cong r_2 \cong r \text{ for amplitude variations}$$

$$\theta_1 \cong \theta_2 \cong \theta \text{ for amplitude variations}$$

Thus, substituting into equation 25:

$$E_t = \hat{a}_\theta j\eta \frac{kI_o l}{4\pi r} e^{-jkr} |\cos \theta| \left\{ \frac{e^{\left(jkd\frac{1}{2}\cos\theta + j\beta\frac{1}{2}\right)}}{1} + \frac{e^{\left(-jkd\frac{1}{2}\cos\theta - j\beta\frac{1}{2}\right)}}{1} \right\} \text{ Factor out } e^{-jkr} \text{ and } \cos \theta$$

$$E_t = \hat{a}_\theta j\eta \frac{kI_o l}{4\pi r} e^{-jkr} |\cos \theta| \left\{ e^{j\frac{1}{2}(kd \cos \theta + \beta)} + e^{-j\frac{1}{2}(kd \cos \theta + \beta)} \right\}.$$

Recalling Euler's formula for Cosine:

$$\cos \phi = \left(\frac{e^{j\phi} + e^{-j\phi}}{2} \right) \text{ and } \phi = \frac{1}{2}(kd \cos \theta + \beta).$$

The electric field can be reduced to:

$$E_t = \hat{a}_\theta j\eta \frac{kI_o l}{4\pi r} e^{-jkr} |\cos \theta| \left(\frac{2}{1} \right) \left\{ \frac{e^{j\frac{1}{2}(kd \cos \theta + \beta)} + e^{-j\frac{1}{2}(kd \cos \theta + \beta)}}{2} \right\}.$$

$$E_t = \hat{a}_\theta j\eta \frac{kI_o l}{4\pi r} e^{-jkr} |\cos \theta| (2) \left\{ \cos \left[\frac{1}{2} (kd \cos \theta + \beta) \right] \right\}. \quad (32)$$

Equation 32 shows that the entire field of the array is equal to the single element contribution multiplied by the array factor. Therefore,

$$\hat{a}_\theta j\eta \frac{kI_o l}{4\pi r} e^{-jkr} |\cos \theta| \text{ is the single element contribution to total E field.}$$

And

$$(2) \left\{ \cos \left[\frac{1}{2} (kd \cos \theta + \beta) \right] \right\} \text{ is the array factor (AF) for a } N = 2 \text{ element array.}$$

$$AF_N = N \cos \left[\frac{1}{2} (kd \cos \theta + \beta) \right] \text{ is the normalized AF.} \quad (33)$$

To summarize, the array factor is a function of the number of array elements (N), the wavenumber (k); distance between elements (d); phase shift (β) between each antenna feed; and the angle θ to the object. For the Virtual SATCOM design, the distance will be fixed and β will be controlled to focus the field in the θ direction for a given frequency.

4.12 N-Element Linear Array

Figure 30 is a multi-element array showing the location of the phase shifter and the summation of the input from each antenna.

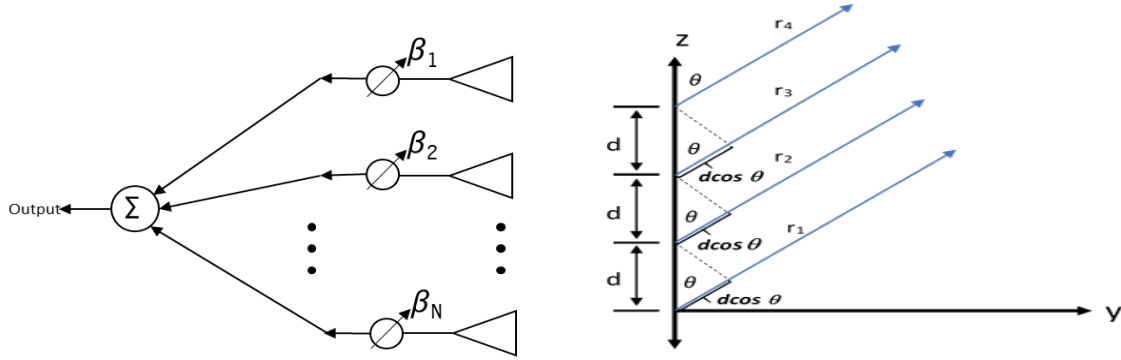


Figure 30. On the left is a diagram of an N element array that is evenly spaced with uniform amplitude. On the right is a diagram of the antenna pattern of N= 4 element array with separation of distance (d) and signal direction angle of θ relative to antenna array axis (Z).

To calculate the array factor, assuming uniform amplitude and spacing, the array factor can be generalized to N elements. The Array Factor is:

$$AF = 1 + e^{j\psi} + e^{i2\psi} + \dots e^{j(N-1)\psi} \text{ where } \psi = kd \cos \theta + \beta.$$

$$AF = \sum_{n=1}^N e^{j(n-1)\psi}.$$
(34)

Multiply both sides by $e^{j\psi}$

$$AF(e^{j\psi}) = e^{j\psi} (1 + e^{j\psi} + e^{i2\psi} + \dots e^{j(N-1)\psi}) = e^{j\psi} + e^{i2\psi} + \dots e^{j(N)\psi}.$$

Now subtract AF from $AF(e^{j\psi})$.

$$AF(e^{j\psi}) - AF = e^{j\psi} + e^{i2\psi} + \dots + e^{j(N)\psi} - 1 - e^{j\psi} - e^{i2\psi} \dots - e^{j(N-1)\psi}.$$

$$AF(e^{j\psi} - 1) = -1 + e^{j(N)\psi}.$$

With a little manipulation and factoring:

$$AF = e^{j\frac{N-1}{2}\psi} \left(\frac{\sin\left(\frac{N}{2}\psi\right)}{\sin\left(\frac{1}{2}\psi\right)} \right).$$
(35)

If the reference point is the physical center of the array, then the array factor of equation 36 reduces to:

$$AF = \frac{\sin\left(\frac{N}{2}\psi\right)}{\sin\left(\frac{1}{2}\psi\right)}. \quad (36)$$

For small values of ψ , the above equation can be approximated to:

$$AF \approx \left[\frac{\sin\left(\frac{N}{2}\psi\right)}{\left(\frac{1}{2}\psi\right)} \right]. \quad (37)$$

If the array factor is normalized in equation 38:

$$AF_{normalized} = AF_n = \left(\frac{1}{N} \right) \left[\frac{\sin\left(\frac{N}{2}\psi\right)}{\left(\frac{1}{2}\psi\right)} \right] = \left[\frac{\sin\left(\frac{N}{2}\psi\right)}{\left(\frac{N}{2}\psi\right)} \right]. \quad (38)$$

As shown in equation 38, AF_n is a form of $|(\sin x)/x|$ as graphed in Figure 31.

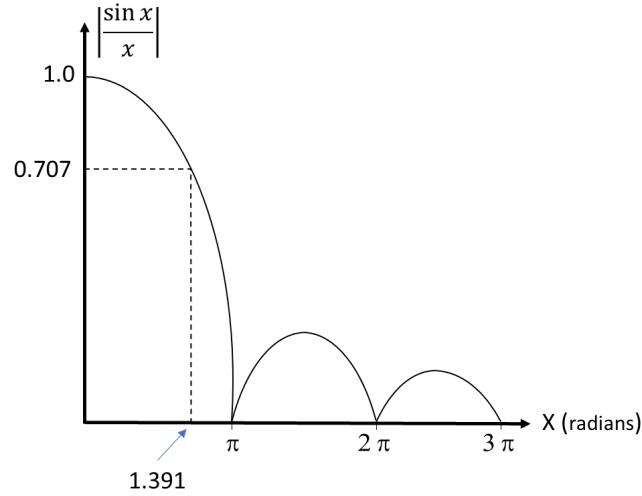


Figure 31. Graph of $|(\sin x)/x|$.

The limit of $\lim_{\delta x \rightarrow 0} \left(\frac{\sin x}{x} \right) = 1$. Therefore, the maximum value of the normalized array factor occurs when:

$$\frac{\psi}{2} = \frac{1}{2}(kd \cos \theta + \beta) = \pm m\pi$$

$$\theta_{(\text{maximum})} = \cos^{-1}\left(\frac{\lambda}{2\pi d}\right)(-\beta \pm 2m\pi) \quad (39)$$

Since AF_n is proportional to total E field and E^2 is proportional to power, then the half-power normalized array factor is equal to $\frac{1}{\sqrt{2}}$ or approximately 0.707. Thus,

$$\frac{\sin x}{x} = .707, \text{ so } x = \pm 1.391 \quad (40)$$

Applying equation 39 to equation 40:

$$\frac{N}{2}\psi = \frac{N}{2}(kd \cos \theta + \beta) = \pm 1.391 \quad (41)$$

Now substituting $k = 2\pi/\lambda$ and solving for the half-power angle, $\theta_{\text{half power}}$ is:

$$\theta_{\text{halfpower}} = \cos^{-1}\left[\frac{\lambda}{2\pi d}\left(-\beta \pm \frac{2.782}{N}\right)\right] \quad (42)$$

The half-power beamwidth $\Theta_{\text{half power}}$ can be found by subtracting the θ_{max} from $\theta_{\text{half power}}$ then multiplying by 2.

$$\theta_{\text{halfpower}} = 2\left|\theta_{\text{max}} - \theta_{\text{halfpower}}\right| \quad (43)$$

Substituting 39 and 42 into 43 gives:

$$\theta_{\text{halfpower}} = 2\left[\left(\cos^{-1}\left(\frac{\lambda}{2\pi d}\right)(-\beta \pm 2m\pi)\right) - \left(\cos^{-1}\left[\frac{\lambda}{2\pi d}\left(-\beta \pm \frac{2.782}{N}\right)\right]\right)\right] \quad (44)$$

At the first maximum, when $m=0$, equation 44 reduces to:

$$\theta_{\text{halfpower}} = 2\left|\frac{\pi}{2} - \cos^{-1}\left(\pm \frac{2.782\lambda}{2\pi dN}\right)\right| \quad (45)$$

As the number of array elements increases, the \cos^{-1} term approaches $\pi/2$ and a half-power beamwidth becomes narrower. The length of the array is equal to Nd . For an array with many elements,

the length can be approximated as $N \cdot d$. In other words, the half-power beamwidth is a function of array length, not the number of antennas alone. If the number of elements is doubled but the spacing is reduced by half, the half-power beamwidth would be the same.

$$L = (N - 1)d \cong Nd$$

$$\theta_{halfpower} = 2 \left| \frac{\pi}{2} - \cos^{-1} \left(\pm \frac{2.782\lambda}{2\pi L} \right) \right| \quad (46)$$

Table 5 is a list of the broadside HPBW for a different number of elements (N) at frequencies of 7, 14, and 28 MHz. The distance between elements is 10 meters throughout. Table 5 shows that a 100-element array would bring the beam width to approximately 2° at the low end (7 MHz) and 0.5° at the high end (28MHz). In the Virtual SATCOM design, a 200-element array was selected. The basis was the narrow beam size without driving the number of elements to an unreasonable size. For perspective, a standard 10,000-foot runway is just over 3 km in length. Therefore, a Virtual SATCOM system could fit inside a typical size airfield.

4.13 Virtual SATCOM Radiation Pattern Analysis Using MATLAB

A MATLAB program was used to develop and visualize the array's pattern. Different size arrays and different element types and sizes were tested. The objective was to find an array that would perform across the system's frequency envelope from 7- 28 MHz. The requirement is a clean narrow beam with a minimum of 20 dBi of gain. This is not a trivial engineering requirement, as that system must operate

Table 5. Half Power Beam Width (HPBW) for Arrays at select frequencies

HALF POWER BEAMWIDTH (HPBW) BROADSIDE ARRAYS				
Frequency (MHz)		7	14	28
Lambda (m)		42.857	21.429	10.714
Distance between elements (m)		10.000		
Number of Array Elements	Total Array Length	7 MHZ Half Power Beamwidth (Degrees)	14 MHZ Half Power Beamwidth (Degrees)	28 MHZ Half Power beamwidth (Deg)
2	10	143.169	56.640	27.442
4	30	56.640	27.442	13.622
8	70	27.442	13.622	6.799
10	90	21.877	10.889	5.438
20	190	10.889	5.438	2.718
40	390	5.438	2.718	1.359
50	490	4.350	2.175	1.087
100	990	2.175	1.087	0.544
150	1490	1.450	0.725	0.362
200	1990	1.087	0.544	0.272
250	2490	0.870	0.435	0.217

across two full octaves of frequency (7-14MHz and 14-28 MHz). Testing was performed using monopole and dipole antennas. The best results obtained were 200 dipoles or monopoles with 10-meter spacing between elements. Figures 32 through 35 are images of a 200-element monopole array at 7, 14, 21 and 28 MHz. Tapering was applied to reduce sidelobes. These images are in free space; however, in a real array the ground plane would attenuate the energy below the axis and the back lobe would be suppressed leaving only one-quarter of the antenna radiating into free space. The images show excellent directivity from the horizon to a very high elevation angle. For long range communication, the low elevation angles from 5-30° are the most important, but higher elevations will be required for shorter range propagation.

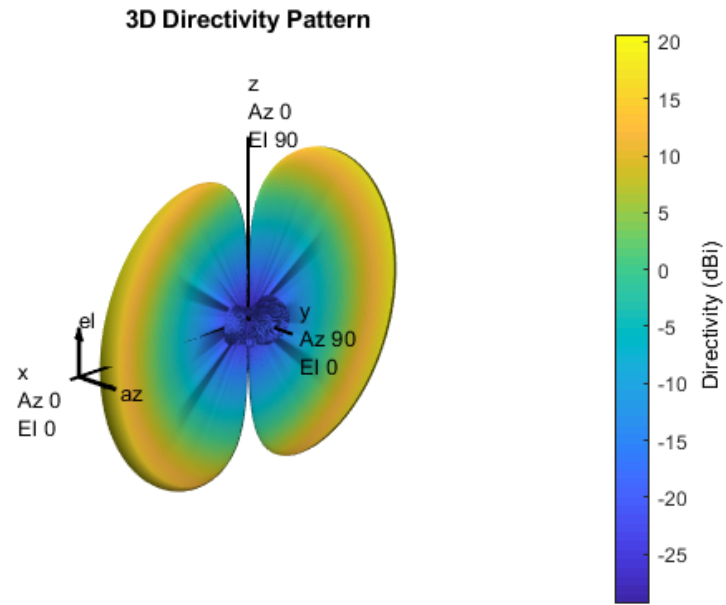


Figure 32. Shows 3D pattern of 200 dipole element array at 7 MHz with 10 m spacing.

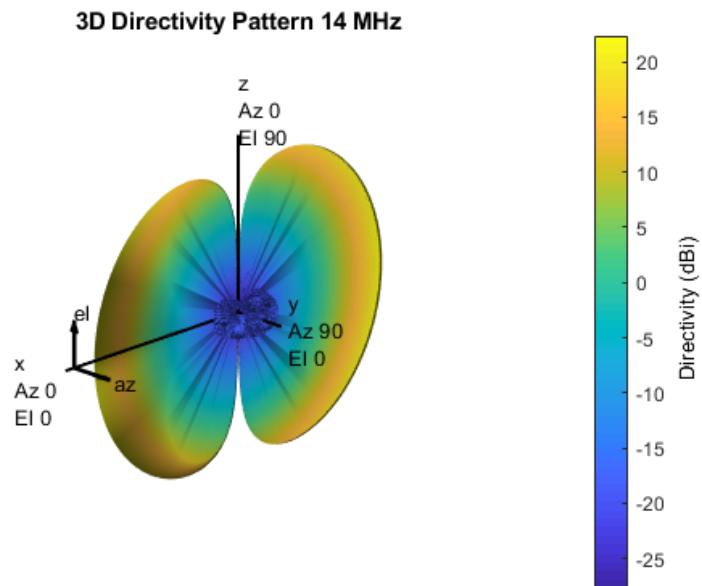


Figure 33. Shows 3D pattern of 200 dipole element array at 14 MHz with 10m spacing.

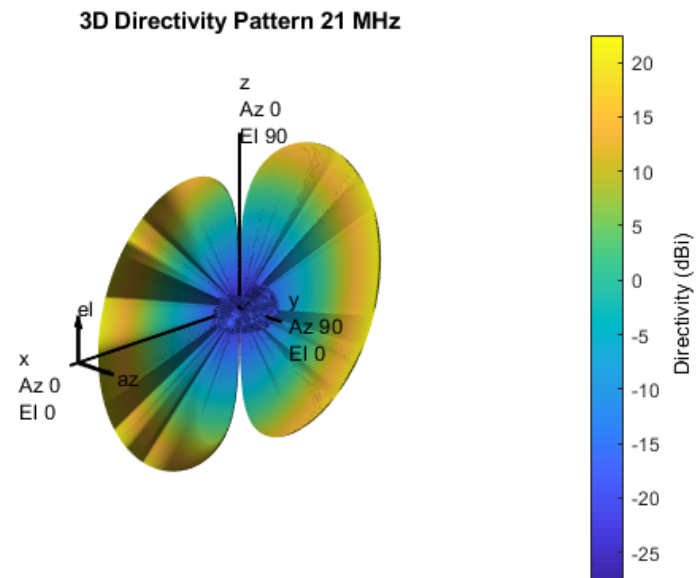


Figure 34. Shows 3D pattern of 200 dipole element array at 21 MHz with 10m spacing.

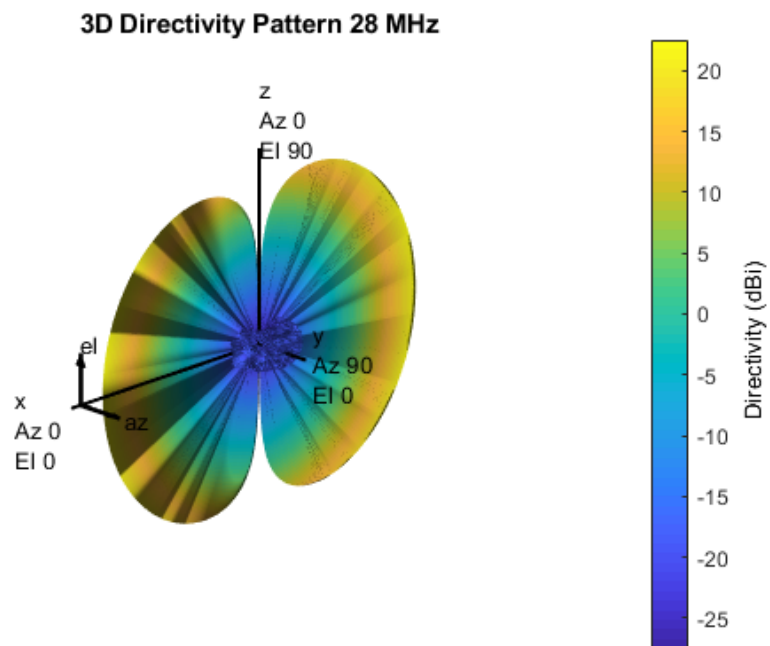


Figure 35. Shows 3D pattern of 200 dipole element array at 28 MHz with 10m spacing.

4.14 Phase Steering

The system requires the array at the ground station to have the capability to steer the narrow beam to the intended mobile unit. By controlling the phase excitation (β) in equation 47, the antenna's focus can be adjusted. In the figures above, the phase excitation is zero and the focus is broadside at 90° to the array. This assumes a plus or minus 60° field of view i.e. θ range of $30^\circ \leq \theta \leq 150^\circ$. Hence, phase excitation must be as follows:

$$\psi = kd \cos \theta + \beta = 0 \text{ so } \beta = -kd \cos(\theta) \quad (47)$$

For example, if θ is 60° then $\beta = -kd \cos(60^\circ)$. Therefore, by controlling the progressive phase difference between the elements, the max radiation can be pointed in any direction to form a scanning array. In an array operating at 7 MHz, $\lambda = 42.8$ m, and $d = 10$ m then $\beta = -214.3^\circ$ for 60° off broadside angle.

4.15 Directivity and Gain

Directivity is a parameter of an antenna system that measures the degree to which the radiation emitted is concentrated in a single direction. It is included in the systems antenna gain. In electromagnetics, antenna gain is an important performance number that combines the antenna's directivity and electrical efficiency. At a transmitting antenna, the gain describes how well the antenna converts input power into radio waves pointed in a specified direction. At a receiving antenna, the gain describes how well the antenna converts radio waves arriving from a specified direction into electrical power. When no direction is specified, gain is understood to refer to the peak value of the gain. A plot of the gain as a function of direction is called the radiation pattern. Our system design requires a narrow beam width to segregate, and this will have a secondary effect of increasing the gain of the ground station. Moreover, this will affect the power at the receiver and positively impact the signal to noise ratio.

Gain is related to directivity by antenna efficiency factors as:

$$\begin{aligned} G_0 &= e_0 D \text{ and } e_0 = e_r e_c e_d \\ G_0 &= e_0 D \end{aligned} \quad (48)$$

where:

e_0 = total efficiency (dimensionless)
 e_r = reflection (mismatch) efficiency $e_r = (1 - |\Gamma|^2)$
 e_c = conduction efficacy
 e_d = dielectric efficacy
 Γ = voltage reflection coefficient at the input of the antenna.
 Z = reference impedance

$$\Gamma = \frac{Z_{in} - Z_{out}}{Z_{in} + Z_{out}} \quad (49)$$

$$VSWR = \text{voltage standing wave ratio} = \frac{1 + |\Gamma|}{1 - |\Gamma|}$$

The antenna is most efficient when $Z_{out} = Z_{in}$, and Γ approaches zero. The variable Z is the impedance of the system between the transmitter or the antenna, the transmission line to the antenna, and the antenna. It is a complex quantity and a function of the frequency, resistance, capacitance and inductance of the system. A VSWR below 2.0 is considered excellent. This is important because this system is using a focused beam at wide bandwidth to avoid interference with other users of the spectrum. Therefore, the higher the gain, the higher spectral separation from other users and the higher the signal to noise and interference. Controlling the impedance increases the efficiency and results in higher received power at the receiver. The Virtual SATCOM system selected LPDA antenna elements because they have controllable impedance across a larger bandwidth. Besides controlling gain in the desired direction, the antenna system reduces the power of unwanted human-made interference and noise from outside the focused beam.

A more precise definition of directivity is defined as the ratio of radiation intensity in a direction from the antenna compared to the radiation intensity averaged over all directions. The average radiation intensity (U_0) is equal to the total power radiated by the antenna divided by 4π .

$$U_0 = \frac{P_{rad}}{4\pi} \quad (50)$$

$$D_{max} = \frac{U_{max}}{U_0} = \frac{4\pi U_{max}}{P_{rad}} \quad (51)$$

4.16 Radiation Intensity and Radiation Power Density

Electromagnetic waves used to transport information across wireless channels have energy. The Poynting vector is a parameter that describes this power as written in equation 52.

$$\mathcal{W} = \mathcal{E} \times \mathcal{H} \quad (52)$$

where:

\mathcal{W} = instantaneous Poynting vector (W/m²)

\mathcal{E} = instantaneous electric field intensity (V/m)

\mathcal{H} = instantaneous magnetic field intensity (A/m)

Note: script letters are used to indicate instantaneous fields, while Roman letters are used to represent their complex counterparts. By integrating the Poynting vector normal component over a surface, the instantaneous power density can be determined.

$$\mathcal{P} = \oint\oint_S \mathcal{W} \cdot d\mathbf{s} = \oint\oint_S \mathcal{W} \cdot \hat{\mathbf{n}} da \quad (53)$$

where

$$\begin{aligned} \mathcal{P} &= \text{instantaneous power density (W)} \\ \mathbf{n} &= \text{unit vector normal to the surface} \\ da &= \text{infinitesimal area of the closed surface (m}^2\text{)} \end{aligned}$$

To find the time average Poynting vector for periodic signals, we convert to a complex phasor form:

$$\begin{aligned} \mathcal{W} = \mathcal{E} \times \mathcal{H} &= \frac{1}{2} \text{Re}[\mathbf{E} \times \mathbf{H}^*] + \frac{1}{2} \text{Re}[\mathbf{E} \times \mathbf{H}^* e^{j2\omega t}] \\ W_{\text{avg}}(x, y, z) &= [\mathcal{W}(x, y, z, t)]_{\text{avg}} = \frac{1}{2} \text{Re}[\mathbf{E} \times \mathbf{H}^*] \text{ (W/m}^2\text{)} \end{aligned} \quad (54)$$

The factor of ½ appears because the E and H fields represent peak values, not root mean square (RMS) values. The second term in the top equation is a rotating vector and, therefore, averages to zero and is not included in equation 54.

Based on equations 53 and 54, the average power radiated can be written as:

$$\begin{aligned} P_{\text{rad}} = P_{\text{av}} &= \oint\oint_S \mathbf{W}_{\text{rad}} \cdot d\mathbf{s} = \oint\oint_S \mathbf{W}_{\text{av}} \cdot \hat{\mathbf{n}} da \\ P_{\text{rad}} &= \frac{1}{2} \oint\oint_S \text{Re}[\mathbf{E} \times \mathbf{H}^*] \cdot d\mathbf{s} \text{ (W)} \end{aligned} \quad (55)$$

4.17 Radiation Intensity of Antenna Arrays

The radiation intensity is defined as the power radiated from an antenna per unit solid angle. Another way of thinking about radiation intensity is normalized power density with respect to range loss ($1/r^2$).

$$\begin{aligned} U &= r^2 W_{\text{rad}} \quad \text{or} \\ W_{\text{rad}} &= \frac{U}{r^2} \end{aligned} \quad (56)$$

where:

U = radiation intensity (Watts/unit solid angle)
 W_{rad} = radiation power density (W/m²)
 r = distance from antenna element.

The array factor is a multiplier of the electric field (E). Thus, the square of the array factor is proportional to radiation intensity.

$$U(\theta) = [AF_n]^2 = \left[\frac{\sin(\frac{N}{2}kd \cos \theta)}{\frac{N}{2}kd \cos \theta} \right]^2 = \left[\frac{\sin(\psi)}{\psi} \right]^2 \quad (57)$$

$$\psi = \frac{N}{2}kd \cos \theta$$

Since the array factor is normalized between 0 to 1, radiation intensity has a max value of 1.0.

For a broadside array, this occurs at $\theta = 90^\circ$ or $(\pi/2 \text{ rad})$. Thus, the average intensity (U_0) is

$$U_0 = \frac{1}{4\pi} P_{\text{rad}} = \frac{1}{2} \int_0^\pi \left[\frac{\sin(\psi)}{\psi} \right]^2 \sin \theta d\theta \quad (58)$$

$$\psi = \frac{N}{2}kd \cos \theta, \quad d\psi = -\frac{N}{2}kd \sin \theta$$

$$U_0 = \frac{1}{2} \int_0^\pi \left[\frac{\sin\left(\frac{N}{2}kd \cos \theta\right)}{\frac{N}{2}kd \cos \theta} \right]^2 \sin \theta d\theta$$

Therefore, equation 58 can be written as:

$$U_0 = -\frac{1}{Nkd} \int_{+Nkd/2}^{-Nkd/2} \left[\frac{\sin(\psi)}{\psi} \right]^2 d\psi = \frac{1}{Nkd} \int_{-Nkd/2}^{+Nkd/2} \left[\frac{\sin(\psi)}{\psi} \right]^2 d\psi \quad (59)$$

For a large array with large N, the $(Nkd/2)$ term can be approximated by extending the limits to infinity.

$$U_0 = \frac{1}{Nkd} \int_{-Nkd/2}^{+Nkd/2} \left[\frac{\sin(\psi)}{\psi} \right]^2 d\psi = \frac{1}{Nkd} \int_{-\infty}^{+\infty} \left[\frac{\sin(\psi)}{\psi} \right]^2 d\psi \quad (60)$$

Since

$$\int_{-\infty}^{+\infty} \left[\frac{\sin(\psi)}{\psi} \right]^2 d\psi = \pi$$

This reduces to:

$$U_0 = \frac{\pi}{Nkd} \quad (61)$$

Applied to Directivity:

$$D_0 = \frac{U_{\max}}{U_0} = \frac{(1)}{U_0} \cong \frac{(1)Nkd}{\pi} = \frac{N\left(\frac{2\pi}{\lambda}\right)d}{\pi} = 2N\frac{d}{\lambda} \quad (62)$$

The total length of the array is:

$$L = (N - 1)d \quad (63)$$

If $N \gg d$ then this can be reduced to:

$$\begin{aligned} N &= \frac{L}{d} + 1 \\ L &= (N - 1)d = Nd \end{aligned} \quad (64)$$

For large $L \gg \lambda$ and $\lambda > d$, equation 81 can be rewritten as:

$$D_0 = 2N\frac{d}{\lambda} = 2\left(\frac{L}{d} + 1\right)\frac{d}{\lambda} = 2\left(\frac{L}{\lambda} + \frac{d}{\lambda}\right) \quad (65)$$

For large broadside arrays ($L \gg \lambda$) this can be approximated as:

$$D_0 \cong 2\left(\frac{L}{\lambda}\right) \quad (66)$$

Restating this, the directivity of the large array is not a function of the number of elements or the spacing between them, but it is a function of the total length compared to the wavelength. For example, if the system requires a directivity of 20 dB at 7 MHz then:

$$\begin{aligned} 10 * \log_{10}\left(\frac{2L}{\lambda}\right) &= 20_{dB} \\ \log_{10}(2) + \log_{10}(L) - \log_{10}(\lambda) &= 2.0 \\ \log(L) &= 2.0 - \log(2) + \log(\lambda), \quad \lambda = 43 \\ \log(L) &= 2 - 0.3 + 1.6 = 3.3 \\ 10^{\log(L)} = L &= 10^{2 - \log 2 + \log \lambda} = 10^{1.7 + \log \lambda} \\ L &= 2100m \end{aligned}$$

Table 6. Directivity across the Virtual SATCOM Spectrum

Frequency (MHz)	Array Length L (m)	Wavelength λ (m)	Directivity D_o (dBi)
7	1990	43	19.6
14	1990	21.5	22.7
21	1990	14.3	24.5
28	1990	10.7	25.7
Note: The average directivity for a 200-element array with 10 m spacing is 23.13 dBi.			

Table 6 shows the directivity of the 200 elements Virtual SATCOM array at different frequencies. In this design, 7 MHz is the lowest frequency and longest wavelengths; consequently, this drives the total array length. The design goal of 20 dB of directivity results in an array length of 2100 m. In the design of the Virtual SATCOM array, we limited the design to 200 elements spaced at 10 m, resulting in a 1990 m array used from 7 to 28 MHz.

4.18 Non-Uniform Amplitude of Array Elements.

The analysis to this point assumes uniform spacing and uniform amplitude and a progressive phase shift. Now non-uniform amplitude with equal spacing will be considered in this section as seen in Figure 24. Numerous possible amplitude schemes could be applied. The complexity of the system has increased because two variables, phase (β) and amplitude weighting (w), must be calculated for each antenna element. However, the goal is to design a ground-based adaptive array of fixed geometry that can manipulate amplitude and phase to focus signal energy at a mobile receiver and extract transmitted energy from a mobile transmitter. Additionally, the system must operate at high speed while reacting to a dynamic channel path that changes as the ionosphere changes. Therefore, a design will include the ability to adjust both phase and amplitude weighing at each antenna element.

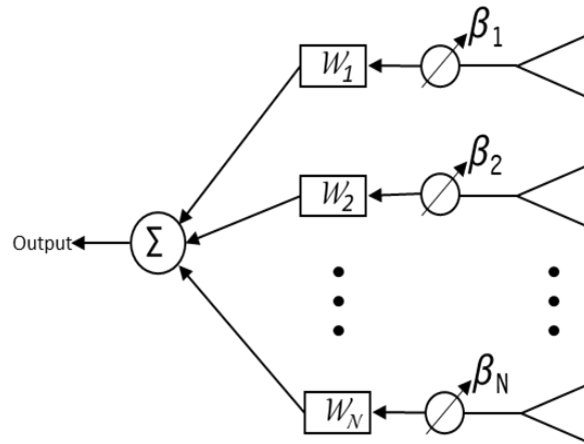


Figure 36. Diagram of Non-uniform amplitude array. Each of the N elements has its output modified by a phase shift (β) and amplitude weighting (W). By choosing different weighting algorithm, the radiation pattern of the array can be improved. This is particularly useful in reducing the sidelobes of the array.

Three commonly discussed amplitude weighting algorithms are uniform amplitude, binomial, and Dolph-Tschebyscheff (also called Chebyshev). Each algorithm has advantages and limitations. The uniform array where all amplitudes are the same has the narrowest beam but can have unacceptably high sidelobes as compared to the binomial, which has the smallest sidelobes. The Dolph-Tschebyscheff has a slightly wider beam but lower sidelobes over the uniform weighting. The binomial has a practical weakness in that for arrays with many elements, it results in a wide variation between the amplitude of elements. This would not be practical for a system with hundreds of elements. The Dolph-Tschebyscheff broadside array has many practical applications. This array suppresses the sidelobes and is a compromise between binomial and uniform array.

The application of this method does not increase the directivity of the main beam. In fact, it slightly widens the half-power beamwidth of the main beam. It is very effective in reducing the amplitude in the direction of sidelobes. If both a narrow main beam and sidelobe suppression are required, a slightly larger array with Dolph Tchebyscheff tapering will yield the desired beam width and sidelobe suppression. Amplitude weighting is called element weighting factors and denoted as w_n . The AF is now a factor of element amplitude (w_n); wavelength (λ); uniform distance between elements (d); angle of the signal of interest (θ) relative to array axis, and a progressive phase shift (β). In a broadside array looking at 90° the phase shift is zero. Element weighting adds a degree of complexity when calculating the element amplitude for each antenna element. The advantage of the Dolph-Tchebyscheff approach is that

the designer can design the level of sidelobe suppression required for all angles outside the main beam of the array.

$$AF_{2M}(even) = \sum_{n=1}^M w_n \cos[(2n-1)u] \quad (67)$$

$$AF_{2M+1}(odd) = \sum_{n=1}^{M+1} w_n \cos[2(n-1)u] \quad (68)$$

where:

$$u = \frac{\pi d}{\lambda} \cos \theta \quad (69)$$

The method introduced by Dolph in 1946 [43] for uniform spaced linear arrays, applies a class of polynomials developed by Tchebyscheff. These polynomials have equal amplitudes of magnitude 1 in the range between -1 and 1. In Figure 27, a comparison of a large uniformly linear array is presented. Each subfigure shows the directivity of a 200-element array with element spacing at 10 meters apart. The Y-axis is directivity, and the X-axis is azimuth angle. Zero degrees is broadside to the array. As the diagrams on the left indicate, as the frequency increases from 7 MHz to 28 MHz, the sidebands increase. In the transmit mode of the high-power array significant amounts of energy would be propagating in the wrong directions. This would cause considerable interference for other users of the spectrum. When operating in the receive mode, the side lobes would allow additional noise and interference into the front end of the system that would reduce SNR and increase BER.

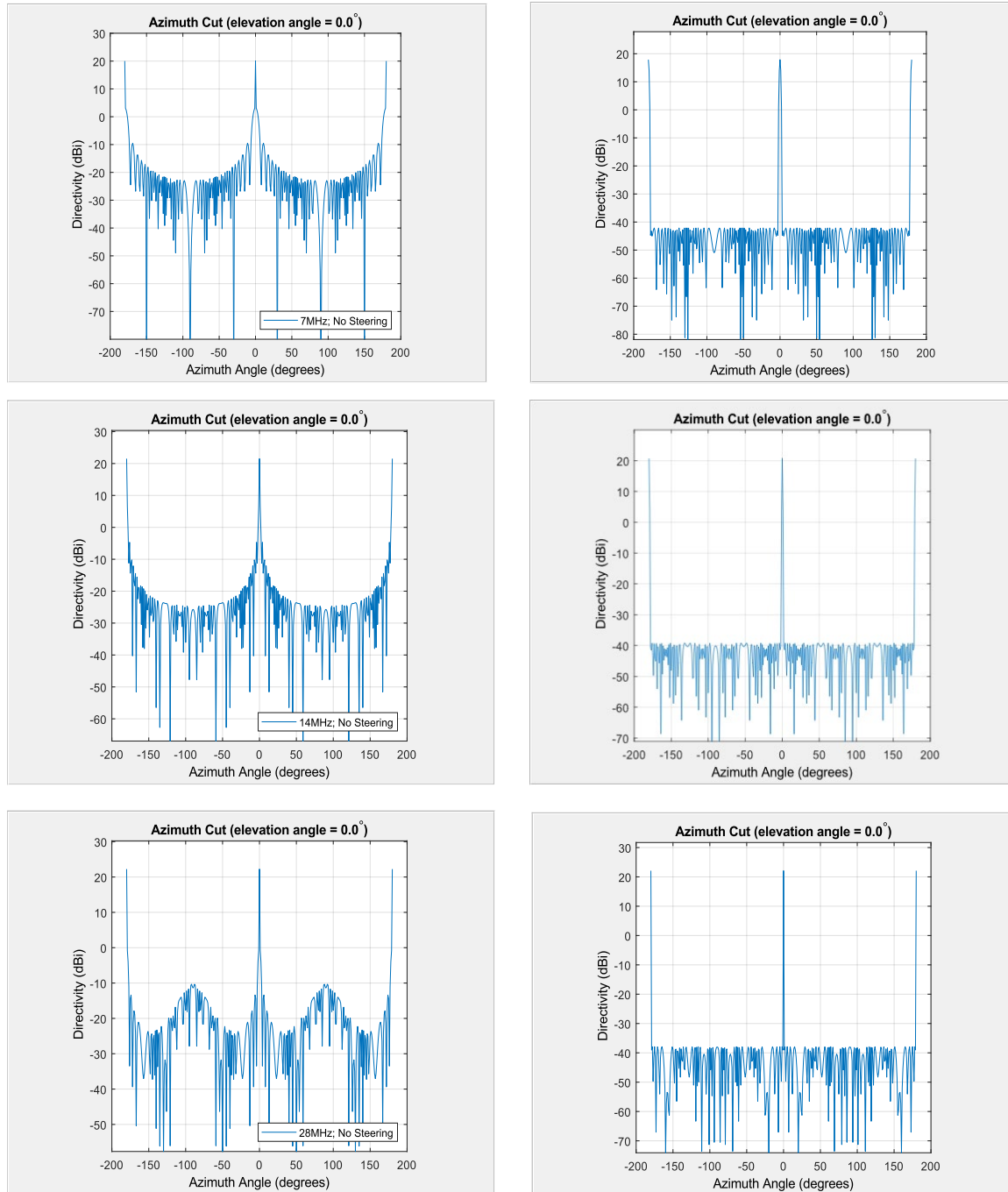


Figure 37. Aperture gain of a 200-element isotropic array with uniform spacing of 10m at 7, 14 and 28 MHz. The figures on the left do not have weighting and on the right is the same array with Dolph-Tschebyscheff weighting set to -60 dB to suppress the sidelobes. Clearly seen is the narrow main beam with ~20 dBi of gain and all sidelobes with -40 dBi of sidelobe suppression at the 3 frequencies.

4.19 Smart Antennas

Smart antennas are systems that use adaptive antenna phasing and weighting to sync with a changing channel condition to keep the antenna on target. This technique can establish nulls. Effective use of nulls will filter out interference and jamming in real-time. As previously discussed, HF Skywave channel conditions are continually changing, with the adaptive beamforming antenna in this system, the beam can be adjusted continuously to keep reliable signal energy on the mobile transceiver. That same adaptive array system will place nulls in the direction of substantial interference and thus reject the intrusion. Figure 38 shows how the array can be modified to provide the adaptive capability.

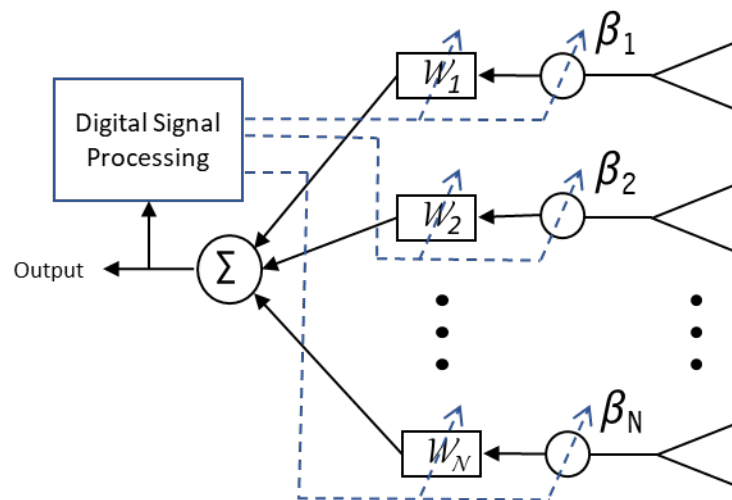


Figure 38. Diagram of a smart antenna array with a digital signal processor that will sense the output of the array and then adjust each element's excitation weighting and phase to improve the quality of the output.

By adding a digital signal processor (DSP) to the system, the output of the array can be evaluated. It will then automatically change the weighing and phase angles of each element to improve the quality of the antenna output. The concept of adaptive arrays dates to WWII. However, the advancements in digital signal processing to provide robust integrated circuits coupled with advance software has enabled the high-speed computing necessary to control an array with many antenna elements.

Figures 38 and 28 are diagrams that show how a notional smart antenna array system would dynamically control the weighting (w_n) of each element. The signal is input into the digital antenna controller, where adaptive weighting and phase are applied to amplify and transmit the narrow beam in

the desired direction while at the same time attenuating the interference arriving from an undesired direction.

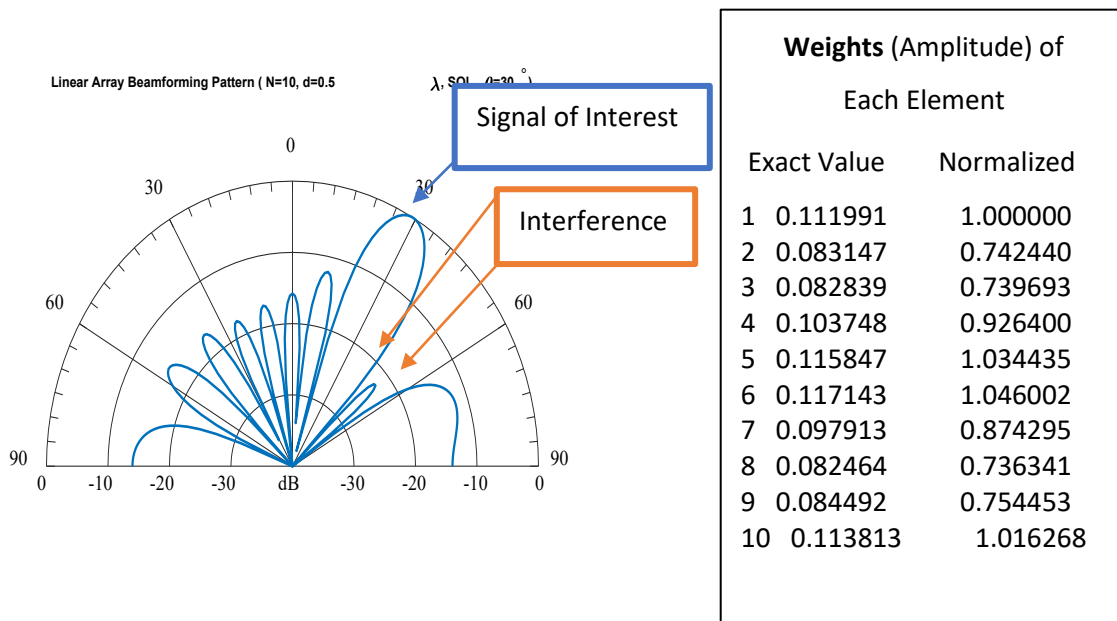


Figure 39. Diagram shows how a notional smart antenna would adjust the weighting to a 10-element array to reduce directivity in the direction of interference and increase directive in the direction of the signal of interest.

4.20 Analysis Performance Degradation Due to Non-Linearity and Phase Noise

Nonlinearity and phase noise are two important factors that can negatively affect system performance. Figure 40 shows a theoretical amplifier that is linear across all power levels. In real amplifiers, the output at high power may not be linear as the power drops off at higher levels. This can be a significant issue in any amplitude modulated signal, i.e. QAM signals.

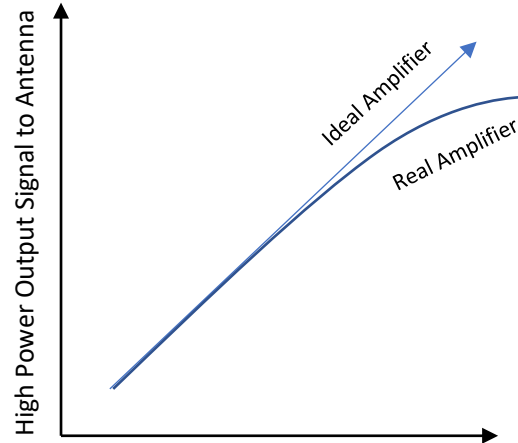


Figure 40. Diagram shows the power fall off of an amplifier at high power.

An orthogonal frequency division multiplex (OFDM) signal modulation uses many subcarriers to transmit symbols in parallel. Each subcarrier is modulated with quadrature amplitude modulations (QAM). A QAM modulation is a complex modulation that uses both amplitude and phase to represent the transmitted symbol. The nonlinearity of the transmitter affects the amplitude, and phase noise affects the phase of the transmitted symbol. Both conditions must be controlled.

Nonlinearity is present at the upper (high) limits of a power amplifier (PA), as shown in Figure 40. In this region, the output power is not linear with respect to the input power. In [44] the authors provide an analysis process to determine the effect on BER with respect to phase noise and nonlinear effects on OFDM signals.

In Virtual SATCOM, two methods are presented to address this issue. The first is to limit the input to the PA to ensure output is well within the linear response. In the Virtual SATCOM design, each antenna element has a dedicated power amplifier. This system employs 5 kW PA but limits output to 1 kW. An array of 200 elements with max power limited to 1 kW results in the cumulative power of 200 kW.

Perhaps a more elegant approach to this issue is the use of digital predistortion filters, as shown in Figure 41. This is a method to extend linearization to reduce adjacent channel interference (ACI) in systems like OFDM that have varying envelope modulation schemes. Digital baseband predistortion is a highly cost-effective way to linearize power amplifiers (PAs). Most existing architectures assume that the PA has a memoryless nonlinearity. For wider bandwidth applications such as wideband orthogonal frequency-division multiplexing (W-OFDM), PA memory effects can no longer be ignored. In [44] and

[45], a new technique was proposed for adaptation of a digital pre-distorter that considers memory effects in power amplifiers. This method has shown positive results. In summary, the nonlinearity of analog components can be managed and controlled with proper system design and application of digital feedback controls.

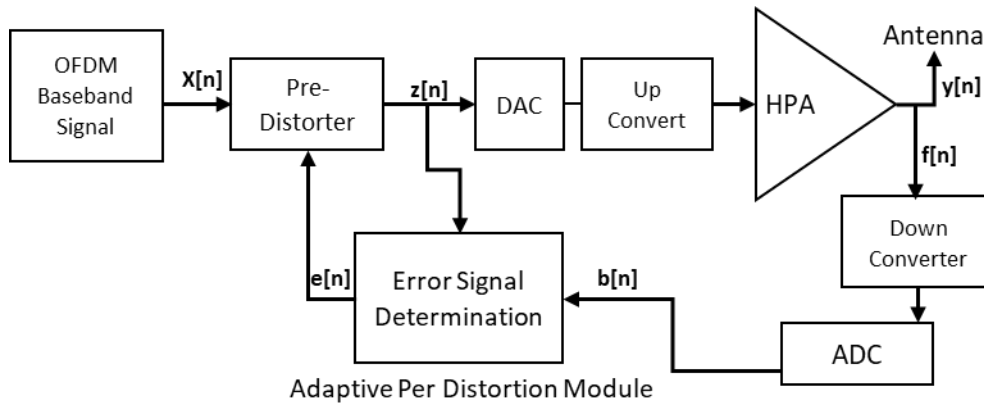


Figure 41. Adaptive Pre-Distorter will adjust input to amplifier and maintain linear output.

4.21 Signal Processing for Virtual SATCOM

In this section, signal processing will be discussed in more detail. In the previous chapters, we have shown that an antenna array can be constructed to focus signal energy into a narrow beam to generate significant SNR across a wide bandwidth. In this section, the discussion will address the signal processing necessary to accommodate the bandwidth of the system.

Considering that a typical HF channel is 3 kHz of bandwidth, it is not a trivial management exercise to manage 3 MHz of bandwidth. The preference of the Virtual SATCOM system is to use an already developed and approved standard and then organize and modify as required to meet the unique Virtual SATCOM approach. Two approaches will be discussed; the first is LTE (long term evolution). LTE is used extensively in mobile cellular systems but at higher frequencies, e.g. 900 MHz, and at much shorter ranges. The LTE standard supports a bandwidth of 1.3, 3.5, 10, and 20 MHz. LTE OFDM uses 15 kHz subchannels to move information in parallel efficiently. OFDM has an excellent performance in the high multipath cellular environment.

The second approach is to use a military standard HF waveform. The current US DoD standard is MILSTD188-110D. The 110D standard supports bandwidths from 3 – 48 kHz. This waveform has developed the FEC and interleaving protocols for the HF environment. This is predominantly a serial single tone modulation; as the data rate and bandwidth of 110D increase, the symbol speed increases.

Further discussion of best modulation schemes will be discussed after a discussion of the environmental factors that affect data rate. The two major performance degraders are delay spread and inter-symbol interference. Doppler spread is another degrader but will not be studied because it is typically only a few hertz at the distances and frequencies of this system.

4.22 Delay Spread

One of the significant challenges with HF skywave channel paths is the delay spread due to the multipath of signals reflecting off layers from different altitudes in the E, F1, and F2 layers. Additionally, the ray path is influenced by the Earth's magnetic field. Transmitted signal rays are split into ordinary and extraordinary waves. If the paths are of different lengths (Figure 42), then the time of arrival at the receiver or time delay will be split leading to a delay spread. In digital communications, delay spread leads to inter symbol interference (ISI). For example, in Figure 43, if a serial signal is being transmitted at 1 million symbols per sec (1 Msps), then each symbol is 1 μ sec in length. However, if the time delay or delay spread (σ_τ) between two paths is more significant, say 3 μ sec, then the second path will interfere with the symbol of the fourth symbol of the first path causing inter-symbol interference (ISI). This frequently results in incorrect data reception. A solution to this symbol overlap is to increase the transmitted signal time (T_s) to prevent multipath rays from arriving outside the period for that signal. In the example, if the period of each symbol was increased to 10 μ sec with the same delay spread of 3 μ sec, the receiver would have a much higher probability of detecting the correct symbol.

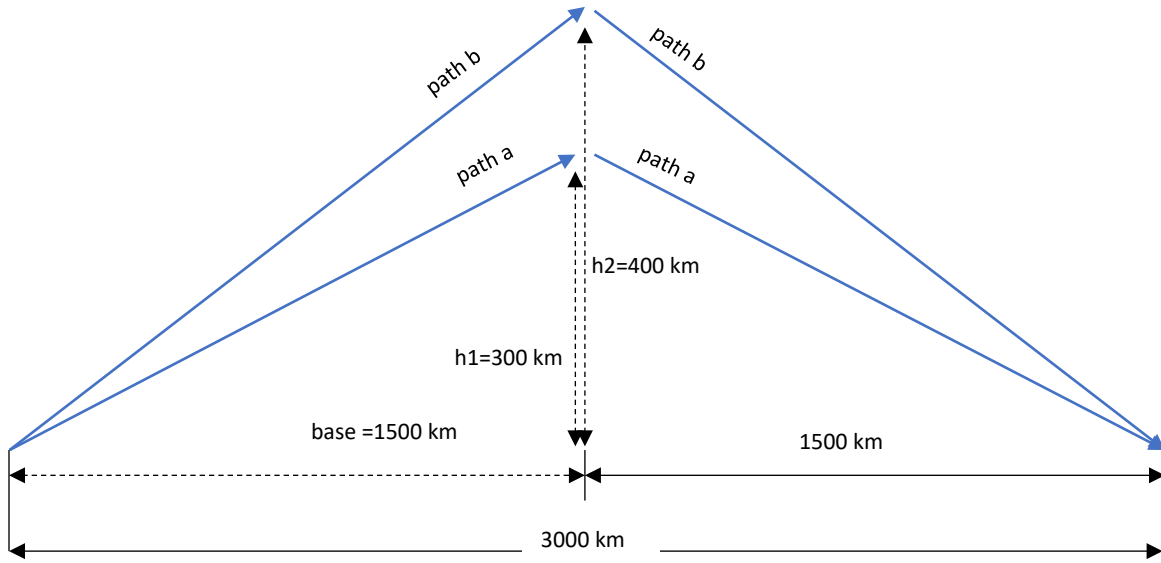


Figure 42. Diagram of two ray paths. One at a refraction altitude of 300 km and the other at a refraction altitude of 400 km. Path (b) is longer and signals on path (b) will arrive after the signals on path (a) causing multipath interference.

4.23 Flat Fading

Flat fading (good fading) occurs when the bandwidth of the signal is much less than the coherence bandwidth. In the scenario depicted in Figure 42 and Equation 65, path b is 46 km longer resulting in a delay of 153 μ sec. The reciprocal of delay spread (σ_τ) is coherence bandwidth (B_c). In this case, the coherence bandwidth is $(1/153 \mu\text{sec}) = B_c = 6.5$ kHz.

$$\begin{aligned}
 a &= 2\sqrt{(1500^2) + (300^2)} = 3059\text{km} \\
 b &= 2\sqrt{(1500^2) + (400^2)} = 3105\text{km} \\
 b - a &= 46\text{km} \therefore \text{delay} = 153\mu\text{sec}
 \end{aligned}
 \tag{70}$$

A way to ensure flat fading is to design a modulation where the signal bandwidth is less than the coherence bandwidth. For example, the signal symbol speed of a MILSTD 188-110D 3 kHz modulation is 2.4 kHz, and the signal bandwidth (B_s) is 1.8 kHz. This is below the coherence bandwidth of 6.5 kHz and is therefore an excellent choice.

$$B_s \ll B_c \tag{71}$$

The signal transmit time is $1/B_s$, so in this example, the T_s is 417 μsec , which is much greater than the delay spread. Then the signal symbol transmit time is much greater than the RMS delay spread.

$$T_s \gg \sigma_\tau \quad (72)$$

Therefore, a solution to delay spread is to increase the signal duration, so the signal period includes all multipath signals. For a long-range skywave transmission, the following diagram presents the geometry.

There are many references to delay spread in the literature. In [28] page 285, Fabrizio estimates coherence bandwidth at 100 kHz or less for OHR systems, and this equates to a σ_τ of 10 μsec . However, [12] p 114 sites typical time delay between 0.5 and 2 msec for communications systems, resulting in a coherent bandwidth between 500 Hz and 2 kHz. The difference between the two very different perspectives is the OTHR focuses the energy in a narrow azimuth beam. Therefore, there is less probability that energy will follow multiple paths from different azimuth angles. Still, the multipath from ionosphere layers stacked in altitude may cause multiple elevation paths including the ordinary and extraordinary wave previously discussed. Another paper developed to test wideband signals shows delay spread consistent with Fabrizio. In [30] the MITRE authors tested a 1 MHz wideband HF channel to measure Doppler shift and delay spread. The results show mean delay spread of 10-20 μsec and a doppler shift of a few Hz.

In summary, flat fading (good fading) occurs when the bandwidth of the signal is much less than the coherence bandwidth. Therefore, the signal transmit time is much longer than the RMS delay spread.

4.24 Inter Symbol Interference

Inter-symbol interference is the result of a delay spread that is greater than the symbol transmit time. As shown in Figure 43, if the first symbol in the path (b), arrives at the receiver during the fourth symbol from the path (a), the receiver will be unable to convert the signal energy into the proper symbol, and the bit error rate will increase. In HF skywave propagation, neither path (a) or (b) are the direct lines of sight; both are refracted signals that suffer approximately the same propagation loss and are consequently at the same power level in the receiver.

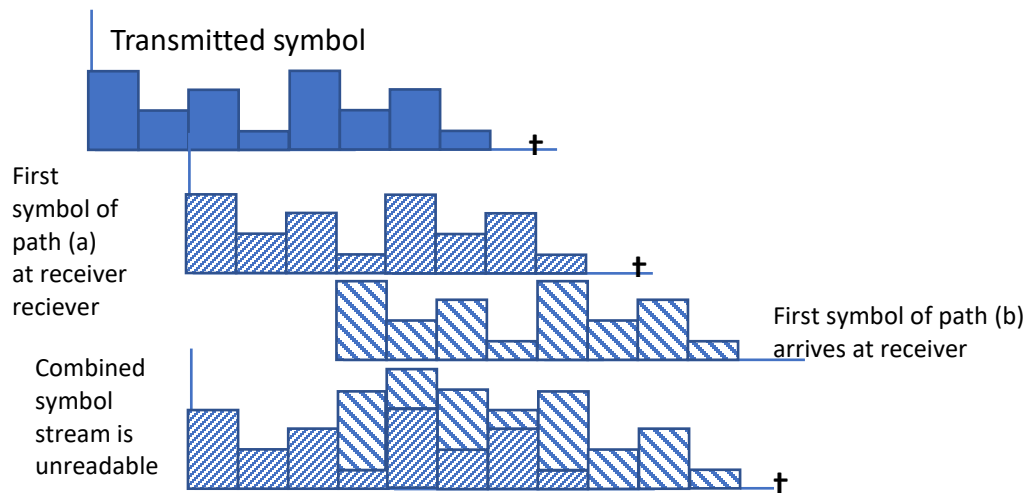


Figure 43. Diagram shows how delay spread causes inter-symbol interference. The second signal in a multipath propagation environment will affect the receiver's ability to decode the signal.

4.25 The Magnitude of Signal Processing

Signal processing in Virtual SATCOM is significant but is well within the capabilities of current technologies. The system will follow the logic path in Figure 44.

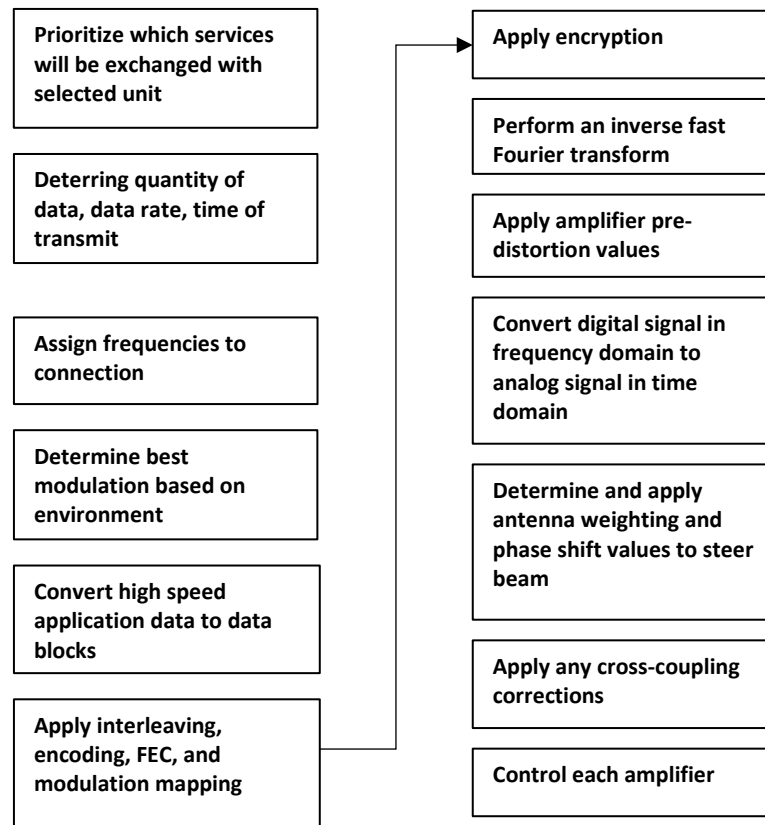


Figure 44. Functional diagram of digital processing in the Virtual SATCOM system.

The first two significant areas of significant digital processing are the transmitter and the receiver functions. In the transmit phase, high-speed serial channels from many different services are prioritized. Selected services are parsed into many parallel channels mixed with OFDM subchannels frequencies and then converted to time-domain signals for transmission. The receiver must accomplish the same process in reverse.

The next area of significant processing is antenna control. The antenna controller must adjust amplitude and phase at each one of the 200 antennas to ensure the correct steering of the beam. This includes the addition of interference nulling and cross-coupling rejection. The virtual SATCOM phased array antenna in this design has 200 elements. This is not a small number; however, it is minor compared with radar phased array systems used in many military applications. For example, the SPY-1 phased array radar on many US Navy ships used 4,350 radiators that are digitally controlled to steer the beam in both azimuth and elevation.

These processes are not small; however, compared to other comparable systems, they are well within the capabilities of current technology. Another example is the 4th generation LTE standard that operates on 1.5, 3, 5, 10, and 20 MHz bandwidths with many subchannels. At a bandwidth of 20 MHz, each subchannel has 15 kHz of subchannel spacing, so there are 1333 OFDM subchannels to process. The Flex 6600 direct sampling SDR transceiver, a high-end amateur HF radio, uses an SDR processor that will sample at 245.6 Msps, with a maximum bandwidth of 14 MHz. The Flex CDRX-3200 can process 32 different signals at the same time with a 200-kbps data rate and time stamp resolution of 1 ns.

4.26 OFDM

The Virtual SATCOM design requires an ultra-wide bandwidth. The Orthogonal Frequency Division Multiplex (OFDM) modulation fits well into this design. As discussed in Goldsmith [31] and Proakis [11] OFDM is a multicarrier modulation that converts a high-speed serial digital data into many parallel sub-streams at a slower signal speed. Each data stream is mapped to an analog symbol and assigned to a sub frequency channel. Each analog subchannel is orthogonal to the next subchannel frequency. The orthogonality results in sidelobe cancellation between adjacent subchannels. The resulting RF consists of many closely spaced modulated carriers. Next, the narrow bandwidth subchannels are combined into a single wide bandwidth signal and transmitted. OFDM has an advantage over frequency division multiplex (FDM) because the guard band between each subchannel is eliminated. OFDM employs an IFFT (Inverse Fast Fourier Transform) process that converts the time domain bitstream into frequency domain signals. Before transmission, a digital to analog process combines the subchannels into a signal time-division signal. At the receiver, the time domain signal is decomposed by a Fast Fourier Transform (FFT) back into the unique sub-channel frequencies for signal detection. The subchannels are recombined into a high-speed serial channel. OFDM has been used in many high data rate wireless systems because of the many advantages it provides; some examples include WIFI, LTE, and WiMAX. One key benefit is a satisfactory performance in a multipath environment which is needed in this Virtual SATCOM system.

4.27 Virtual SATCOM Data Block Design

As seen in 0, all high-speed digital data applications on the left will be assigned to data blocks depending on the needs of the mobile platform and bandwidth available. The data blocks help organize the flow of services to the mobile unit. Each data block will carry four data MILSTD 188-110D signals with two for 48 kHz channels and two 24 kHz channels. This waveform was designed for performance and robustness in the HF spectrum. This mode is almost identical to STANAG 4285. Serial D is a series of wideband high-frequency radio (WBHF) waveforms and coding specifications for bandwidths of 3, 6, 9, 12, 15, 18, 21, 24, 30, 36, 42, and 48 kHz. Data rates of 75 through 240,000 bps are supported.

Not all applications on the left will be scheduled for all platforms. This will have to be managed. This flexible design will allow the data to be efficiently tailored for the mobile unit. All ships may not want the same data feeds and different data feeds have various restrictions. For example, NIPRNET, SIPRNET and JWICS have different classifications and different security encryption standards. This data architecture provides the capability to keep the application separated as required in different MILSTD 188-110D channels.

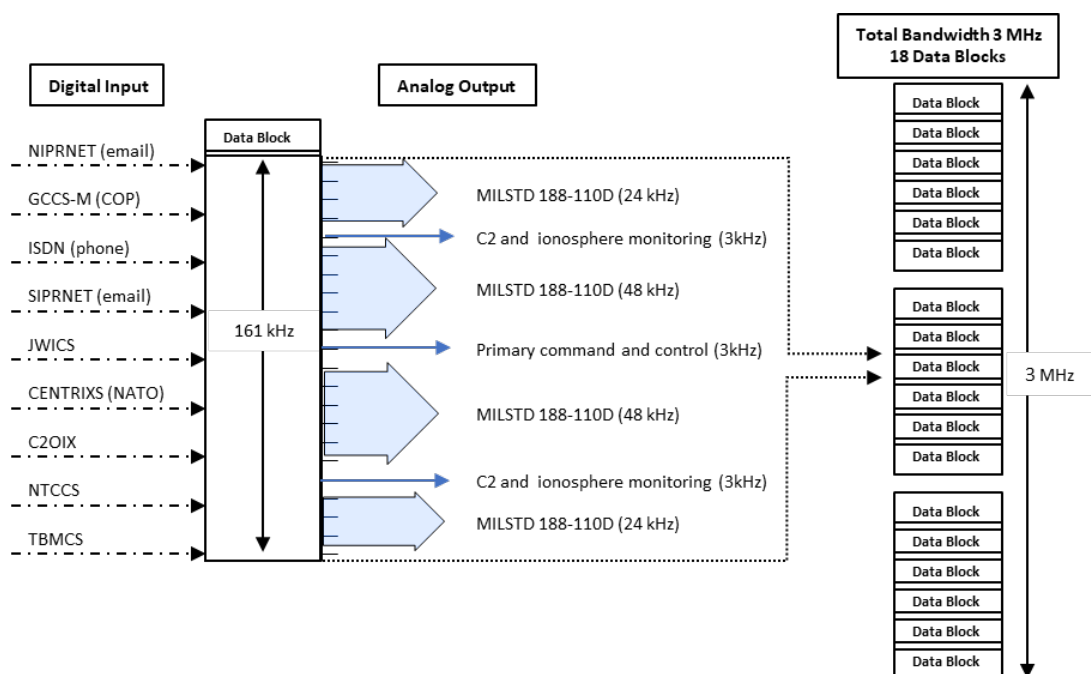


Figure 45. The diagram shows how high-speed applications are sorted into data blocks for transmission.

In addition to the four data channels, three other 3 kHz channels are provided. These serve other low data rate function. The most important is the quality of service feedback, and other control systems commands necessary to maintain the link. One of the channels will be designated for voice connectivity. This could be an analog channel, but the preference is to move to a digital voice modulation to provide cleaner voice communications without the loud hiss of an analog SSB connection. The total bandwidth of each data block is 161 kHz and includes a total of eight guard bands of 1 kHz between each channel within the data block.

$$\text{Total bandwidth for one block} = (2 \times 48) + (2 \times 24) + (3 \times 3) + (8 \times 1) = 161 \text{ kHz.}$$

A 3 MHz total bandwidth will hold 18 separate data blocks. If the bandwidth is less than 3 MHz, then the number of blocks can be reduced. In some situations, the base station may transmit 3 MHz and the mobile unit will receive 3 MHz, but then the ship will only transmit 1 MHz of bandwidth back to the base station. This will require the management of applications to meet asymmetric information exchange requirements. One solution is to use different frequencies for the forward link and backlink. As indicated in Chapter 1, the ship has two receive antennas with the bandwidth to receive a 3 MHz signal. To transmit from mobile, the mobile unit will use its directional antenna with the extra gain to ensure satisfactory SNR at low power.

4.28 Weakness of MILSTD 188-110D Appendix D, Wide Bandwidth Channels.

MILSTD188-110D was introduced in Chapter 1. It is the DoD standard for HF digital communications. However, there are some weaknesses when operating in wideband modes. 110D is a serial mode design; the symbols are transmitted in sequence. Different symbol modulations are available i.e. BPSK, QPSK, QAM, etc., but the symbols are transmitted one after the other as specified by the symbol rate (B_s). The symbol rate for a 3 kHz channel is 2400 symbols/sec. The symbol rate increases as bandwidth increases. As the symbol rate increases, the symbol transmit time decreases. As the transmit time decreases, the energy per bit also decreases.

More importantly, at some point, the delay spread is longer than symbol transmit time and inter-symbol interference becomes a factor. In Table 7, the symbol rate is listed for each MILSTD 188-110D. Using the delay spread calculated above based on Figure 33, the coherence bandwidth of 6532 Hz is determined. As shown, all bandwidths above 6 kHz may have difficulty except in a very stable ionosphere and short ranges where the delay spread is very low. The conclusion we have drawn is that MILSTD 188-110D wideband modulation is not a robust standard for long-range HF operations.

Table 7. Comparison of MILSTD Symbol Rate and Delay Spread

MILSTD 188-110D Bandwidth	Symbol Rate B_s	Transmitted Signal Time T_s	Delay Spread σ_τ	Coherent Bandwidth B_c	Delta $T_s - \sigma_\tau$
(kHz)	(sym/sec)	(μsec)	(μsec)	(Hz)	(μsec)
3	2400	417	153	6536	263.67
6	4800	208	153	6536	55.33
9	7200	139	153	6536	-14.11
12	9600	104	153	6536	-48.83
15	12000	83	153	6536	-69.67
18	14400	69	153	6536	-83.56
21	16800	60	153	6536	-93.48
24	19200	52	153	6536	-100.92
27	21600	46	153	6536	-106.70
30	24000	42	153	6536	-111.33
33	26400	38	153	6536	-115.12
36	28800	35	153	6536	-118.28
39	31200	32	153	6536	-120.95
42	33600	30	153	6536	-123.24
45	36000	28	153	6536	-125.22
48	38400	26	153	6536	-126.96

4.29 Our Solutions to MILSTD188-110D Wideband Modulation High Symbol Rate.

One tact to increase the symbol rate is to use only 3 kHz channels. The 3 kHz channel has a bandwidth of 1800 Hz and a symbol rate of 2400 Hz. This generates a 417 msec transmit time which is much longer than the delay spread, so ISI is not a factor under most conditions. However, if a 1 kHz guard band is added between each 3 kHz channels, in 3 MHz there are 750 channels. This would require an impractical number of radio demodulators on the mobile units.

The Virtual SATCOM solution is a hybrid solution of MILSTD 188-110D WBHF and OFDM modulation. In 0, there are 26 OFDM subchannels spaced 1800 Hz apart within the 48 kHz channel. In this configuration, each subchannel is mapped to a modulation scheme. Like the 3 kHz channel, the symbol rate is 2400 sps. If the modulation scheme is 16-QAM the data rate is 6400 bps. The gross data rate is 4bits times 2400 bps or 9600 bps. However, header and CRC bits reduce the payload data rate to 6400 bps. If this is multiplied 26 times for each subchannel, the payload data rate is 166 kbps. The MILSTD 188-110D 48 kHz serial waveform has a data rate of 96 kbps. This results in a 20% increase in data speed but still at a 417 μ sec symbol transmit time compared to a 26 μ sec for the standard MILSTD 188-110D modulation. The OFDM is the better choice for long haul digital HF modulations. Table 8

shows a comparison of Virtual SATCOM hybrid MILSTD 188-110D on the top half of the table against the standard MILSTD188-110D data rates below.

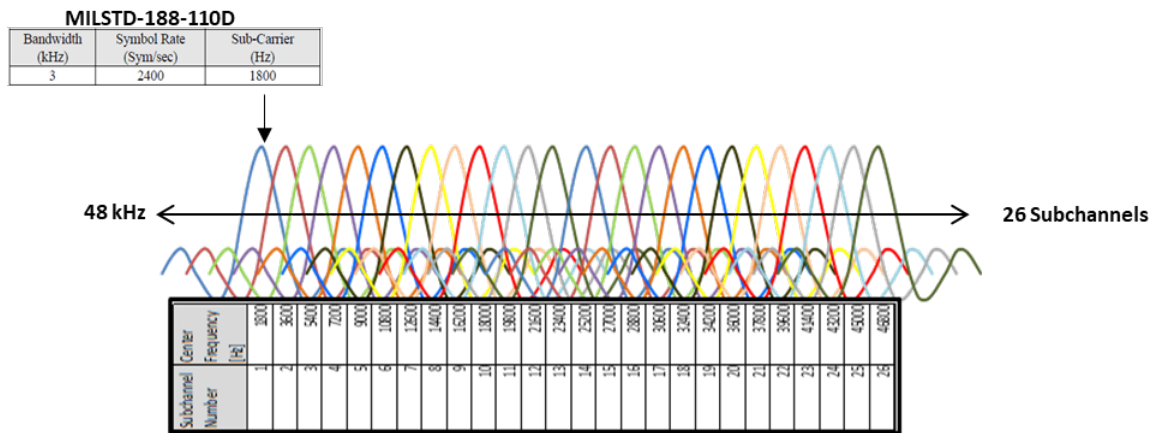


Figure 46. Diagram of 26 OFDM subchannels, each subchannel is 1800 Hz wide

Table 8. Virtual SATCOM Modulation using MILSTD188-110D Modified with OFDM

Wave Number		0	1	2	3	4	5	6	7	8	9	10	11	12	13
Modulation		Walsh	BPSK	BPSK	BPSK	BPSK	BPSK	QPSK	8PSK	16QAM	32QAM	64QAM	64QAM	256QAM	QPSK
Bandwidth	Number of Subcarrier														
	1800Hz/subcarrier														
[kHz]		[Hz]	[Hz]	[Hz]	[Hz]	[Hz]	[Hz]	[Hz]	[Hz]	[Hz]	[Hz]	[Hz]	[Hz]	[Hz]	[Hz]
3	1	75	150	300	600	1200	1600	3200	4800	6400	8000	9600	12000	16000	24000
6	3	225	450	900	1800	3600	4800	9600	14400	19200	24000	28800	36000	48000	72000
9	5	375	750	1500	3000	6000	8000	16000	24000	32000	40000	48000	60000	80000	120000
12	6	450	900	1800	3600	7200	9600	19200	28800	38400	48000	57600	72000	96000	144000
15	8	600	1200	2400	4800	9600	12800	25600	38400	51200	64000	76800	96000	128000	192000
18	10	750	1500	3000	6000	12000	16000	32000	48000	64000	80000	96000	120000	160000	240000
21	11	825	1650	3300	6600	13200	17600	35200	52800	70400	88000	105600	132000	176000	264000
24	13	975	1950	3900	7800	15600	20800	41600	62400	83200	104000	124800	156000	208000	312000
27	15	1125	2250	4500	9000	18000	24000	48000	72000	96000	120000	144000	180000	240000	360000
30	16	1200	2400	4800	9600	19200	25600	51200	76800	102400	128000	153600	192000	256000	384000
33	18	1350	2700	5400	10800	21600	28800	57600	86400	115200	144000	172800	216000	288000	432000
36	20	1500	3000	6000	12000	24000	32000	64000	96000	128000	160000	192000	240000	320000	480000
39	21	1575	3150	6300	12600	25200	33600	67200	100800	134400	168000	201600	252000	336000	504000
42	23	1725	3450	6900	13800	27600	36800	73600	110400	147200	184000	220800	276000	368000	552000
45	25	1875	3750	7500	15000	30000	40000	80000	120000	160000	200000	240000	300000	400000	600000
48	26	1950	3900	7800	15600	31200	41600	83200	124800	166400	208000	249600	312000	416000	624000

MILSTD 188-110D	Waveform Number	0 Walsh	1 BPSK	2 BPSK	3 BPSK	4 BPSK	5 BPSK	6 QPSK	7 8PSK	8 16QAM	9 32QAM	10 64QAM	11 64QAM	12 256QAM	13 QPSK
	Bandwidth (kHz)														
	3	75	150	300	600	1200	1600	3200	4800	6400	8000	9600	12000	16000	2400
	6	150	300	600	1200	2400	3200	6400	9600	12800	16000	19200	24000	32000	
	9	300	600	1200	2400	-	4800	9600	14400	19200	24000	28800	36000	48000	
	12	300	600	1200	2400	4800	6400	12800	19200	25600	32000	38400	48000	64000	
	15	300	600	1200	2400	4800	8000	16000	24000	32000	40000	48000	57600	76800	
	18	600	1200	2400	4800	-	9600	19200	28800	38400	48000	57600	72000	90000	
	21	300	600	1200	2400	4800	9600	19200	28800	38400	48000	57600	76800	115200	
	24	600	1200	2400	4800	9600	12800	25600	38400	51200	64000	76800	96000	120000	
	30	600	1200	2400	4800	9600	16000	32000	48000	64000	80000	96000	120000	160000	
	36	1200	2400	4800	9600	12800	19200	38400	57600	76800	96000	115200	144000	192000	
	42	1200	2400	4800	9600	14400	19200	38400	57600	76800	96000	115200	160000	192000	
	48	1200	2400	4800	9600	16000	24000	48000	72000	96000	120000	144000	192000	240000	

4.30 Software Defined Radios (SDR) Meet digital Signal Procession Requirements

A critical thinker might ask, “HF communication has been around for a long time, so why is a high data rate solution proposed now?” The answer is the technological advance of the SDR. Software Defined Radios are the drivers for the digital signal processing required in this Virtual SATCOM design. SDR uses Analog-to-Digital Converters (ADCs) to digitize the received analog signal. The ADC today can digitize the analog electromagnetic spectrum at a nano second rate. This fast process allows the ADC to move closer to the antenna and reduce the analog hardware circuits. This enables the SDR to move quickly across the spectrum to decode complex signals.

The SDR receivers are the principal research focus for Ultra-Wide-Band (UWB). The idea of these UWB receivers is to convert the noisy RF signal coming directly from the antenna to the digital domain. Consequently, all the analog processing processes are removed, and the message is converted directly to the digital domain to be processed by the digital processor. The processing of the signal in the digital domain preserves high accuracy and resolution with fewer high-cost analog components.

The best approach towards SDRs procession is the use of programmable hardware such as field-programmable gate arrays (FPGA). Examples of FPGA based SDR platforms are Airblue and Xilinx Zynq. Although FPGAs consume more power and occupy more area than ASICs, the programmability feature is the reason behind their increasing adoption in a wide range of applications. FPGAs can be quickly reprogrammed, and their cost is within a few tens to a few thousands of dollars. Advantages of FPGA include attractive hardware processing advantages, such as high-speed performance, low power consumption, and portability, compared to other processors [46]. In Hussein [47], a presentation of a Time-Based Analog-to-Digital Converter (TADC) is considered an essential block in designing SDR receivers because it exhibits higher speed and reduced power consumption compared to the conventional ADC, especially, at scaled CMOS technologies.

In summary, state of the art in digital signal processing and phased array antenna control are well within the magnitude of the signal processing requirements of a 200-element array operating over a bandwidth of 3 MHz.

CHAPTER FIVE

CONCLUSIONS

The Achilles heel of modern networked warfare for maneuver forces like the Navy is the communication satellite. The Navy has become dependent on high-speed SATCOM data. Adversaries are poised to attack with capable weapons, including RF jamming, cyber-attack, directed energy, and physical kinetic attack.

This research presents an innovative alternative -- non-satellite signal paths to support long-range wireless network communications for mobile platforms. It provides a significant improvement over current HF systems that is comparable to SATCOM signal speeds.

The ionosphere has limitations, but modern signal processing technologies can compensate for these limitations. The ionosphere is a dynamic medium, but we designed a frequency-agile HF OTH communication system that can provide mobile platforms with high data rates via a base station relay.

Our analysis using the PHaRLAP model has shown that the ionosphere can accommodate an ultra-wideband signal. Additional research is needed to refine the channel conditions at other locations in the future.

Our innovative concept acknowledges the practicality that a wideband signal must be constrained to prevent interference with other users of the spectrum. Our solution is a narrow-focused beam that negates interference outside the beam. The application of a narrow beam, high gain, and high-power signal results in a strong signal to noise ratio that will increase data rate and lower bit error rate. Wide bandwidth and reliable SNR result in high data speed.

Antenna elements for wide bandwidth signals are different than narrowband signals. Our design selected LPDA antenna elements for its wide frequency properties. More detailed analysis with a better software tool like FEKO or CST that model EM radiation patterns will provide a precise design that can be prototyped and tested.

Though more study is required, Virtual SATCOM is a disruptive technology that can augment or replace DOD's long-range wireless communications requirement and mitigate the risk of satellite disruption.

REFERENCES

- [1] Department of Defense, "ANNUAL REPORT TO CONGRESS, Military and Security Developments Involving the People's Republic of China 2016," DoD RefID: 117FA69, Washington DC, 2016.
- [2] Federal Communications Commission, " FCC Spectrum Auctions and Secondary Markets Policies: An Assessment of the Distribution of Spectrum Resources Under the Spectrum Screen by Mobile Future," FCC, Washington DC, 2013.
- [3] J. M. Thomason and Headrick, "Applications of High-frequency Radar," *RadioScience*, Vols. Volume 33, Number 4, no. July-August 1998, pp. 1045-1054, 1998.
- [4] C. Cox, An Introduction to LTE: Lte, LTE-advanced, SAE and 4G Mobile Communicaton, West Sussex, United Kingdom: John Wiley and Sons Ltd, 2012.
- [5] T. L. Endicott, "A WARRIOR'S MINDSET, KEY TO WINNING IN SPACE," US Air Force , Peterson Air Force Base, Colorado, 2017.
- [6] M.Gruss, "Pentagon Says 2013 Chinese Launch May Have Tested Antisatellite Technology," *Space News*, 14 May 2015.
- [7] Defense Acquisition Management Information Retrieval (DAMIR), "Selected Acquisition Report (SAR) Mobile User Objective System (MUOS) RCS: DD-A&T(Q&A)823-345," Defense Acquisition Management Information Retrieval (DAMIR), Washington DC, March 23, 2016.
- [8] G. I. Seffers, "Navy Satellite System Approved for Expanded Operational Use," *Signal Magazine*, pp. Posted on <https://www.afcea.org/content/navy-satellite-system-approved-expanded-operational-use>, 2 August 2018.
- [9] C. E. Shannon and W. Weaver, The Mathematical Theory of Communicaiton, Chicago, IL: University of Illinois Press, 1949.
- [10] W. L. Stutzman and G. A. Thiele, Antenna Theory and Design, USA: John Wiley & Sons, Inc, 1981.
- [11] J. G. Proakis and M. Salehi, Communications Systems Engineering, Second Edition, Upper Saddle River, NJ: Prentice Hall, 2002.
- [12] E. E. Johnson, R. I. Desourdis, G. D. Earle, S. C. Cook and a. Jens C Ostergaard, Advance High-Frequency Radio Communications, Norwood MA: Artech House INC, 1997.

- [13] K. G. Budden, The propagation of radio waves, The theory of radio waves on low power in the ionosphere and magnetosphere, Cambridge: Cambridge University Press, 1985.
- [14] M. A. Cervera and T. J. Harris, "Modeling ionospheric disturbance features in quasi-vertically incident ionograms using 3-D magnetoionic ray tracing and atmospheric gravity waves" in, J. Geophys. Res. Space Physics, 119, 431– 440, 8 January 2014," *Journal of Geophysical Research: Space Physics*, vol. 119, p. 431– 440, 2014.
- [15] J. C. Coleman, "A direction-sensitive model of atmospheric noise and its application to the analysis of HF receiving antennas," *RADIO SCIENCE* 10.1029/2000RS002567, vol. 37, no. 3, p. 1031, 2002.
- [16] D. J. Cecil, D. E. Buechler and Blakeslee, "Gridded lightning climatology from TRMM-LIS and OTD: Dataset description," *Atmospheric Research*, pp. 404-414, 2014.
- [17] M. Kotaki, "Global Sistribution of Atmospheric radio noise derived from thunderstorm activity," *Journal of Atmospheric and Terrestrial Physics*, vol. 46, no. 10, pp. 867-877, 1984.
- [18] A. Oliveira-Cosa, M. Tegmark, B. M. Gaensler, J. Jonas, T. L. Landecker and P. Reich, "A model of diffuse Galactic radio emission from 10 MHz to 100 GHz," *Monthly Notices of the Royal Astronomical Society*, vol. 388, no. doi:10.1111/j.1365-2966.2008.13376.x, pp. 247-260, 2008.
- [19] L. H. Pederic and M. A. Cervera, "Semiempirical Model for Ionospheric Absorption based on the NRLMSISE-00 atmospheric model," *Radio Science*, vol. 49, no. doi:10.1002/2013RS005274, pp. 81-93, 2014.
- [20] L. H. Pederick and M. A. Cervera, "Semiempirical Model for Ionospheric Absorption based on the NRLMSISE-00 atmospheric model," *Radio Science*, vol. 49, no. doi:10.1002/2013RS005274, pp. 81-93, 2014.
- [21] Alaris Antennas, "<https://www.alarisantennas.com/wp-content/uploads/2018/02/RA10-118-01-RLP10-30-Version-1.3.pdf>," Alaris Antennas, 2020. [Online]. Available: <https://www.alarisantennas.com/products/antenna-selector/>. [Accessed 8 Feb 2020].
- [22] W. Tanenbaum, Computer Networks, Fifth Edition, Boston Massachusetts: Oeasib /edycatuib Inc., 2011.
- [23] United Nations, "ITU Radiocommunication Sector," International Telecommunications Union, [Online]. Available: <https://www.itu.int/en/ITU-R/Pages/default.aspx>. [Accessed 03 November 2019].
- [24] H. Chenjyu, K. Guo and F. Yili, "The sky-wave radar detection performance computing based on the dynamic ionospheric model," *Neurocomputing*, vol. 151, no. Part 3, pp. 1305-1315, 2015.

- [25] J. Haselgrove, "Ray Theory and a New Method for Ray Tracing," in *Physical Society Conference on The Physics of the Ionosphere*, CAVENDISH LABORATORY, CAMBRIDGE, 1955.
- [26] J. Haselgrove, "The Hamiltonian ray path equations,," *Journal of Atmospheric and Terrestrial Physics*, vol. 25, no. 7, p. 397, 1963.
- [27] D. J. Belknap, R. D. Haggarty and and Perry D.B., "Adaptive Singnal Processing for Ionospheric Distortion Correction (ESD-TR-70-30)," Electronic Systems Division, Air Force Systems Command, Bedford, MA, 1970.
- [28] G. Fabrizio, F. Colon, P. Lombardo and A.Farina, "Adaptive beamforming for high-frequency over-the-horizon passive radar," *IET Radar, Sonar and Navigation*,, no. Special Issue – selected papers from IEEE RadarCon 2008, 2009.
- [29] Bin-Yi Liu, "Thesis: HF OVER-THE-HORIZON RADAR SYSTEM PERFORMANCE ANALYSIS," Naval Postgraduate School, Monterey, CA, 2007.
- [30] M. I. Clune, P. B. Fine, J. N. Freedman, C. A. Nissen and b. D. P. and, "Delay and Doppler Spreading Charteristics of the Wide-Bandwidth HF Channel," in *1991 Fifth International Conference on HF Radio Systems and Techniques (Conf. Publ. No.339)*, Edinburgh, UK,, 1991.
- [31] A. Goldsmith, *Wireless Communication*, New York: Cambridge University Press, 2005, p. page 374..
- [32] E. E. Johnson, E. Koski, W. N. Furman, M. Jorgenson and a. J. Nieto, *Third-Generation and Wideband HF Radio Communications*, Norwood: Artec House, 2012.
- [33] Department of Defense (DoD) , "DEPARTMENT OF DEFENSEINTERFACE STANDARD INTEROPERABILITY AND PERFORMANCE STANDARDS FOR DATA MODEMS (MIL-STD-188-110D)," US Air Force Sustainment Center, Oklahoma City, OK, 2017.
- [34] V. d. C. Van Troyen, "Ionsoheric Modeling Based on Oblique Chirp-Sounders," in *Forth International Conference on HF Radio Systesms and Techniques*, London, UK,, 1988.
- [35] J. C. Coleman, "A ray tracing formulation and its application to some problems in over the horizon radar," *Radio Science*, , Pages,, vol. Volume 33, no. Number 4, pp. 1187-1197, July-August 1998.
- [36] D. Bilitza, L. McKinnell, B. Reinisch and T. Fuller-Rowel, "The international reference ionosphere today and in the future," *Journal of Geodesy*, vol. 80, no. 12, pp. 909-920, 2011.
- [37] J. C. Coleman, "A General Purpose Ionospheric Ray Tracing Procedure," DSTO Australia Surveillance Research Laboratory, High Frequency Division #SLR-0131-TR, Salisbury, 1993.

- [38] International Telecommunication Union, Radio Communications Sector (ITU-R), "Recommendation ITU-R P.372-12, Radio Noise," International Telecommunication Union, Geneva, 2015.
- [39] H. K. Sen and A. A. Wyller, "On the generalization of the Appleton-Hartree magnetoionic formulas," *Journal of Geophysical Research*, vol. 65, no. 12, pp. 3931-3950, 1960.
- [40] J. M. Picone, A. E. Hedin and D. P. Drob, "NRLMSISE-00 empirical model of the atmosphere:," *Journal of Geophysical Research: Statistical comparisons and scientific issues*, vol. 107, no. A12, p. 1468, 2002.
- [41] C. A. Balanis, *Antenna Theory Analysis and Design*, 4th edition., Hoboken, NJ: Wiley and Son's Inc, 2016.
- [42] R. Mantha, "Log-Periodic Dipole Antenna (LPDA) version 1.0.0.0 Design of a Log-Periodic Dipole Antenna," Mathworks, Houston, 2014.
- [43] C. L. Dolph, "A Current Distribution for Broadside Arrays Which Optimizes the Relationship between Beam Width and Side-Lobe Level.," *Proceedings of the IRE*, vol. 34, pp. 335-348., 1946.
- [44] W. Jian, C. Yu, J. Wang, J. Yu and L. Wang, "A Digital Adaptive Predistortion Method of OFDM Power Amplifier,," in *2009 International Conference on Networks Security, Wireless Communications and Trusted Computing*, Wuhan, Hubei, 2009.
- [45] P. Varahram, J. Dooley, K. Finnerty and R. Farrell, "A low complexity pre-distortion scheme for power amplifier linearization in wideband applications," *INTERNATIONAL JOURNAL OF COMMUNICATION SYSTEMS*, vol. 30, no. DOI: 10.1002/dac.3177, p. 3177, 2017.
- [46] R. Akeela and B. Dezfouli, ""Software-defined Radios: Architecture, State-of-the-art, and Challenges",," *Computer Communications*, vol. 128, pp. 106-125, September 2018.
- [47] A. S. Hussein, M. Fawzy, M. W. Ismail, M. Refky and a. H. Mostafa, "A 1 Gs/S 6-Bit Time-Based Analog-to-Digital Converter (T-ADC) for Front-End Receivers," in *26th International Conference on Microelectronics (ICM)*, Doha, Qatar, 2014.
- [48] International Telecommunications Union Radio Communication Sector (ITU-R), "Recommendation ITU-R P.832-4, World Atlas of Ground Conductivities," International Telecommunication Union, Geneva, 2015.
- [49] J. G. S. M. Proakis, *Communication Systems Engineering*, 2nd Ed., Upper Saddle River, New Jersey: Prentice Hall, 2002.
- [50] W. Jian, C. Yu, J. Wang, J. Yu and L. Wang, "A Digital Adaptive Predistortion Method of OFDM Power Amplifier," in *International Conference on Networks Security, Wireless Communication and Trusted Computing*, 2009;10.1109/NSWCTC.2009.180.

- [51] L. H. Pederic and M. A. Cervera, "Modeling the interference environment in the HF band," *Radio Science*, vol. 51, no. doi:10.1002/2015RS005856, pp. 82–90, doi:10.1002/2015RS005856, 2016.
- [52] L. H. Pederick and M. A. Cervera, "A Directional HF Noise Model: Calibration and Validation in Australian Region," *Radio Science*, vol. 51, pp. 25-39, 2016.
- [53] Department of Defense USA, "Selected Acquisition Reprot (SAR) Mobile User Objective System (MUOS) RSC: DD-A&T 823-345," US Department of Defense, Defense Acquisition Management Information Retrieval. , Washington DC, December 2017.

APPENDIX A

Appendix A shows the MATLAB programs support the dissertation.

Noise references

Beam steering

```
% Path    C:\Users\denni\Documents\MATLAB\dec 2018 lpda matlab
% Design of a Log-Periodic Dipole Antenna (by Ramann Mantha)

% This design is based on the initial assumption that the directivity
(D0) (ranging from 7dB-11.5dB in accordance with fig 11.13 in Balanis)
and bandwidth (fL and fH) are given
clc;
D0 = input('\nEnter the Value of Directivity = ');
fL = input('\nEnter the Lower cut-off frequency (in MHz) = ');
fH = input('\nEnter the Upper cut-off frequency (in MHz) = ');

if D0 == 7;
sigma = 0.135;
tau = 0.77;

elseif D0 == 7.5;
    sigma = 0.145;
    tau = 0.83;

elseif D0 == 8;
    sigma = 0.157;
    tau = 0.865;

elseif D0 == 8.5;
    sigma = 0.17;
    tau = 0.90;

elseif D0 == 9;
    sigma = 0.172;
    tau = 0.93;

elseif D0 == 9.5;
    sigma = 0.178;
    tau = 0.945;

elseif D0 == 10;
    sigma = 0.18;
    tau = 0.957;

elseif D0 == 10.5;
    sigma = 0.182;
    tau = 0.97;
```

```

elseif D0 == 11;
    sigma = 0.19;
    tau = 0.975;
end

fprintf('\nsigma = %f\n\n', sigma);
fprintf('tau = %f\n\n', tau);
alpha = atand((1-tau)/(4*sigma));
fprintf('alpha = %f\n\n', alpha);

% Bandwidth of active region is denoted by "Bactreg" and slightly
higher
% bandwidth is denoted by "Bs"
Bactreg = 1.1+7.7*((1-tau)^2)*cotd(alpha);
fprintf('Bactreg = %f\n\n', Bactreg);
Bs = (fH/fL)*Bactreg;
fprintf('Bs = %f\n\n', Bs);

% Number of elements is denoted by N
ln = @log;
intermediate1 = 1+(ln(Bs)/ln(1/tau));
N = ceil(intermediate1);
fprintf('N = %f\n\n', N);

f1 = 2/((Bs/fH)+(1/fL));
f2 = fH*(2-(f1/fL));
fprintf('f1 = %f\n\n', f1);
fprintf('f2 = %f\n\n', f2);

c = 300;
lambda_max = c/f1;
fprintf('lambda_max = %f\n\n', lambda_max);
L = (lambda_max/4)*(1-(1/Bs))*cotd(alpha);
fprintf('L = %f\n\n', L);
l_max = lambda_max/2;
fprintf('l_max = %f\n\n', l_max);

for i = 1:1:N-1;
    intermediate2 = ((tau)^(i-1))*(l_max);
    l_i = (tau)*intermediate2;
    fprintf('l_i = %f\n', l_i);
end

R_max = l_max/(2*tand(alpha));
fprintf('\nR_max = %f\n\n', R_max);

for j = 1:1:N-1;
    intermediate3 = ((tau)^(j-1))*(R_max);
    R_j = (tau)*intermediate3;
    fprintf('R_j = %f\n', R_j);
end

```

```

L_actual = R_max - R_j;
fprintf('\nL_actual = %f\n\n', L_actual);

spacing_factor = ((R_max) - ((R_max) * (tau))) / (2 * (l_max));
fprintf('spacing_factor = %f\n\n', spacing_factor);

```

Input/Output

Enter the Value of Directivity = 7

Enter the Lower cut-off frequency (in MHz) = 7

Enter the Upper cut-off frequency (in MHz) = 28

sigma = 0.135000

tau = 0.770000

alpha = 23.070412

Bactreg = 2.056340

Bs = 8.225360

N = 10.000000

f1 = 4.580642

f2 = 37.677431

lambda_max = 65.493000

L = 33.768004

l_max = 32.746500

l_i = 25.214805

l_i = 19.415400

l_i = 14.949858

l_i = 11.511391

l_i = 8.863771

l_i = 6.825103

l_i = 5.255330

l_i = 4.046604

l_i = 3.115885

R_max = 38.441543

R_j = 29.599988

R_j = 22.791991

R_j = 17.549833

R_j = 13.513372

R_j = 10.405296

$R_j = 8.012078$
 $R_j = 6.169300$
 $R_j = 4.750361$
 $R_j = 3.657778$
 $L_{\text{actual}} = 34.783765$
 $\text{spacing_factor} = 0.135000$

Copyright (c) 2014, Ramann Mantha
 All rights reserved.

Redistribution and use in source and binary forms, with or without modification, are permitted provided that the following conditions are met:

- * Redistributions of source code must retain the above copyright notice, this list of conditions and the following disclaimer.

- * Redistributions in binary form must reproduce the above copyright notice, this list of conditions and the following disclaimer in the documentation and/or other materials provided with the distribution

- * Neither the name of nor the names of its contributors may be used to endorse or promote products derived from this software without specific prior written permission.

THIS SOFTWARE IS PROVIDED BY THE COPYRIGHT HOLDERS AND CONTRIBUTORS "AS IS"

AND ANY EXPRESS OR IMPLIED WARRANTIES, INCLUDING, BUT NOT LIMITED TO, THE

IMPLIED WARRANTIES OF MERCHANTABILITY AND FITNESS FOR A PARTICULAR PURPOSE ARE

DISCLAIMED. IN NO EVENT SHALL THE COPYRIGHT OWNER OR CONTRIBUTORS BE LIABLE

FOR ANY DIRECT, INDIRECT, INCIDENTAL, SPECIAL, EXEMPLARY, OR CONSEQUENTIAL

DAMAGES (INCLUDING, BUT NOT LIMITED TO, PROCUREMENT OF SUBSTITUTE GOODS OR

SERVICES; LOSS OF USE, DATA, OR PROFITS; OR BUSINESS INTERRUPTION) HOWEVER

CAUSED AND ON ANY THEORY OF LIABILITY, WHETHER IN CONTRACT, STRICT LIABILITY,

OR TORT (INCLUDING NEGLIGENCE OR OTHERWISE) ARISING IN ANY WAY OUT OF THE USE

OF THIS SOFTWARE, EVEN IF ADVISED OF THE POSSIBILITY OF SUCH DAMAGE.

C:\Users\denni\Dropbox\Disertation (Watson



LPDAMultiAntenna
ArrayNov10_2018.m

```

clc;      % Clear the command window.
close all; % Close all figures (except those of imtool.)
workspace; % Make sure the workspace panel is showing.
fontSize = 20;

% Create the lpda antenna object
%
% Parameters
BoardLength = 100;
BoardWidth = 100;
Height = .025;
StripLineWidth = 0.0625;
FeedLength = 0.014;
ArmLength = [3.115885 4.046604 5.255330 6.825103 8.863771 11.511391
14.949858 19.415400 25.214805];
ArmWidth = [25e-03 25e-03 25e-03 25e-03 25e-03 25e-03 25e-03 25e-03
25e-03];
ArmSpacing = [3.657778 4.750361 6.169300 8.012078 10.405296 13.513372
17.549833 22.791991 29.599988];
Substrate = dielectric('Air');
lumped_elements = lumpedElement('Impedance',50);
tilt_angle = [90 90 0];
tilt_axis = [0 0 1; 0 0 1; 0 0 1];
% Object creation
lpdipole = lpda('BoardLength', BoardLength, ...
    'BoardWidth', BoardWidth, ...
    'Height', Height, ...
    'StripLineWidth', StripLineWidth, ...
    'FeedLength', FeedLength, ...
    'ArmLength', ArmLength, ...
    'ArmWidth', ArmWidth, ...
    'ArmSpacing', ArmSpacing, ...
    'Substrate', Substrate, ...
    'Load', lumped_elements, ...
    'Tilt', tilt_angle, ...
    'TiltAxis', tilt_axis);

show(lpdipole)
figure;

% Script generated by antennaDesigner

% Define plot frequency
plotFrequency = 14000000;
% Define frequency range
freqRange = (7:0.5:28) * 1e6;

```

```

lamda=300e6/plotFrequency

% Define antenna
% myantenna=dipole('Length',lamda/2,'Width',0.02) % Dipole
%
myantenna=monopoleTopHat('Height',5,'Width',0.02,'GroundPlaneWidth',10
,'GroundPlaneLength', 10, 'TopHatWidth', 2, 'TopHatlength', 2)
% myantenna=monopole('Height',5,'Width',0.02,'GroundPlaneWidth',
5,'GroundPlaneLength', 5)
%myantenna=bowtieTriangular('Length',10,'FlareAngle',85)
myantenna=lpdipole
    antennaObject = myantenna

% show for myantenna
show(antennaObject)
title('Antenna Diagram')
% pattern for myantenna
figure;%fig1 Antenna Diagram

pattern(antennaObject, plotFrequency)
title('Antenna Element Pattern')
figure;%fig2 pattern

patternAzimuth(antennaObject, plotFrequency)
title('Azimuth')
figure;%fig3 patternAzimuth

% elevation for myantenna
patternElevation(antennaObject, plotFrequency)
title('Elevation')
figure;%fig4 patternElevation

% s11 for myantenna
s=sparameters(antennaObject,freqRange);
rfplot(s)
title('S11 Plot')
figure;%fig5

% VSWR of Antenna element
v = vswr(myantenna, freqRange);
plot(v)
title('VSWR Plot')
figure;%fig6

%% ---- Code added to create the ULA -----

% Elevation and azimuth angles
el = -090:090; % Elevation Angles
az = -180:180; % Azimuth Angles

% Generate the magnitude pattern for specified azimuth and elevation

```

```

[pat,az,el] = pattern(antennaObject,plotFrequency,az,el);

% Create a phased.CustomAntennaElement with the magnitude pattern
hAntenna = phased.CustomAntennaElement('MagnitudePattern',pat, ...
'ElevationAngles',el, 'AzimuthAngles',az);

% Create the ULA Object
numElements = 200; % Number of elements
elemSpacing = 10 % Element Spacing set to 10n or can apply Lamda/2
spacing with the following physconst('LightSpeed')/(2*plotFrequency);
taper = chebwin(numElements,40); %Apply Chebyshev Window (Taper to
reduce sidelobes) set to -60dB;
hULA =
phased.ULA(numElements,elemSpacing,'Element',hAntenna,'Taper',taper);

% bw=beamwidth(hULA.pattern,14e6,0:1:360,45,10)

% Plot the pattern of the ULA
hULA.pattern(plotFrequency);

for x=1:5;
    a=0:.5:2;
    [Directivity] = pattern(hULA,14e6,a,15);
    % y(x)=[Directivity]
    % [Directivity1] = pattern(hULA,14e6,0.5,15)
    % [Directivity2] = pattern(hULA,14e6,1.0,15)
    % [Directivity3] = pattern(hULA,14e6,1.5,15)

end
plot(a,Directivity);
title('Directivity');

```

```

%MATLAB Code from Sensor Array Analyzer App

%Generated by MATLAB 9.4 and Phased Array System Toolbox 3.6

clear
%Generated on 24-Aug-2018 07:37:15
%Create a uniform linear array withOUT taper
h = phased.ULA;
h.NumElements = 200;
h.ElementSpacing = 10.000;
h.ArrayAxis = 'y';

% Create a uniform linear array with taper
h1 = phased.ULA;
h1.NumElements = 200;
h1.ElementSpacing = 10.000;
h1.ArrayAxis = 'y';

% Calculate Taper   %t2
<
-
    sll = 60;   %t2
<
-
    wind = chebwin(200, sll)';   %2
<
-
    h1.Taper = wind; %2
%Create Isotropic Antenna Element
el = phased.IsotropicAntennaElement;
h.Element = el;

%Assign frequencies and propagation speed
F = 280000000;
PS = 3000000000;

%Create figure, panel, and axes
fig1 = figure;
panel = uipanel('Parent',fig1);
hAxes = axes('Parent',panel,'Color','none');
NumCurves = length(F);
%Plot 2d graph
fmt = 'rectangular';
cutAngle = 0;
pattern(h1, F, -180:180, cutAngle, 'PropagationSpeed', PS, 'Type', ...
    'directivity', 'CoordinateSystem', fmt );
pattern(h1, F, -180:180, cutAngle, 'PropagationSpeed', PS, 'Type', ...
    'directivity', 'CoordinateSystem', fmt );
axis(hAxes,'square')

fig2 = figure;
panel = uipanel('Parent',fig2);

```



```

hAxes = axes('Parent',panel,'Color','none');
NumCurves = length(F);
%Plot 2d graph
fmt = 'rectangular';
cutAngle = 0;
pattern(h, F, -180:180, cutAngle, 'PropagationSpeed', PS, 'Type', ...
        'directivity', 'CoordinateSystem', fmt );
axis(hAxes,'square')

%Create legend
legend_string = cell(1,NumCurves);
lines = findobj(gca,'Type','line');
for idx = 1:NumCurves
    [Fval, ~, Fletter] = engunits(F(idx));
    legend_string{idx} = [num2str(Fval) Fletter 'Hz; No Steering'];
end
legend(legend_string, 'Location', 'southeast');

```

APPENDIX B

Appendix B shows the copyright approvals for figures within the dissertation.

2/27/2020

Manage Account



Marketplace™

Special Requests > Special Request Details

Review Cart

Antenna Theory : Analysis and Design

GENERAL INFORMATION

Request ID	Request Date
600008176	26 Feb 2020
Request Status	Price
Accepted	0.00 USD

ALL DETAILS

ISBN-13:	9781118642061
Type of Use:	Republish in other published product
Publisher:	Wiley
Portion:	Chart/graph/table/figure

LICENSED CONTENT

Publication Title	Antenna Theory : Analysis and Design	Country	United States of America
Author/Editor	Balanis, Constantine A.	Rightsholder	John Wiley & Sons - Books
Date	12/28/2015	Publication Type	e-Book
Language	English		

REQUEST DETAILS

Portion Type	Chart/graph/table/figure	Distribution	Worldwide
Number of charts / graphs / tables / figures requested	2	Translation	Original language of publication
Format (select all that apply)	Print, Electronic	Copies for the disabled?	No
Who will republish the content?	Academic institution	Minor editing privileges?	No
		Incidental promotional use?	No

https://marketplace.copyright.com/rs-ui-web/manage_account/special-requests/details/4ca4a712-4809-4295-9743-a9b71168e5a4

1/2

2/27/2020

Manage Account

Duration of Use	Life of current edition	Currency	USD
Lifetime Unit Quantity	Up to 499		
Rights Requested	Main product		

NEW WORK DETAILS

Title	Dissertation: VIRTUAL SATCOM: LONG RANGE BROADBAND DIGITAL COMMUNICATIONS	Produced by	Old Dominion University Norfolk VA
Author	Dennis Watson	Expected publication date	2020-05-08

ADDITIONAL DETAILS

The requesting person / organization to appear on the license	Dennis Watson
---	---------------

REUSE CONTENT DETAILS

Title, description or numeric reference of the portion(s)	Figures 11.13 and 11.14	Title of the article/chapter the portion is from	Chapter 11
Editor of portion(s)	NA	Author of portion(s)	Balanis, Constantine A.
Volume of serial or monograph	NA	Issue, if republishing an article from a serial	NA
Page or page range of portion	609-611	Publication date of portion	2015-12-28

COMMENTS

 Add Comment / Attachment

26 Feb 2020 10:48:59 AM, by Dennis Watson
For my dissertation

 Review Cart

2/27/2020

Manage Account



Marketplace™

Special Requests > Special Request Details



Review Cart

Radio science

Article Semiempirical Model for Ionospheric Absorption based on the NRLMSISE-00 atmospheric mo...

GENERAL INFORMATION

Request ID	Request Date
600008181	26 Feb 2020
Request Status	Price
Accepted	0.00 USD ?



ALL DETAILS

ISSN:	1944-799X
Type of Use:	Republish in other published product
Publisher:	American Geophysical Union
Portion:	Chart/graph/table/figure

LICENSED CONTENT

Publication Title	Radio science	Rightholder	John Wiley & Sons - Books
Article Title	Semiempirical Model for Ionospheric Absorption based on the NRLMSISE-00 atmospheric model	Publication Type	e-Journal
		URL	http://www.agu.org/journals/rs/
Author/Editor	American Geophysical Union.	Start Page	81
		Issue	2
Date	01/01/1966	Volume	49
Language	English		
Country	United States of America		

REQUEST DETAILS

2/27/2020

Manage Account

Portion Type	Chart/graph/table/figure	Distribution	Worldwide
Number of charts / graphs / tables / figures requested	1	Translation	Original language of publication
Format (select all that apply)	Print, Electronic	Copies for the disabled?	No
Who will republish the content?	Academic institution	Minor editing privileges?	No
Duration of Use	Life of current edition	Incidental promotional use?	No
Lifetime Unit Quantity	Up to 499	Currency	USD
Rights Requested	Main product		

NEW WORK DETAILS

Title	Dissertation Title:VIRTUAL SATCOM: LONG RANGE BROADBAND DIGITAL COMMUNICATIONS	Produced by	Old Dominion University, Norfolk VA USA
Author	Dennis Watson	Expected publication date	2020-05-08

ADDITIONAL DETAILS

The requesting person / organization to appear on the license	Dennis Watson
---	---------------

REUSE CONTENT DETAILS

Title, description or numeric reference of the portion(s)	Figure 1. Newtral and ion densities generate by IRI-2012 and NRLMSISE-00	Title of the article/chapter the portion is from	Semiempirical Model for Ionospheric Absorption based on the NRLMSISE-00 atmospheric model
Editor of portion(s)	Cervera, M. A.; Pederick, L. H.	Author of portion(s)	Cervera, M. A.; Pederick, L. H.
Volume of serial or monograph	49	Issue, if republishing an article from a serial	2
Page or page range of portion	81-93	Publication date of portion	2014-02-05

COMMENTS



Add Comment / Attachment

26 Feb 2020 11:09:49 AM, by Dennis Watson

For my dissertation.

From: Ramann Mantha <ramannbharadwaj91@gmail.com>

Sent: Saturday, November 23, 2019 9:23 PM

To: dwats017@odu.edu

Subject: Re: MATLAB Central Contributor Question

Hello Mr. Watson,

Thank you for the email. Yes, I hereby grant you permission to cite my Matlab program/code in your dissertation references. Please forward me a final copy of the reference page from your dissertation so that I can save it for my records.

Ramann Mantha

Sent from my iPhone

On Nov 23, 2019, at 13:38, dwats017@odu.edu wrote:

Mr Ramann Mantha,

I used your MATLAB program to design a LPDA antenna for my Dissertation at Old Dominion University. Title: VIRTUAL SATCOM: LONG RANGE BROADBAND DIGITAL COMMUNICATIONS. My project is based on a beam forming aperture of many LPDA antennas to focus the High Frequency energy into narrow beam. I used your program to design the aperture elements. LPDA was selected due to wide bandwidth and beam forming performance capabilities.

Request permission to site you and your MATLAB program in my paper.
Did you publish a paper that explains the program?

Respectfully,

Dennis Watson
PHD Candidate
Old Dominion Universtity
Norfolk VA
dwats017@odu.edu
757-406-9526

APPENDIX C

Dissertation presentation.

VIRTUAL SATCOM: LONG RANGE BROADBAND DIGITAL COMMUNICATIONS

A Dissertation Presentation Submitted to the Faculty of
Old Dominion University in Partial Fulfillment of the
Requirements for the Degree of Doctor of Philosophy
Electrical and Computer Engineering
by

Dennis G Watson

Department of Electrical and Computer Engineering
Frank Batten College of Engineering and Technology
Old Dominion University, Norfolk Virginia, USA
February 27, 2020



Presented to:

Linda Vahala (Director)
Dimitrie Popescu (Member)
Otilia Popescu (Member)
Jose Fernandez (Member)



All Rights Reserved



Naval Strategy Depends on Robust Long-Range Communications



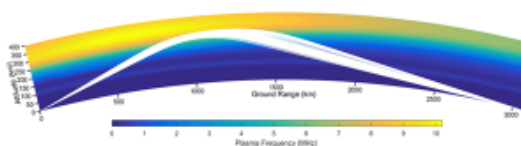
Current Naval strategy called Distributed Maritime Operations (DMO) requires.

- US Navy is mobile and needs high capacity wireless networks.
- Beyond Line of Sight (BLOS) communications is paramount.
- Navy needs an Alternatives to satellite communications

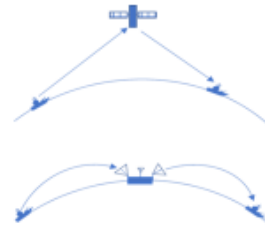
Why Virtual SATCOM:

- Virtual SATCOM is an innovative way to provide BLOS communications that is fast, robust, affordable, repairable and upgradable.
- SATCOM is vulnerable, expensive, and fragile.
- Virtual SATCOM is robust, and affordable with high data speed.

HF Skywave uses the charged ionosphere above earth to refract signals at long range.



Virtual SATCOM moves relay point from space to surface.



All right reserved, Old Dominion University



What is Innovative?

Land base vice space base relay segment: High power with high bandwidth on narrow steerable beam yields high data rate

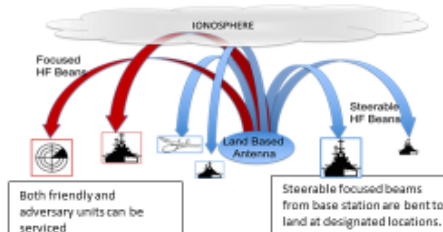
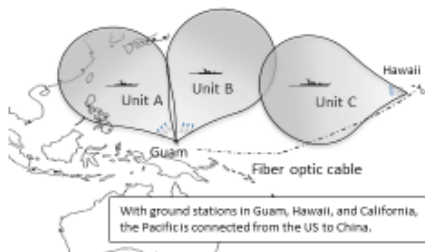


Innovative

- Active Electronic Scanned Array (AESA) for communication channel.
 - Directional beamforming antenna array
 - High gain on target
 - High power transmitter
- Wide Band Channels -- 3 MHz vs 3kHz
 - Yields high data rate (>10 Mbps)
- Increasing HF usefulness in 21st Century
 - Frequency reuse, Low Prob of Detect, Anti-Jam
- Changing the pyridine on how to communicate on HF

Contribution of this work:

1. I developed a viable innovative concept and design that will change Military communications.
2. Completed tradeoff analysis of data rate vs frequency, bandwidth, noise level, antenna gain & power and efficiency.
3. Modified a RF propagation program to analysis the ionosphere across four seasons and time of day in various locations. Results confirm bandwidth is available almost 24/7.
4. Designed a wide band LPDA antenna for 7-28 MHz frequency range for large antenna array.
5. Designed and modeled a 200-element array to show the beamforming capabilities.
6. Designed a command and control network to monitor and adjust parameters in real time.
7. Developed a modulation scheme using MILSTD188-110D with OFDM modulation to enable high data rate in harsh multipath environment.



All right reserved, Old Dominion University



Virtual SATCOM Design Flowchart (1)



Need—DoD requires robust BLOS Command and Control

- Long-range
- Reliable
- High data speed
- Low Probability of Detection, and Denial

Current Weakness
Current HF system is long range, but:

- Slow data speed
- High probability of detection
- Not reliable

- Data speed > 10 Mbps
- High reliability communication
- Lower the probability of detection
 - Use off the shelf equipment
 - Upgradeable & repairable

- Ray propagation model based on accepted mathematics (Hasegrove equations)
- PHaRLAP model developed by DTSC
 - Model uses IRI database
 - Robust accurate model
 - Designed for radar analysis

**Solution –
Virtual
SATCOM**

**Key Design
Parameters**

**Ionosphere
Modeling &
Analysis**

Current Weakness

Current SATCOM system is high data speed, but:

- SATCOM is vulnerable
- SATCOM is expensive
- SATCOM cannot be:
 - Repaired or upgraded

- Relay station—high-pwr & gain antenna at base station
- Wide bandwidth (3 MHz)
- Narrow beam width (1°)
- Electronically steerable beam
- 200 kW Transmitter
- Broadband antenna (7-28 MHz)
- Agile detection and frequency control

- We modified PHaRLAP program to support communications vice radar analysis
- Tested off east coast into Atlantic and from Guam looking North in Pacific
- Tested day and night and sessional
- **Modeling shows adequate spectrum available**

All right reserved, Old Dominion University



Virtual SATCOM Design Flowchart (2)



Mobile Station

Antenna & Power Limited
Three antenna configuration

- Gain > 2- 6 dBi
- Low power TX < 100 W
- Agile Automatic Link

- Two wideband duo-conical antennas
- One directional/steerable LPDA antenna
 - Uses off the shelf equipment
 - Software defined Radio with ALE
 - Upgradeable & repairable
- Receives sounding to determine real time propagation information
- Mobile reports, at LPI power, via JS8, on C2 channel, its position and optimum frequency
- Mobile establish communication's at low data rate and ramps up to optimum on subchannels.
 - Monitors & adjusts data rate of each subchannel.

**Antenna
Array
Design**

**Antenna
Element
Design**

**Operations
and other
Infrastructure**

Base Station

Large Array for High-PWR TX and highly sensitive RX

- Aperture Gain > 20 dBi
- TX Power > 200 kW
- Uniform linear array
- Two-kilometer aperture of
 - 200 elements
 - Spaced 10 m apart
- Electronically steerable in azimuth and range
- Agile frequency adjustment across 7-28 MHz
- Mechanically fixed, no moving parts

Each Element

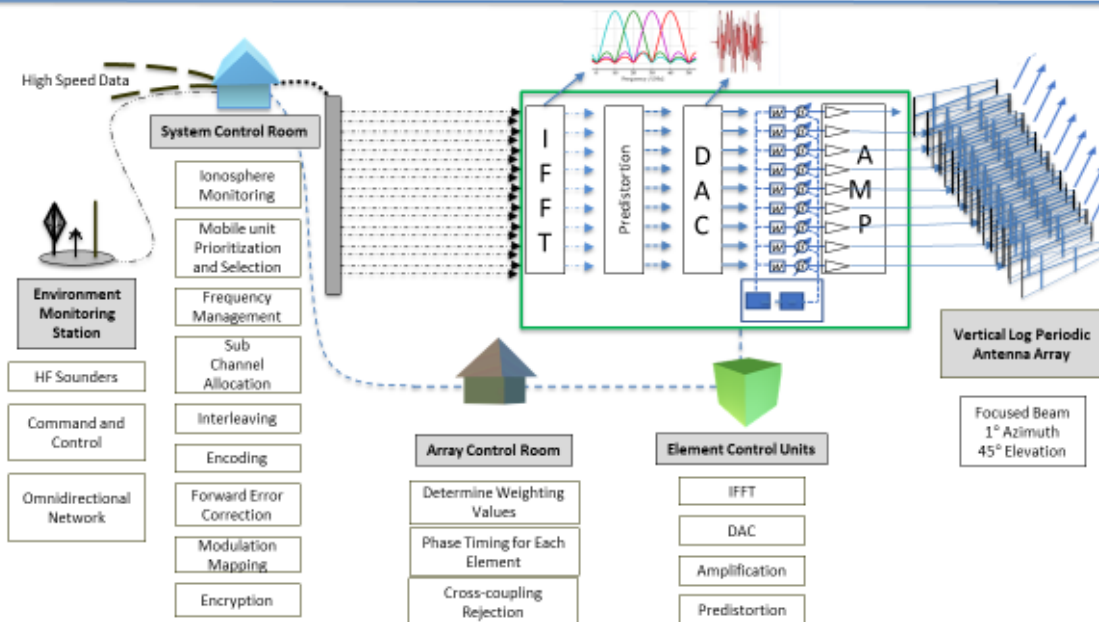
- Vertical Log Periodic Dipole antenna
 - Wide bandwidth
 - Increased gain for optimum elevation angles
- Each element has unique transmitter for DAC and amplification. 200 total elements with 1 kW TX.
- Each element is controlled by master control stations applying weighting and phase control to aim antenna and suppress sidelobes and interference.

Operations

- Omni directional soundings (7-28 MHz) to inform passband.
- Low pwr (LPI) control signals for check-in and agile ops.
- Command and Control (C2) using JS8 modulation
 - JS8 is an FSK(B) 50 Hz signal with significant FEC.
- Electronic surveillance system to detect interference and jamming.

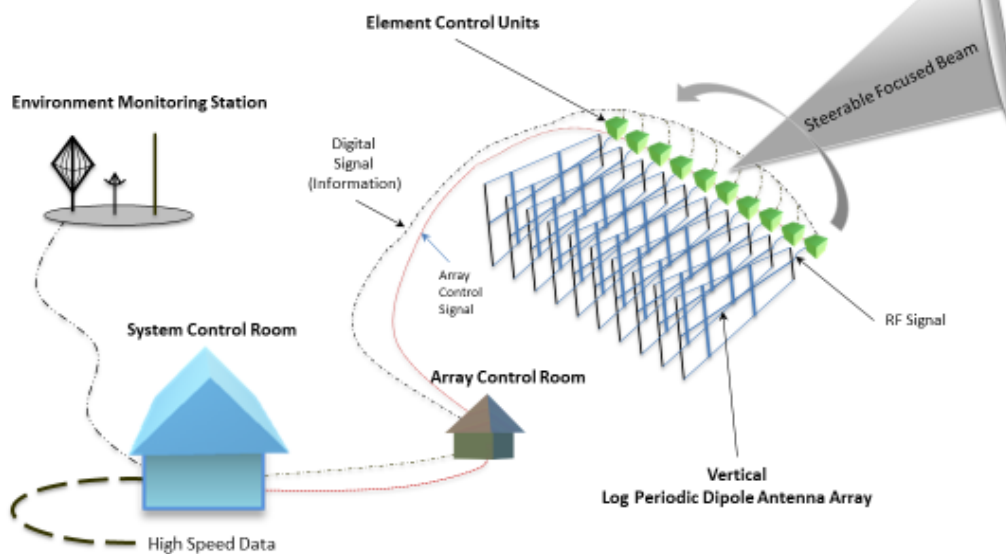
All right reserved, Old Dominion University

Diagram of Virtual SATCOM Transmitter



All right reserved, Old Dominion University

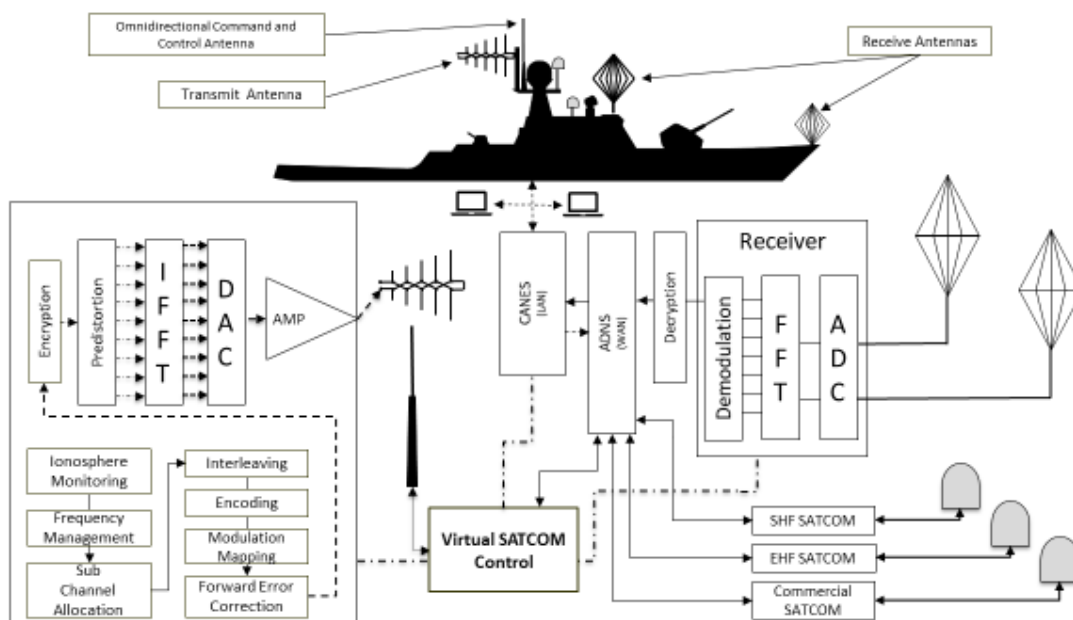
Virtual SATCOM Systems Diagram



All right reserved, Old Dominion University



Diagram of Virtual SATCOM Mobile System



All right reserved, Old Dominion University

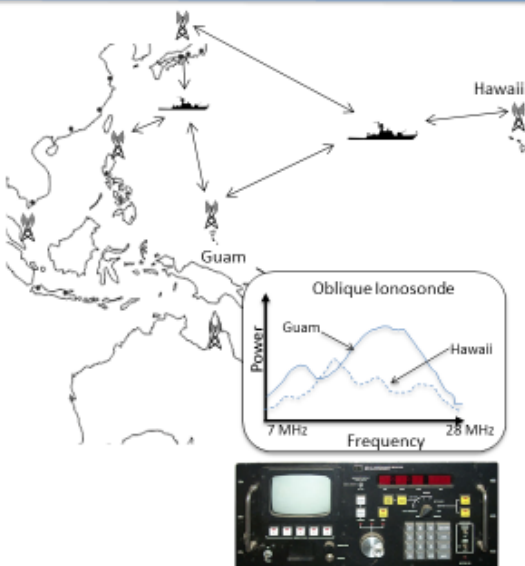


Omnidirectional Command and Control Network and Sounders



How communications is established :

- Omnidirectional oblique ionosphere sounding is transmitted by base station (Guam and Hawaii) to mobile platforms to establish best frequencies for communication
 - Provides real time propagation information.
 - Tx Sweeps FMCW beacon from 7 to 28 MHz.
 - Mobile units only receive signals with good propagation parameters.
 - Mobile units relay location and best frequency for communications on C2 frequencies of 10, 15, 20 & 25 MHz using narrowband modulation using JS8 Modulation.
 - Base station will respond on check-in frequency with directional communication's frequency, modulation, etc.



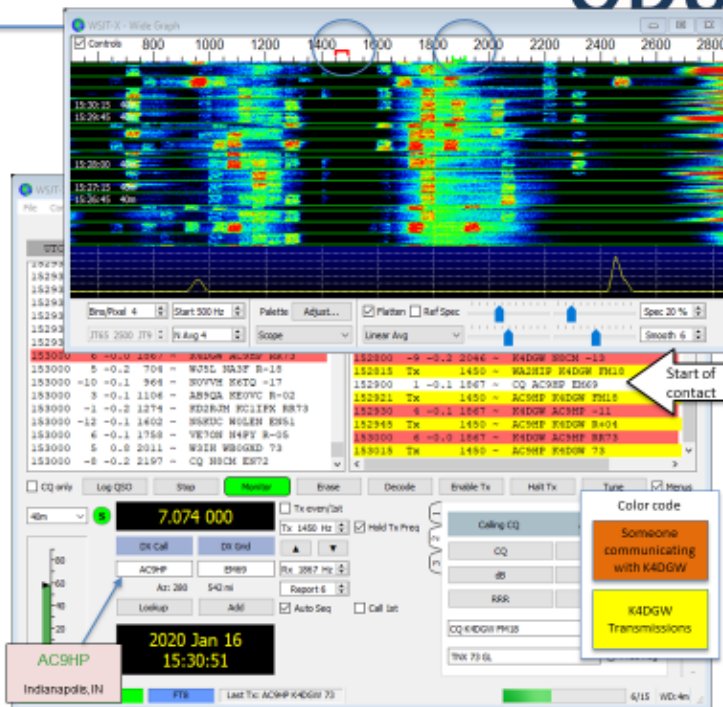
All right reserved, Old Dominion University



Command and Control (C2) Narrowband, low data rate, low power



- FT8 is an open source code that transmits call sign, position and power level of a received signal back to the requesting unit.
- The modulation has had great success with thousands of contacts each day
- Signal parameters:
 - Transmit and receive sequence period length: 15 s
 - Bandwidth: 50 Hz within a 3 kHz window.
 - Modulation is 8-FSK, tone at a frequency spacing of 6.25 Hz
 - Message length: 76 bits + 12-bit CRC
 - Forward error correction (FEC) code: Low density parity check (LDPC) at (174,87)
 - Time slot is divided into 79 time intervals
 - 58 intervals allotted for the message + FEC + CRC
 - 21 intervals allotted for SYNCH TONES
 - Synchronization is a 7x7 Costas arrays transmitting 7 Synch tones at start, middle, and end of message.
 - 79-time intervals, of 0.16 second duration, so each symbol is transmitted for 0.16 s.
 - Total message duration: 12.64 seconds
 - Decoding threshold: -20 dB
 - Multi-decoder finds and decodes all signals in passband of 3 kHz
 - Optional auto-sequencing and auto-reply
- To the right, K4DQW is responding to a CQ request from AC9HP. K4DQW is TX on 1450 to 1500 Hz above 7.074 MHz.
- AC9HP is TX on 1867 to 1917 Hz above 7.048 MHz.
- The two stations are 542 miles apart and K4DQW is transmitting at 25 Watts.



Command and Control Network



How to establish communications:

- Directional AESA signal is transmitted by base station to mobile platforms to establish communication
 - Once locked on, base station will initiate communications at narrow bandwidth and slow data rate then increase bandwidth as propagation environment is determined.
 - Once connected mobile and base station use Agile ALE techniques to maintain best link.
 - Mobile unit will transmit quality of service via set aside frequencies to help maintain high throughput data flow.





Command and Control Network



How to establish communications:

- Directional AESA signal is transmitted by base station to mobile platforms to establish communication
 - Once locked on, base station will initiate communications at narrow bandwidth and slow data rate then increase bandwidth as propagation environment is determined.
 - Once connected mobile and base station use Agile ALE techniques to maintain best link.
 - Mobile unit will transmit quality of service via set aside frequencies to help maintain high throughput data flow.



All right reserved, Old Dominion University



Information Theory

How Bandwidth and Noise Power Affect Virtual SATCOM Link Budget



• Information Theory

$$C = B \log_2 (1 + SNR)$$

$$SNR = \frac{P_r}{BN_0}$$

• Link Budget

$$\frac{P_r}{P_t} = G_t G_r \left(\frac{\lambda}{4\pi R} \right)^2$$

$$P_{r,dB} = P_{t,dB} + G_{t,dB} + G_{r,dB} - P_L, \quad P_{L,dB} = 20 \log \left(\frac{4\pi R}{\lambda} \right)$$

For Virtual SATCOM:

- If bandwidth is 3 MHz and Signal/Noise Ratio is 15 (12 dB), then capacity is 12 Mbps.
- If bandwidth is 3 kHz the capacity is only 12 kbps.
- As bandwidth increase, SNR decreases, so P_r must be increased to maintain the same SNR.

- Virtual SATCOM will need 42 dB of P_r to account for the increased bandwidth (30 dB of bandwidth and 12 dB of SNR).
- Virtual SATCOM must increase P_t and G_t to meet the desired SNR.
- Virtual SATCOM base station produces:
 - $G_t \rightarrow +20$ dBi
 - $P_t \rightarrow 200$ kW which is 23dB over 1kW TX

All right reserved, Old Dominion University

Forward Link

Where:

- P_R is power at receiver [W]
- P_T is power at transmitter 200000 [W], 53 dB
- G_T is gain of transmitter 20 [dBi]
- G_R is gain of receiver 2 [dBi]
- Wavelength λ of carrier 20 [m]
- R is range TX to RX 3000 [km]
- Path Loss is -126 dB
- N_0 is Noise Pwr -140 dBW/Hz
- B is Bandwidth 3MHz
- Data Rate C 10 Mbps

$$P_R = 53 + 20 + 2 - 126 = -51 \text{ dBW or } 8 \mu\text{W}$$

$$SNR_{dB} = \left(\frac{P_R}{N_0 B} \right) = -51 - (-140 + 65) = 24_{dB}$$

$$E_b = \frac{P_R}{C} = \frac{8 \mu\text{W}}{10 \text{ Mbps}} = \frac{8 \times 10^{-6}}{1 \times 10^7} = 8.0 \times 10^{-13} \left[\frac{\text{W}}{\text{b}} \right]$$

$$\frac{E_b}{N_0} = \frac{8.0 \times 10^{-13}}{-140 \text{ [dBW / Hz]}} = \frac{8.0 \times 10^{-13}}{1 \times 10^{-14}} = 80 = 19 \text{ dB}$$

Back Link

Where:

- P_R is power at receiver [W]
- P_T is power at transmitter 100 [W], 20dB
- G_T is gain of transmitter 6 [dBi]
- G_R is gain of receiver 20 [dBi]
- Wavelength λ of carrier 20 [m]
- R is range TX to RX 3000 [km],
- Path Loss is -126 dB
- N_0 is Noise Pwr -150 dBW/Hz
- B is Bandwidth 1 MHz, 60 dB
- C is Data Rate 1 Mbps

$$P_{R(GS)} = 20 + 20 - 126 = -86 \text{ dBW or } 10 \text{ nW}$$

$$SNR_{dB} = \left(\frac{P_R}{N_0 B} \right) = -86 - (-150 + 60) = 10_{dB}$$

$$E_b = \frac{P_R}{C} = \frac{10 \text{ nW}}{1 \text{ Mbps}} = \frac{10 \times 10^{-9}}{1 \times 10^6} = 1 \times 10^{-14} \left[\frac{\text{W}}{\text{b}} \right]$$

$$\frac{E_b}{N_0} = \frac{1 \times 10^{-14}}{-150 \text{ [dBW / Hz]}} = \frac{1 \times 10^{-14}}{1 \times 10^{-15}} = 10 = 10 \text{ dB}$$

All right reserved, Old Dominion University

Scenario	Freq [MHz]	C [Mbps]	E_b/N_0 [dB]	SNR [dB]	$\log_{10}(1+SNR)$	SMR	B [Hz]	No [W/Hz]	P _r [W]	P _r [dBW]	P _t [W]	P _t [dBW]	G _t [dB]	G _r [dB]	P _L [dB]	Freq [Hz]	Lambda [m]	Range [m]	L [dB]	$E_b \cdot P_r / C$
Operator Input	x						x	x					x		x			x		
Forward Link	7	28.267	18.62	28.36	5.42	689.1	32*06	1.0E-14	2.06E-05	-46.87	200000	53	30	2	118.88	7.00E+06	42.88	3E+06	3	7.27E-13
	14	22.286	13.63	22.34	7.43	171.3	32*06	1.0E-14	5.14E-06	-42.89	200000	53	30	2	124.90	1.40E+07	21.43	3E+06	3	2.51E-13
	28	16.360	8.66	16.32	9.45	82.9	32*06	1.0E-14	1.28E-06	-48.91	200000	53	30	2	130.92	2.80E+07	10.71	3E+06	3	7.86E-14
Forward Link Low bandwidth BW=1 MHz	7	11.006	22.71	33.13	11.01	2059.2	32*08	1.0E-14	2.06E-05	-46.87	200000	53	30	2	118.88	7.00E+06	42.88	3E+06	3	1.87E-12
	14	5.003	17.58	27.13	9.01	513.8	32*08	1.0E-14	5.14E-06	-42.89	200000	53	30	2	124.90	1.40E+07	21.43	3E+06	3	5.70E-13
	28	7.016	12.63	21.09	7.02	126.9	32*08	1.0E-14	1.28E-06	-48.91	200000	53	30	2	130.92	2.80E+07	10.71	3E+06	3	1.83E-13
Forward Link Low Gain G1=14 dBi	7	22.306	13.64	22.36	7.44	171.3	26*04	1.0E-14	5.14E-06	-42.87	200000	53	24	2	118.88	7.00E+06	42.88	3E+06	3	2.21E-13
	14	18.281	8.59	18.34	9.46	82.9	26*04	1.0E-14	1.28E-06	-48.89	200000	53	24	2	124.90	1.40E+07	21.43	3E+06	3	7.93E-14
	28	10.666	4.81	10.52	5.56	10.8	26*04	1.0E-14	5.23E-07	-64.91	200000	53	24	2	130.92	2.80E+07	10.71	3E+06	3	5.03E-14
Forward Link High RX/TX losses	7	26.283	16.10	26.36	8.63	348.3	26*04	1.0E-14	1.03E-05	-49.87	200000	53	30	2	118.88	7.00E+06	42.88	3E+06	6	6.07E-13
	14	19.321	11.25	19.34	6.46	85.8	26*04	1.0E-14	2.06E-06	-54.89	200000	53	30	2	124.90	1.40E+07	21.43	3E+06	6	1.33E-13
	28	15.488	6.79	15.52	4.48	21.5	26*04	1.0E-14	5.44E-07	-61.91	200000	53	30	2	130.92	2.80E+07	10.71	3E+06	6	4.78E-14
Forward Link Average	16.333	16.772	12.973	21.28	8.48	556.1	32*06	1.0E-14	6.19E-06	-55.14	200000	53	30.50	2	124.90	1.63E+07	25.00	3E+06	5.75	5.82E-13
Back Link Reduced Noise & BW Tx=100W, 6 dBi	7	4.705	1.47	16.13	4.74	26	16*06	1.0E-15	2.06E-08	-75.88	200	20	6	20	118.88	7.00E+06	42.88	3E+06	3	5.66E-15
	14	2.355	0.33	8.33	1.90	6	16*06	1.0E-15	6.45E-09	-61.90	200	20	6	20	124.90	1.40E+07	21.43	3E+06	3	2.23E-15
	28	1.178	0.33	2.08	1.59	2	16*06	1.0E-15	1.61E-09	-67.92	200	20	6	20	130.92	2.80E+07	10.71	3E+06	3	1.18E-15
Back Link Average	16.333	3.409	0.711	8.33	5.62	11	16*06	1.0E-15	1.13E-08	-61.902	200	20	6	20	124.90	1.63E+07	25.00	3E+06	3	2.94E-15
Ship to ship 1000km	7	2.127	1.47	5.66	2.23	2.7	12*06	1.0E-15	2.68E-09	-66.24	200	20	6	2	106.34	7.00E+06	42.86	3E+06	3	1.95E-15
	14	0.941	1.47	-0.34	0.94	0.9	12*06	1.0E-15	9.20E-10	-60.26	200	20	6	2	116.36	1.40E+07	21.43	3E+06	3	9.78E-16
	28	0.299	1.47	-6.58	0.30	0.2	16*06	1.0E-15	2.30E-10	-86.38	200	20	6	2	121.38	2.80E+07	10.71	3E+06	3	7.70E-16
Ship to Ship Average	16.333	1.356	1.47	-0.38	1.28	1.6	12*06	1.0E-15	1.61E-09	-80.26	200	20	6	2	115.38	1.63E+07	25.00	3E+06	3	1.13E-15

Varied: frequency, bandwidth, antenna gain, power, efficiency, range and link direction

All right reserved, Old Dominion University

The PHaRLAP model is based on the Hamilton principal. Dr. Jennifer Haselgrove was the first to derive the Hamiltonian ray tracing equations for HF radio waves through the ionosphere. These equations have been extensively used to study HF radio wave propagation and are the basis of the PHaRLAP program.

$$\frac{dx}{d\tau} = \frac{c}{n} \left(\cos \chi + \sin \chi \frac{1}{n} \frac{\partial n}{\partial \chi} \right)$$

$$\frac{dz}{d\tau} = \frac{c}{n} \left(\sin \chi - \cos \chi \frac{1}{n} \frac{\partial n}{\partial \chi} \right)$$

$$\frac{d\chi}{d\tau} = \frac{c}{n^2} \left(\cos \chi \frac{1}{n} \frac{\partial n}{\partial z} - \sin \chi \frac{1}{n} \frac{\partial n}{\partial x} \right)$$

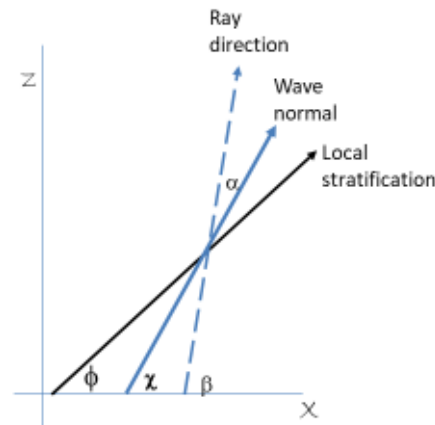
Where

χ = angle between the wave normal and the respective axis;

c = speed of light in vacuum.

n = refractive index = c/v

v = velocity of wave



All right reserved, Old Dominion University

The model process:

- Cut the ionosphere into a grid and calculate the index of refraction using electron density in each grid element.
- With the grid index of refraction, signal frequency, and elevation angle, the model can calculate the refraction angle to determine the propagation path from transmit to reception.

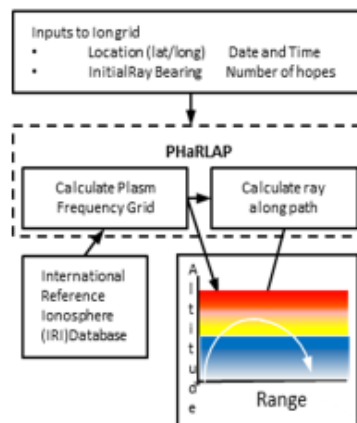
We modified the PHaRLAP program: We modified the MATLAB code to analyze one-way communication to a precise location. Then ran from different locations and times.

We modified PHaRLAP for single hop, point to point, analysis.

- We Ran the new program at numerous frequencies / elevations, recording rays landing at a precise locations from ground station
 - Ran the model from ODU on east coast looking east at 3000 km during each season every hour of a day.
 - Ran model every hour for 24 hours on September 2, 2016 to capture the total picture for the day and the results can be seen in Table 1.
 - We input a large range of frequencies and rejected the signals that did not return to the surface at a given locations.
 - Model calculates the ion density using International Reference Ionosphere (IRI) database. IRI is an international project sponsored by United Nations (ITU).

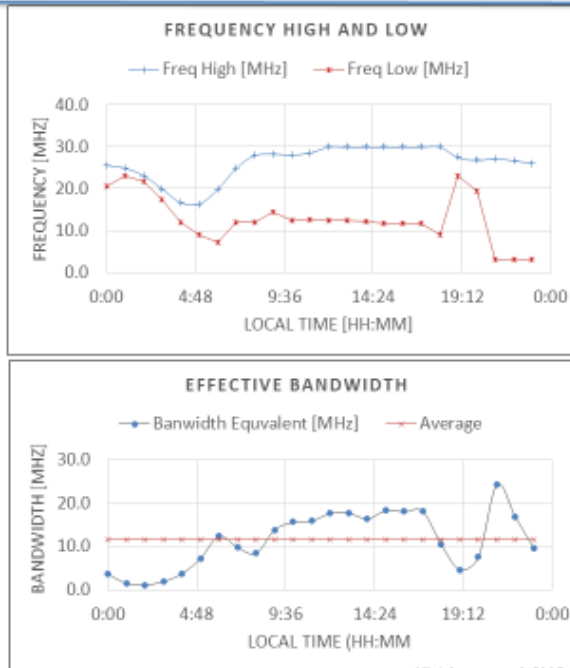
Advantage of our approach:

- Beam steering and frequency adjusted to follow the ionosphere.
- Trading omnidirectional wide beam with narrow bandwidth signal for narrow beam and wide bandwidth signal.
- Narrow beam prevents interference outside the beam and increases SNR while wide bandwidth increases data rate.
- Beam footprint size adjusted as required.





Results of Virtual SATCOM PhaRLAP Analysis



Output of PhaRLAP Guam looking north on September 2, 2016

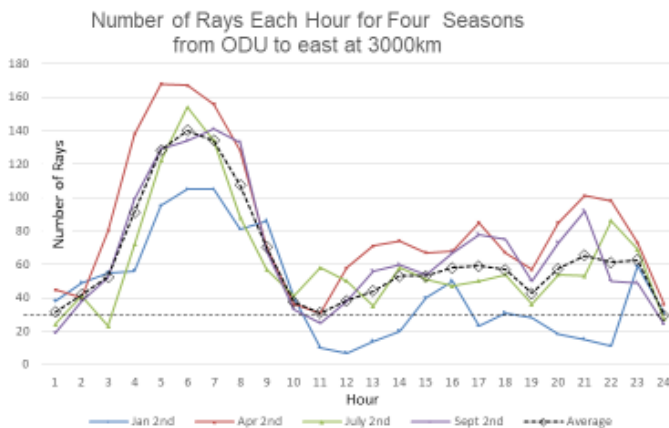
Local Time GUAM	Freq High [MHz]	Freq Low [MHz]	High to Low [MHz]	Count of 100 kHz channels	Bandwidth Equivalent [MHz]
0:00	25.6	20.5	5.1	36	3.6
1:00	24.9	23.1	1.8	15	1.5
2:00	23.1	21.7	1.4	11	1.1
3:00	19.9	17.4	2.5	19	1.9
4:00	16.6	12.0	4.6	37	3.7
5:00	16.3	9.0	7.3	72	7.2
6:00	19.8	7.2	12.6	124	12.4
7:00	24.9	11.9	13.0	98	9.8
8:00	28.0	11.9	16.1	84	8.4
9:00	28.3	14.5	13.8	138	13.8
10:00	28.1	12.4	15.7	156	15.6
11:00	28.6	12.7	15.9	159	15.9
12:00	30.0	12.5	17.5	176	17.6
13:00	30.0	12.4	17.6	177	17.7
14:00	30.0	12.2	17.8	164	16.4
15:00	30.0	11.6	18.4	183	18.3
16:00	30.0	11.6	18.4	180	18.0
17:00	30.0	11.8	18.2	181	18.1
18:00	30.0	8.9	21.1	104	10.4
19:00	27.5	23.0	4.5	46	4.6
20:00	26.8	19.4	7.4	75	7.5
21:00	27.2	3.0	24.2	243	24.3
22:00	26.7	3.0	23.7	168	16.8
23:00	26.1	3.0	23.1	96	9.6
AVERAGE	26.2	12.8	13.4	114.3	11.4

19

All right reserved, Old Dominion University

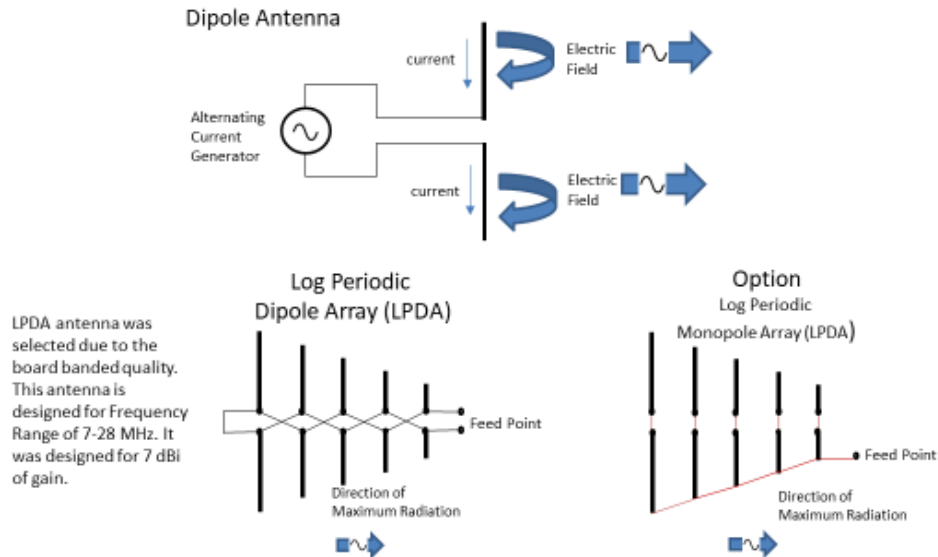


PhaRLAP Model Data From East Coast Looking East for Each Season



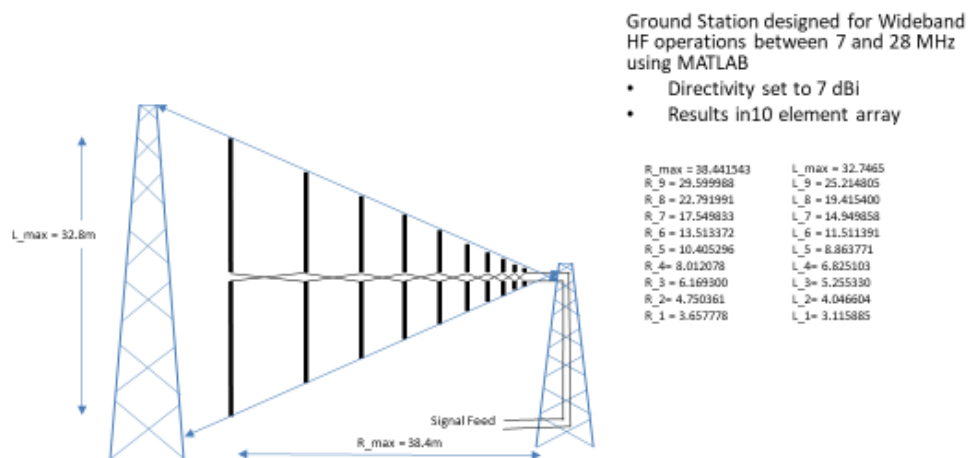
Time of Day	Number of Rays				
	Jan 2nd	Apr 2nd	July 2nd	Sept 2nd	Average
0	38	45	24	19	31.5
1	49	40	41	38	42
2	55	80	23	52	52.5
3	56	138	72	99	91.25
4	95	168	122	129	128.5
5	105	167	154	134	140
6	105	156	154	141	134
7	81	128	88	133	107.5
8	86	70	57	68	70.25
9	40	36	41	33	37.5
10	10	31	58	25	31
11	7	58	50	38	38.25
12	14	71	35	56	44
13	20	74	58	60	53
14	40	67	51	54	53
15	50	68	47	67	58
16	23	85	50	78	59
17	31	67	54	75	56.75
18	28	57	36	50	42.75
19	18	85	54	75	57.5
20	15	101	53	92	65.25
21	11	98	86	50	61.25
22	59	75	69	49	62.5
23	31	36	27	24	29.5

All right reserved, Old Dominion University

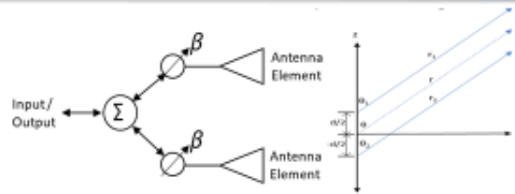


All right reserved, Old Dominion University

21



All right reserved, Old Dominion University



$$\vec{E}_t = \vec{E}_1 + \vec{E}_2 = \hat{a}_\theta j\eta \frac{kI_0 l}{4\pi} \left\{ \frac{e^{-j(kr_1 - \frac{\beta}{2})}}{r_1} |\cos \theta_1| + \frac{e^{-j(kr_2 - \frac{\beta}{2})}}{r_2} |\cos \theta_2| \right\}$$

$$E_t = \hat{a}_\theta j\eta \frac{kI_0 l}{4\pi r} e^{-jkr} |\cos \theta| (2) \left\{ \cos \left[\frac{1}{2} (kd \cos \theta + \beta) \right] \right\}$$

$$\hat{a}_\theta j\eta \frac{kI_0 l}{4\pi r} e^{-jkr} |\cos \theta|$$

Single Element Contribution

$$AF = \sum_{n=1}^N AF_n = N \cos \left[\frac{1}{2} (kd \cos \theta + \beta) \right]$$

Array Factor Contribution

All right reserved, Old Dominion University

23

Table 5 Directivity across the Virtual SATCOM Spectrum

Frequency (MHz)	Array Length L (m)	Wavelength λ (m)	Directivity D_0 (dB)
7	1990	43	19.6
14	1990	21.5	22.7
21	1990	14.3	24.5
28	1990	10.7	25.7

Note: The average directivity for a 200-element array with 10 m spacing is 23.13 dBi.

All right reserved, Old Dominion University



Half Power Beam Width



$$\Theta_{\text{halfpower}} = 2 \left| \frac{\pi}{2} - \cos^{-1} \left(\pm \frac{2.782\lambda}{2\pi L} \right) \right|$$

$$L = (N - 1)d$$

Frequency (MHz)		7	14	28
Lambda (m)		42.857	21.429	10.714
Distance between elements (m)		10.000		
Number of Array Elements	Total Array Length	7 MHz Half Power Beamwidth (Degrees)	14 MHz Half Power Beamwidth (Degrees)	28 MHz Half Power Beamwidth (Deg)
2	10	143.169	56.640	27.442
4	30	56.640	27.442	13.622
8	70	27.442	13.622	6.799
10	90	21.877	10.889	5.438
20	190	10.889	5.438	2.718
40	390	5.438	2.718	1.359
50	490	4.350	2.175	1.087
100	990	2.175	1.087	0.544
150	1490	1.450	0.725	0.362
200	1990	1.087	0.544	0.272
250	2490	0.870	0.435	0.217

Note: As the number of array elements increases so L increase and the \cos^{-1} term approaches $\pi/2$ and the half power beamwidth becomes narrower.

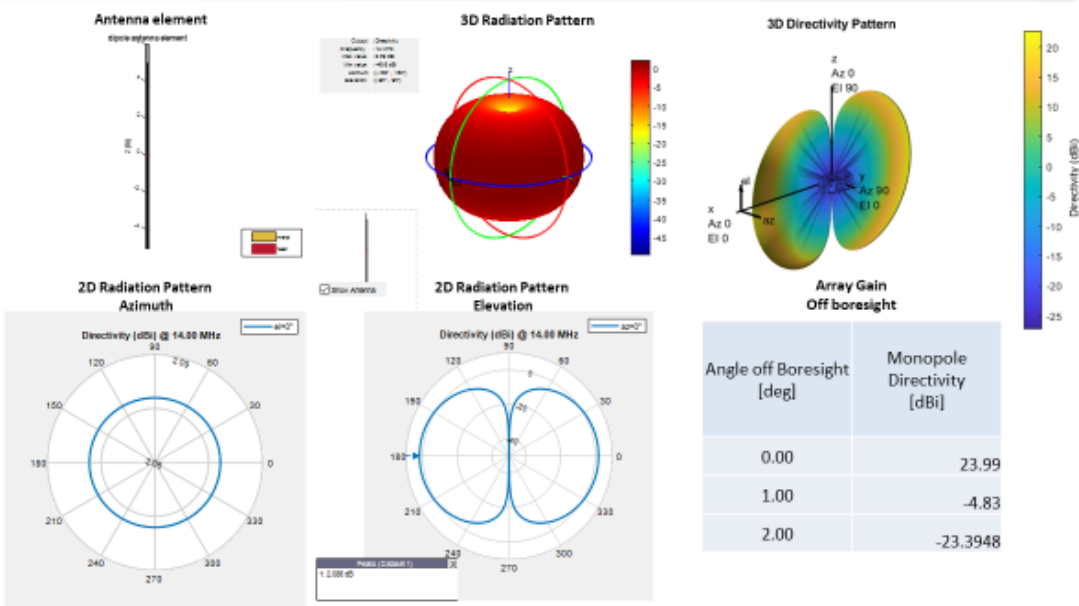
Frequency MHz	λ m	Distance Between Elements m	Number of Elements #	Array Length (N*d)-d m	Half Power Beamwidth degrees
7	42.86	10	200	1990	1.09
8	37.50	10	200	1990	0.95
9	33.33	10	200	1990	0.85
10	30.00	10	200	1990	0.76
11	27.27	10	200	1990	0.69
12	25.00	10	200	1990	0.63
13	23.08	10	200	1990	0.59
14	21.43	10	200	1990	0.54
15	20.00	10	200	1990	0.51
16	18.75	10	200	1990	0.48
17	17.65	10	200	1990	0.45
18	16.67	10	200	1990	0.42
19	15.79	10	200	1990	0.40
20	15.00	10	200	1990	0.38
21	14.29	10	200	1990	0.36
22	13.64	10	200	1990	0.35
23	13.04	10	200	1990	0.33
24	12.50	10	200	1990	0.32
25	12.00	10	200	1990	0.30
26	11.54	10	200	1990	0.29
27	11.11	10	200	1990	0.28
28	10.71	10	200	1990	0.27
Average	20.143	10	200	1990	0.511

All right reserved, Old Dominion University



Antenna Pattern at 14 MHz

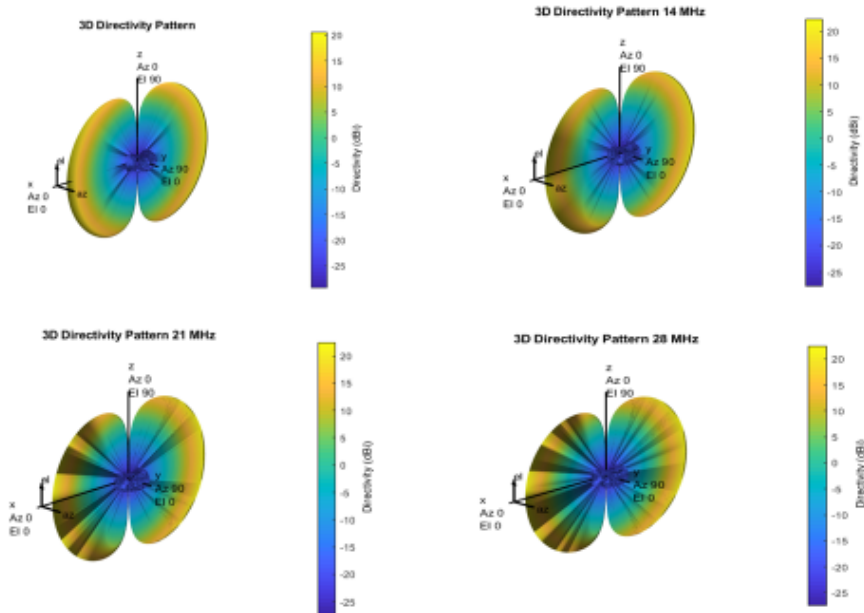
Antenna element



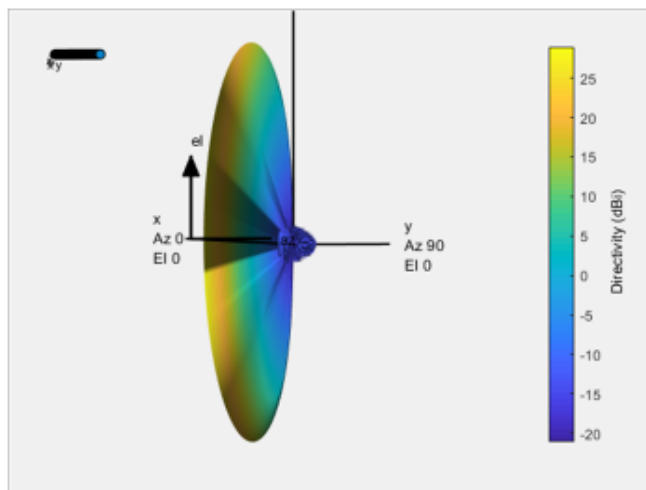
All right reserved, Old Dominion University



Virtual SATCOM Antenna Pattern
200 Elements Spaced 10m Apart
Designed with MATLAB Antenna Designer



Virtual SATCOM Array of 215 x 2 Antennas
Designed with FEKO EM Software

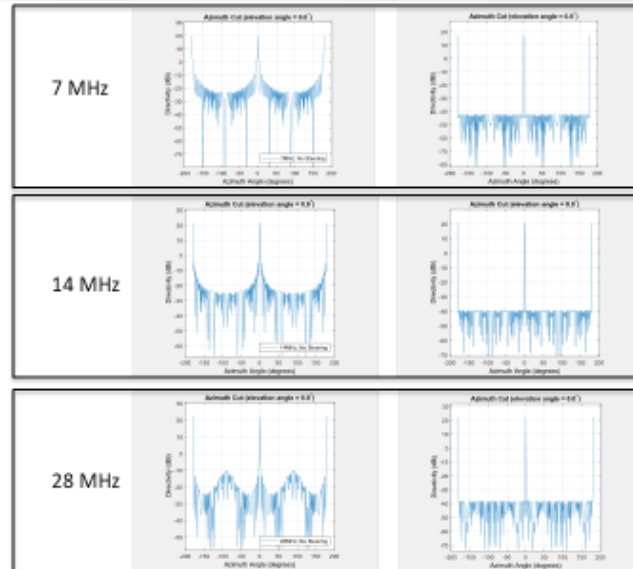
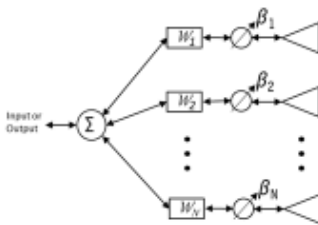


Applying static weighting to antenna array weighting to reduce sidelobes. Here tapering is Chebyshev at -60 dB.

Program run at 7, 14 and 28 MHz, figures show both weighting and no weighting.

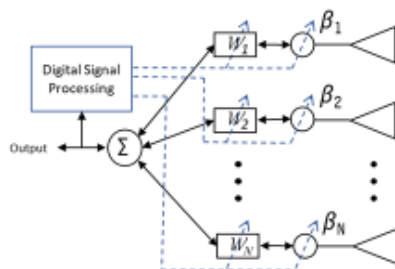
$$AF = (w_1)e^{j\psi} + (w_2)e^{j2\psi} + \dots + (w_N)e^{j(N-1)\psi}$$

where $\psi = kd \cos \theta + \beta$

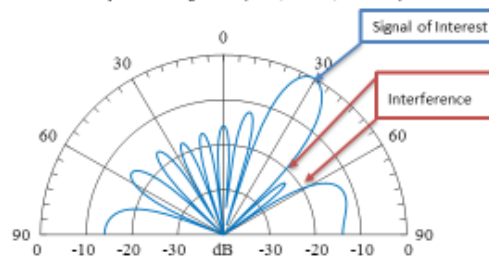


All right reserved, Old Dominion University

29



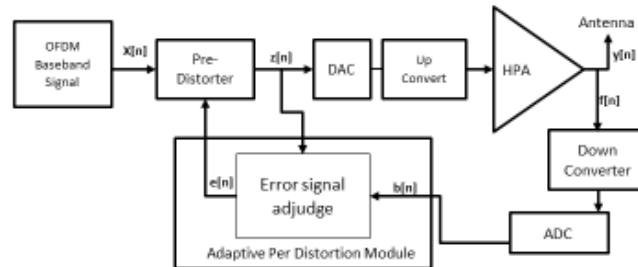
Linear Array Beamforming Pattern (N=10, d=0.5 λ, SOI θ=30°)



Weights (Amplitude) of Each Element		
Exact Value	Normalized	
1	0.111991	1.000000
2	0.083147	0.742440
3	0.082839	0.739693
4	0.103748	0.926400
5	0.115847	1.034435
6	0.117143	1.046002
7	0.097913	0.874295
8	0.082464	0.736341
9	0.084492	0.754453
10	0.113813	1.016268

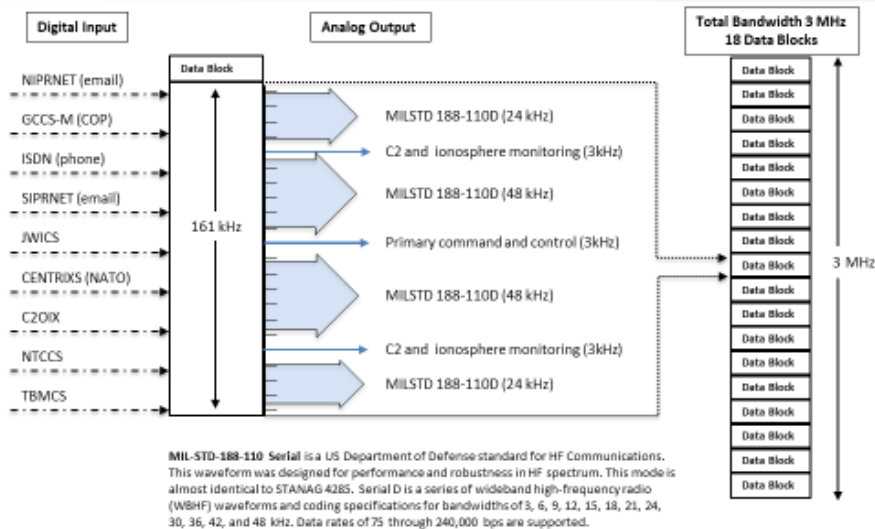
Beta (Phase in degrees) of Each Element		
Exact Value	Normalized	
1	-14.473807	0.000000
2	-101.715237	272.758570
3	-175.671905	198.801902
4	-260.708822	113.764985
5	-354.843926	19.629881
6	-455.168801	279.305006
7	-549.507350	184.966457
8	-633.767842	100.705965
9	-707.795679	26.678128
10	-798.283267	296.190540

All right reserved, Old Dominion University



Adaptive Pre-Distorter will adjust input to amplifier to maintain linear output

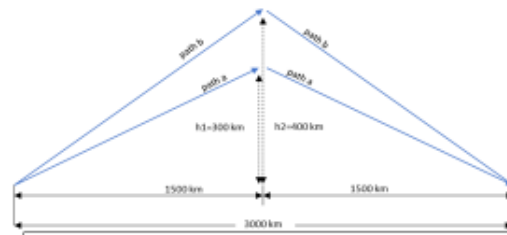
All right reserved, Old Dominion University



All right reserved, Old Dominion University

MILSTD-188-110D Symbol Rate

Bandwidth (kHz)	Symbol Rate (Sym/sec)	Sub-Carrier (Hz)
3	2400	1800
6	4800	3300
9	7200	4800
12	9600	6300
15	12000	7800
18	14400	9300
21	16800	10800
24	19200	12300
30	24000	15300
36	28800	18300
42	33600	21300
48	38400	24300

Calculation of Delay Spread (σ_t) at range of 3000 km


In multipath example; ray path (a) is refracted at 300 km, ray path (b) is refracted at 400 km. Path (b) is 46 km longer with a delay spread (σ_t) of 153 μ sec behind path (a). When transmit signal time (T_s) is less than delay spread inter-symbol interference will result.

Comparison of MILSTD Symbol rate and Delay Spread

MILSTD 188-110D Bandwidth (kHz)	Symbol Rate R_s (Sym/sec)	Transmitted Signal Time T_s (μ sec)	Delay Spread σ_t (μ sec)	Coherent Bandwidth B_c (Hz)	Delta $T_s - \sigma_t$ (μ sec)
3	2400	417	153	6536	263.67
6	4800	208	153	6536	55.33
9	7200	139	153	6536	-14.11
12	9600	104	153	6536	-48.83
15	12000	83	153	6536	-69.67
18	14400	69	153	6536	-83.56
21	16800	60	153	6536	-93.48
24	19200	52	153	6536	-100.92
27	21600	46	153	6536	-106.70
30	24000	42	153	6536	-111.83
33	26400	38	153	6536	-115.12
36	28800	35	153	6536	-118.28
39	31200	32	153	6536	-120.99
42	33600	30	153	6536	-123.24
45	36000	28	153	6536	-125.22
48	38400	26	153	6536	-126.96

A weakness of MILSTD-188-110D:
Transmitted Signal Time is significantly below Delay Spread (σ_t).

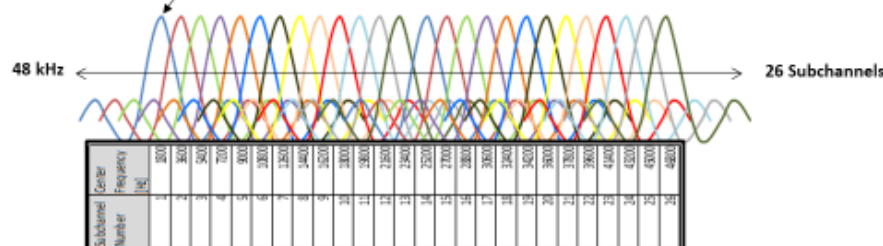
All right reserved, Old Dominion University

MILSTD-188-110D

Bandwidth (kHz)	Symbol Rate (Sym/sec)	Sub-Carrier (Hz)
3	2400	1800

Applying OFDM to MILSTD-188-110D

- Using the MILSTD 3 kHz bandwidth with a 2400 signal interval and 1800 Hz subchannel bandwidth results in 26 orthogonal subchannels within the 48 kHz bandwidth.



All right reserved, Old Dominion University

MILSTD-188-110D

Bandwidth (kHz)	Symbol Rate (Sym/sec)	Sub-Carrier (Hz)
3	2400	1800

Applying OFDM to MILSTD-188-110D

- Applying a 16 QAM modulation (waveform 10) yields 6.4 kbps x16= 166.4 kbps.
- This is faster than the 144 kbps in table above and the symbol duration is 16 time longer.
- A longer symbol rate results in higher E_b/N_0 and lower BER and more resistance to multipath, ISI and fading.
- In better conditions using a 64 QAM modulations results in: 16kbps x 26 = 416 kbps
 - Significantly greater than 240 kbps at a much slower symbol rate.

Virtual SATCOM Modulation using MILSTD188-110D modified with OFDM Modulation

Wave Number	0	1	2	3	4	5	6	7	8	9	10	11	12	13
Modulation	Wave	QPSK	QPSK	QPSK	QPSK	QPSK	QPSK	QPSK	16QAM	16QAM	16QAM	16QAM	16QAM	QPSK
Bandwidth (kHz)	Wave	(Hz)	(Hz)	(Hz)	(Hz)	(Hz)	(Hz)	(Hz)	(Hz)	(Hz)	(Hz)	(Hz)	(Hz)	(Hz)
3	75	150	300	450	600	750	900	1050	1200	1350	1500	1650	1800	2400
6	300	600	1200	1800	2400	3000	3600	4200	4800	5400	6000	6600	7200	9600
9	450	900	1800	2700	3600	4500	5400	6300	7200	8100	9000	9900	10800	14400
12	600	1200	2400	3600	4800	6000	7200	8400	9600	10800	12000	13200	14400	19200
15	750	1500	3000	4500	6000	7500	9000	10500	12000	13500	15000	16500	18000	24000
18	900	1800	3600	5400	7200	9000	10800	12600	14400	16200	18000	19800	21600	28800
21	1050	2100	4200	6300	8400	10500	12600	14700	16800	18900	21000	23100	25200	33600
24	1200	2400	4800	7200	9600	12000	14400	16800	19200	21600	24000	26400	28800	38400
27	1350	2700	5400	8100	10800	13500	16200	18900	21600	24300	27000	29700	32400	43200
30	1500	3000	6000	9000	12000	15000	18000	21000	24000	27000	30000	33000	36000	48000
33	1650	3300	6600	9900	13200	16500	19800	23100	26400	29700	33000	36300	39600	52800
36	1800	3600	7200	10800	14400	18000	21600	25200	28800	32400	36000	39600	43200	57600
39	1950	3900	7800	11700	15600	19500	23400	27300	31200	35100	39000	42900	46800	62400
42	2100	4200	8400	12600	16800	21000	25200	29400	33600	37800	42000	46200	50400	67200
45	2250	4500	9000	13500	18000	22500	27000	31500	36000	40500	45000	49500	54000	72000
48	2400	4800	9600	14400	19200	24000	28800	33600	38400	43200	48000	52800	57600	76800

All right reserved, Old Dominion University

- Developed a feasible and unique communication systems design that can change military communications.
- Propagation prediction through re-programming of MATLAB to analyze ionosphere for ultrawideband communications.
- Developed Concept of narrow beam and wideband signals.
- Completed tradeoff analysis of data rate vs communication parameters to ensure best data speed.
- Designed LPDA element for antenna array for efficient wideband operations between 7 and 28 MHz.
- Designed a 200-element antenna array using MATLAB and FEKO EM software to optimize beam forming and maximize gain.
- Experimented with antenna weighting for Virtual SATCOM array to suppress sidelobes with MATLAB.
- Designed a modulation and frequency allocation scheme for 3 MHz channel using MILSTD 188-110 narrowband modulations in an OFDM architecture.
- Designed a command and control network to monitor and adjust Virtual SATCOM parameters in real time.
- Developed command and control mechanism for units to establish and maintain link.

All right reserved, Old Dominion University



Summary



- Information transfer is the key to modern military operations.
- Increased bandwidth and signal to noise (SNR) are keys to communication speed.
- SATCOM is limited, vulnerability is increasing.
- Ionosphere is nature's satellite and available 24/7
- Directional antennas to increase BW and SNR are the future in communications.
- Digital signal processing in software defined radios using cognitive processes are opening new and exciting opportunities.

We have discovered that the development of a high-speed HF BLOS digital communication system is possible.

VITA

Dennis George Watson

EDUCATION

- National Defense University**, Dwight D. Eisenhower School for National Security and Resource Strategy, Fort McNair, Washington DC 2000
Degree: M.S. National Resource Strategy
 Area of concentration; Space industry and China.
 Completed: Senior Acquisition Course.
- Naval Postgraduate School**, Monterey, CA 1986
Degree: M.S. System Engineering (Electronic Warfare)
 Thesis: "Integration of High-Speed Anti-Radiation Missile (HARM) on EA-6B Aircraft". Area of concentration; Radar, Control Systems, Electromagnetics, Communications, and Digital Systems.
- US Naval Academy**, Annapolis, MD 1980
Degree: B.S. Naval Architecture
 Area of concentration; Naval ship design and weapon systems integration.

SELECT PUBLICATIONS

Naval Engineers Journal, December 2019 No. 131-4, Paper Title: "Virtual SATCOM; Assured Agile Communication in a Satellite Contested Battlefield"

PRESENTATIONS AT PROFESSIONAL MEETINGS

- American Society of Naval Engineers (ASNE), Combat Systems Symposium– 2018 Arlington VA, December 5-6, 2018, Paper Title: "Virtual SATCOM; Assured Agile Communication on a Satellite Contested Battlefield"
- MODSIM World 2018 Norfolk, VA, May 5-7, 2018, Title: "Modeling of the Ionosphere Reveals Wide Bandwidth Available for a Virtual SATCOM Communication System" Paper No. 35
- NATO Innovation Challenge 2017, Old Dominion University, Norfolk VA, October 22, 2017
 Paper Title: "Virtual SATCOM, High-Frequency Communication at SATCOM Speeds Without Space Vehicle Limitations and Vulnerabilities."
- American Society of Naval Engineers (ASNE), Intelligent Ships Symposium 2017, University of Pennsylvania Annenberg Center, Philadelphia, PA, May 24-25, 2017, Paper Title: "Focused High-Frequency Communication Can Mitigate SATCOM Vulnerabilities with Ultra-Wideband Channels"
- 15th International Ionospheric Effects Symposium 2017, Bridging the gap between applications and research involving ionospheric and space weather disciplines, Alexandria, VA, May 9-11, 2017, Paper Title: "Virtual Satellite System for C2, EW, and ISR Without the Vulnerability and Expense of Space Vehicles"

RELATED EXPERIENCE

- | | |
|---|-----------|
| Navy Information Operation Command, Norfolk VA | 2012-2013 |
| Commanding Officer, USS Nashville, LPD-13 | 2002-2003 |
| Commanding Officer, Tactical Electronic Attack Squadron 141 | 1996-1999 |
| Command and Control Warfare Commander, Carrier Group Six | 1994-1996 |
| Program Manager for Logistics, Naval Air Systems Command | 1991-1994 |